TLR4-MEDIATED CALVARIAL BONE REPAIR: INVESTIGATING ITS ROLE AND POTENTIAL USE FOR REGENERATIVE MEDICINE

by

Dan Wang

DMD, Sat Yun-Sen University, China, 2008

Submitted to the Graduate Faculty of

the School of Dental Medicine in partial fulfillment

of the requirements for the degree of

Doctor of Philosophy

University of Pittsburgh

2015

UNIVERSITY OF PITTSBURGH

School of Dental Medicine

This dissertation was presented

by

Dan Wang

It was defended on

March 15th, 2015

and approved by

Mooney P. Mooney, Professor, Departmental of Oral Biology

Elia Beniash, Assioate Professor, Departmental of Oral Biology

Timothy R. Billiar, Professor, Department of Surgery

Dissertation Director: Gregory M. Cooper, Assistant Professor, Department of Plastic Surgery

TLR4-MEDIATED CALVARIAL BONE REPAIR:

INVESTIGATING ITS ROLE AND POTENTIAL USE

FOR REGENERATIVE MEDICINE

Dan Wang, Ph.D

University of Pittsburgh, 2015

Injuries to the craniofacial skeleton have a tremendous economical and social impact on our healthcare system and society. Presently, clinical management of craniofacial trauma remains highly challenging and various efforts have been undertaken to develop and improve existing therapies for craniofacial reconstruction. Among these efforts, mounting evidence has demonstrated that inflammation is among the first events to determine fracture healing outcome. Thus, understanding how inflammation affects bone healing and subsequently modulating inflammation to enhance bone regeneration has become a promising strategy. Toll-like receptor 4 (TLR4) is a member of TLR family that is central to inflammation by virtue of its involvement in host defense for microbial infection as well as tissue regeneration. As such, TLR4 is a potential candidate for investigation and subsequent immune modulation. This work utilized various knockout (KO) mouse models for TLR4 and its associated inflammatory mediators as tools to study the role of inflammation in calvarial bone healing in the absence or presence of bone grafts. In the absence of bone graft, a similar accelerated phenotype was observed between MyD88 KO mice and DC-TLR4 KO (TLR4 depleted in dendritic cells) mice, indicating that dendritic cell expression of TLR4-mediated MyD88 signaling was detrimental for calvarial bone healing. In addition, TLR4 depletion in myeloid cells also resulted in accelerated bone healing via enhanced osteoclastogenesis within a calvarial defect model. However, in the presence of bone graft, inhibited bone healing and decreased osteoclast-mediated graft remodeling was observed in TLR4 KO mice or when TLR4 signaling was locally inhibited, establishing an

important and novel role of TLR4 in graft-based bone repair. Taken together, these data demonstrate that TLR4 signaling and its pathway mediators play an important regulatory role in osteoclastogenesis, highlighting a potential opportunity in which appropriate modulation of TLR4 signaling can be used to initiate early healing in bone defects or assist in bone graft-mediated therapy to improve clinical outcomes.

TABLE OF CONTENTS

LIST OF FIGURES

PREFACE

This thesis would not have been possible without several people whom I would like to acknowledge. I would first and foremost like to thank Dr. Gregory M. Cooper for being my mentor and dissertation director. He has whole-heartedly supported me through failures and successes in my research by being a constant source of encouragement. From him, I have learned many things about research ideas, experimental design, getting "the point" across in my scientific writings, American culture and believing in myself. For these things and more, I will be forever grateful. Thank you.

I would also like to thank Drs. Mark Mooney, Elia Beniash, and Timothy Billiar for their guidance and support as members of my dissertation committee. They hail from diverse academic fields and their advice has been immensely helpful in my research as well as enabled me to gain a better understanding and appreciation of the complexity of bone biology and tissue engineering. I would especially like to thank Dr. Timothy Billiar for initially introducing me to the University of Pittsburgh as a visiting research scholar. This initial opportunity enabled me to subsequently enroll in the Oral Biology Ph.D program. I cannot thank you enough for opening this new door. I would also like to thank Dr. Mark Mooney, who has supported my graduate studies and researches by meticulously arranging details such as my graduate class schedules, administrative matters, and guiding me as a teaching assistant in Gross Anatomy class, just to

name a few. I wanted to thank Dr. Elia Beniash for his delightful classes and discussions on biomineralization which have truly enriched my perspectives of bone biology.

I would also like to thank all the staff from the Department of Oral Biology, University of Pittsburgh. I would like to thank Dr. Manika Govil, Dr. Alejandro Almarza, and Dr. Seth Weinberg. Your advices and discussions we have had on statistics analysis, biomechanical testing and research design was immensely helpful in my experiments. I would also like to thank all the staff who have performed various administrative tasks or otherwise that have enabled me to receive a world-class education here.

I also wanted to thank all my lab mates in Dr. Cooper's Craniofacial Biology Laboratory. It has been a truly research-enriching and fun-filled environment to work in these last four years. I cannot thank you all enough. Through your teachings on research skills or simply the bench-side conversations that we have shared, I have learnt to improve the rigorousness of my research as well as expanded my knowledge of craniofacial biology. I would also like to thank James J. Cray, Adam K. Kubala, and Laura B. Meszaros, who helped to orientate and ease me into my then new and unfamiliar lab environment. I am extremely grateful to all the lab members and especially thank Dr. James R. Gilbert, and Dr. Gwen M. Taylor for their guidance, suggestions and supports. Their willingness to teach me new techniques, involve me in aspects of their research, and dispense both personal and scientific advice has transformed the workplace into a delight full environment to turn up to every day. Thank you so much!

I would also like to thank friends who have made my classes a truly enriching experience. I would especially like to thank my classmates Yang Xu, Loulwah Khalid and Harman Deol for their kind sharing of lecture notes, their help in understanding difficult class topics and the fun times we have shared together.

Lastly, I would like to thank my family. My parents, Jiantang and Qin, my fiancé Dai Fei Elmer Ker, and my doggies Bobbi and Mary. They have been an immense source of encouragement and support for me and this thesis would not have been possible without them.

1.0 INTRODUCTION: NOT ALL BONES ARE EQUIVALENT: COMPARISON OF LONE BONE VERSUS CALVARIAL BONE DEVELOPMENT, STRUCTURE AND HEALING

Craniofacial defects resulting from trauma, surgery, or congenital disorders are notoriously difficult to repair and present a significant burden to the healthcare system. Within the United States, approximately 2 million head injuries are reported annually with an estimated 592,000 cranial surgeries performed in 2006 alone [1-4]. While it is often assumed that regenerative therapies developed to correct defects within the appendicular skeleton will translate for application in craniofacial reconstruction, this is not a fully accurate assumption as there are fundamental differences in the developmental biology and anatomy of the craniofacial and appendicular skeleton. For example, long bones develop via endochondral ossification and require a cartilaginous intermediate whereas most calvarial bones are formed through intramembranous ossification. Moreover, the craniofacial complex includes a number of unique tissues (dura mater, periocranium, suture, and central nervous system), which can have a critical impact on the fracture repair process and regenerative capabilities of calvarial bone. Thus, our current understanding regarding the well-studied microenvironment of long bone fracture repair and their corresponding therapeutic treatment options might not be entirely applicable or appropriate for calvarial bone. Here we present and discuss aspects of development, structure, and repair processes which form a basis for distinction between calvarial bone and long bone.

Understanding the unique properties of calvarial bone and its healing process is essential for the development of tailored therapeutic strategies for skull bone repair [5-7].

1.1 THE DEVELOPMENTAL BIOLOGY OF CALVARIAL BONE

The developmental biology of calvarial bone formation is distinguished from that of long bone formation by virtue of several criteria, including: 1) the embryonic origins of the tissues; 2) the modes of ossification, and; 3) the signaling molecules which govern tissue formation of calvarial bone and long bone may also have differential effects on tissue remodeling and repair.

1.1.1 The Embryonic Origins and Modes of Ossification

Calvarial bone and long bone are composed of cells with different embryonic origins, which have implications on their ability to repair bone. Cells of long bone are derived from lateral plate mesoderm, whereas cells of calvarial region are derived from neural crest and cephalic mesoderm [8,9]. The lateral plate mesoderm and neural crest in turn, are derived from mesoderm and ectoderm germ layers, respectively. Initially, the discovery that bone could be derived from two distinct germ layers was surprising as it contradicted classical germ-layer theory which stated that a specific tissue could be only derived from a particular germ layer. For example, muscle, mesenchyme, connective and vascular tissues were formed from mesoderm whereas nerves and epidermis were formed from ectoderm [10].

The differential embryonic origins of bone tissues and distinct ossification modes may impact the ability to repair bones of the calvarial and axial skeletal systems [11]. Skeletal defects

were created in the mandible (neural crest-derived bone) and tibia (mesoderm-derived bone), and neural crest-derivatives and non-neural crest-derivatives were labeled with GFP and β-galactosidase separately [12]. It was observed that GFP-expressing neural crest-derived skeletal progenitors repaired neural crest-derived mandible and β-galactosidase expressing mesoderm-derived skeletal progenitors repaired the tibia, indicating that there are two separate pools of skeletal progenitor cells that exclusively repair bone according to their embryonic origins [12]. To determine the functional interchangeability of these two pools of skeletal progenitor cells, grafting experiments were performed. Mesoderm-derived skeletal progenitors could not differentiate into osteoblasts after they were transplanted into mandible defects, but neural-derived skeletal progenitors could differentiate into osteoblasts after they were transplanted into tibia [12]. Expression of an important developmental gene, *hoxa11* has been linked to the aforementioned plasticity of neural crest-derived skeletal progenitors [12]. Furthermore, bone progenitors cells from different embryonic origins also exhibit differences in proliferation and osteogenic potential, which translate into more robust bone regeneration. It suggests that the unique characteristics of bone cells from different embryonic origins might have an influence on bone repair. However, the above study does not take into account the potentially confounding effects of cell heterogeneity within their mesoderm- and neural crest-derived cell populations. For example, a recent study reported that a single type of mesoderm-derived skeletal progenitor found in the growth plate of long bone gave rise to at least 8 subpopulations, each with different propensities to form bone, cartilage and stromal cells [13]. As such, even though it appears that embryonic origins may differentially influence the ability of neural crest- and mesoderm-derived skeletal progenitors to repair calvarial and axial skeletal systems, further study is warranted.

Despite of their distinct developmental origins, calvarial bones and long bones both

develop from mesenchymal condensations but ultimately form through distinct modes of ossification. During mesenchymal condensation, mesoderm- and neural-crest derived mesenchymal cells halt their proliferation and form a cluster that is devoid of blood vessels, prior to undergoing stepwise differentiation into skeletal cells [14]. Calvarial bones are primarily formed through intramembranous ossification, although a small subset, including the temporal, occipital, sphenoid, and ethmoid bones, form through a combination of endochondral and intramembranous ossification. During intramembranous ossification, osteoblasts directly differentiate from the pre-osteogenic mesenchymal condensates and secrete bone extracellular matrix to form the ossification center. Subsequently, the osteoblasts continue to differentiate, followed by vascularization and bone marrow formation. In contrast, long bone development proceeds by means of endochondral ossification instead, which requires a cartilaginous template to be formed prior to bone conversion. The endochondral process is characterized by differentiation of mesenchymal stem cells (MSCs) into perichondrial cells and chondroblasts, which are located at the periphery and center of mesenchymal condensates, respectively [14], Upon differentiation into chondroblasts, cells resume proliferation to promote longitudinal bone growth, eventually becoming hypertrophic chondrocytes that secrete mineralized cartilage matrix. This results in a primary ossification center in the bone diaphysis and secondary ossification centers in the bone epiphyses. With subsequent vascularization, osteoblasts and osteoclasts are recruited to resorb the hypertrophic chondrocytes and replace the mineralized cartilage with new bone [15,16]. Thus, calvarial bones and long bones are formed initially from mesenchymal condensations but subsequently utilize intramembranous and endochondral modes of bone ossification, respectively.

1.1.2 Similarities and Differences in Signaling Molecules

Considerable similarity and differences exist in the signaling pathways and gene expression patterns during calvarial and long bone development. As described earlier, both types of bone form mesenchymal condensations prior to undergoing endochondral or intramembranous ossification [17]. Therefore, it is not surprising that the mesenchymal condensation of both calvarial and long bones involve similar signaling pathways and molecular actors including members of the Transforming Growth Factor-Beta (TGF-β), Bone Morphogenetic Protein (BMP) and Fibroblast Growth Factor (FGF) families, transcription factors including *Sox9* and adhesion molecules including cadherins and neural cell adhesion molecule [14]. During the subsequent endochondral or intramembranous ossification, bone- and cartilage-encoding genes are utilized to different extents. Chondrocyte-independent, intramembranous bone formation predominantly utilizes predominantly bone-encoding genes, whereas chondrocyte-dependent, endochondral bone formation utilizes a mix of cartilage- and bone-encoding genes. Bone-encoding genes include *collagen type 1* (*col1a1*), *bmp2* and *bmp6*, whereas cartilage-encoding genes include *sox5*, *sox6*, *sox9*, *indian hedgehog* (*ihh*), *collagen type 2* (*col2a1*) and *collagen type 10* (*col10a1*) [18-20]. For example, the bone-encoding gene COL1A1 forms a major component of bone extracellular matrix that is eventually deposited with hydroxyapatite crystals, producing a calcified matrix that is stiff and resistant to fracture [21] whereas the cartilage-encoding gene COL2A1 forms a major component of cartilage extracellular matrix and deletions to this gene leads to cartilage and skeletal abnormalities [22]. However, some genes including *runx2* are utilized to form both bone and cartilage and thus do not fit neatly into the above classification scheme [23,24]. Despite these exceptions, the differential use of bone- and cartilage-encoding genes by endochondral and intramembranous ossification can affect calvarial and long bone formation

in distinct manners. For example, as a cartilage-encoding gene, IHH is a vital growth factor that regulates the proliferation and differentiation of chondrocytes [11,25,26]. Knockout mice lacking *ihh* ($ihh^{-/-}$) exhibit severe defects in endochondral bone formation with limbs that are severely reduced in size [11,25,26]. In contrast, intramembranous bone formation in $ihh^{-/-}$ mice was less affected and mature osteoblasts that expressed osteocalcin were observed in parietal bone [11,25,26]. Also, *high mobility group box 1* (*HMGB1*) is another gene which differentially affects endochondral bone formation and intramembranous bone formation. HMGB1 is found in chromatin protein and is involved in inflammation and tissue regeneration. HMGB1 also acts as chemotactic agent to osseous cells during endochondral ossification. Recombinant HMGB1 (rHMGB1) stabilized the RANKL/OPG expression ratio and augmented the expression of TNF-α and IL-6 in long bone-derived cell cultures, but not in calvarial bone-derived cell cultures, suggesting that intramembranous and endochondral-derived osteoblasts exhibit a different response towards HMGB1 [27]. This result is further supported by observations that endochondral ossification, but not intramembranous ossification, was significantly impaired in embryonic HMGB1 knockout mice [28].

Thus, as a result of their distinct developmental origins and modes of bone formation, calvarial and long bone skeletal cells utilize different molecular mechanisms to form mineralized bone. Understanding the subtle differences between these molecular pathways will have important implications for identifying the most effective therapies for cranial bone repair.

1.2 STRUCTURAL DIFFERENCES BETWEEN CALVARIAL BONE AND LONG BONE

The craniofacial skeleton protects the brain and supports the structures of the face, whereas the appendicular skeleton protects the internal organs, provides structural support and contour to the body, and interacts with muscle and soft tissues to permit locomotion and movement. The unique organs, such as dura mater, periosteum and suture, and bone marrow directly influence fracture healing within the craniofacial skeletal system.

1.2.1 Dura Mater

The dura mater is a fibrous membrane that surrounds the intracranial and spinal nerve structures. It not only acts as a barrier to protect the central nervous system from traumatic injuries and infection, but is also essential for tissue regeneration. The dura mater has five layers (the bone surface, external median, vascular, internal median, and arachnoid layers) with varying thicknesses, orientations and structures [29]. Functionally, the dura mater is a unique and important source of multipotent mesenchymal cells, whereas bone marrow and periosteum are the most significant sources of osteoprogenitors during long bone formation and remodeling. The dura mater provides paracrine signals which are essential for calvarial defect healing [30]. Dura mater stem cells also showed greater osteogenic differentiation and enhanced matrix synthesis compared to bone marrow stem cells on biodegradable polylactic-co-glycolic acid (PLGA) and tissue culture plastic [31]. This may partially explain the function of dura mater and its resident cells in calvarial bone healing and its roles as being promising candidates for cranial bone tissue engineering [32].

The osteogenic function of dura mater is observed to vary with age. Genome-wide expression analysis showed that juvenile and adult dura mater have different gene expression profiles after rat calvarial fractures. Juvenile dura mater cells expressed more osteogenic and osteoclastogenic differentiation markers than adult dura mater cells [33]. This stark difference in the osteogenic properties of dura mater has been demonstrated in several animal studies where transplantation of juvenile dura into an adult rat resulted in heterotopic membranous ossification [34] whereas transplantation of mature and immature dura mater into calvarial defects of immature animals resulted in reduced and successful bone repair, respectively [35]. Although the precise factors responsible for the differences in regenerative capabilities of immature and mature dura mater are unknown, this difference may partially be due to the impact of mechanical strain on the juvenile dura mater which results from skull growth and expansion. Indeed, clinical observations suggest that calvarial defect healing is most efficient during the period of active intracranial volume expansion, which usually refers to the first two years of life [36-38]. It is possible that the differences in bone healing capacities between children younger and older than two years of age might be partially due to the differences in underlying dura mater function during its developmental processes.

1.2.2 Periosteum

The periosteum induces osteogenesis during endochondral ossification, making it an indispensable player during cartilage repair and long bone fracture healing [39]. The periosteum consists of an outer fibrous layer containing mainly fibroblasts and an inner cambium layer containing nerves, capillaries, osteoblast lineage cells, and undifferentiated cells [40]. Mesenchymal stem cells (MSCs) residing inside the periosteum and bone marrow exhibit

comparable growth kinetics and colony-forming potential [41]. An *in vitro* study demonstrated that upon stimulation with BMP-2 and FGF-2, periosteal cells and bone marrow-derived stromal cells both differentiated into osteoblasts but periosteal cells proliferated faster whereas bone marrow cells were more osteogenic [42]. The periosteum is also a major source of chondrocytes and osteoblasts during callus formation, underscoring its importance in endochondral bone repair. Loss or damage to the periosteum has been observed to result in delayed long bone healing or nonunion [43].

The periosteum has potential applications in long bone tissue engineering [44,45]. Composites of periosteal MSCs and hydroxyapatite ceramics induced bone formation when subcutaneously implanted into syngeneic rats [46]. Periosteum has also been described as essential for allograft performance. Tissue-engineered periosteum used in combination with allograft is superior to allograft alone in femoral defect reconstructions [47]. Artificial periosteum along with incorporated osteogenic-differentiated bone marrow stem cells also showed enhanced osteogenesis [48,49]. Age seems to influence the osteogenic potential of periosteum which is similar to dura mater. It is suggested that juvenile periosteum is more capable of bone regeneration than adult periosteum in a rabbit parietal defect model [50].

Although periosteum is essential in long bone fracture healing, studies suggest that its role in calvarial defect healing may be less crucial when compared to dura mater. A comprehensive study was performed to histologically assess the contributions of periosteum, cortical bone, endosteum, bone marrow and dura mater in rabbit tibial and calvarial bone healing [51]. After creating 10.8 x 4.45 mm tibial or calvarial cortical defects, Teflon cups and films were inserted into the defects in various orientations and positions for 10 – 12 weeks, in order to isolate and prevent specific tissues from participating in bone healing [51]. For example, placement

of the Teflon cup with its orifice/opening facing out towards the periosteum allowed for studying the effects of periosteum-mediated bone healing whereas placement of the Teflon cup with its orifice/opening facing the opposite direction allowed for studying the effects of endosteal- and medullary bone-mediated healing [51]. For tibial bone healing, periosteum was found to play a major role in bone repair whereas cortical bone, endosteum and bone marrow played a less prominent role [51]. For calvarial bone healing, dura mater produced more bone formation than cranial periosteum but both periosteal and dura mater were required for complete bony restoration [51]. Similar results were obtained when bone grafts were implanted into 90 mm^2 rabbit calvarial defects for 10 weeks [52]. Silastic barriers were used to cover the dura mater, cranial periosteum or both dural mater and cranial periosteum to isolate the contributions of various tissues to bone graft-mediated healing, which was assessed using fluorescein labeling [52]. Dura mater was found to improve bone formation throughout the entire graft, whereas periosteum only enhanced bone formation on the periosteal surface of the bone graft [52]. While both periosteum and dura mater showed osteogenic potential, this result suggests that the dura mater is predominantly responsible for the healing outcome in calvarial repair [52]. In addition, autogenous periosteal cells when used in combination with a bovine inorganic apatite and collagen-based biomaterial did not improve bone formation in a rat calvarial defect model when compared to biomaterial alone [53]. Thus, while both dura mater and periosteum show potential for enhancing bone graft repair, further study including cell lineage tracing as well as characterization of the proliferative and osteogenic capabilities of skeletal progenitor cells within these tissues will further delineate their contributions to bone repair and explain why dura mater might be more effective for calvarial bone repair.

1.2.3 Sutures

The cranial suture is a fibrous joint-like organ present in calvarial bone only. Six primary sutures exist which contribute to the growth, healing and elasticity of the skull. The suture is first formed as a thin layer of undifferentiated tissue between two bones, and later presents a serrated pattern after birth [54,55]. It allows the necessary expansion during brain growth, slightly movements of cavlarial bones and absorption of mechanical forces to protect the underneath central nervous system. Abnormal sutures growth largely influence the development of calvarial bone and brain, like the formation of craniosynostosis due to the prematurely ossification of sutures. Differential gene expression profiles have been implicated in fused and patent sutures [56]. Besides its role aforementioned, suture also serves as an intramembranous bone growth site. The roles of suture resident cells or suture expressing transcription factors and growth factors on bone development and regeneration have been implicated [57]. Some of suture-expression osteogenic factors, such as Runx2, Nel-like molecule-1 (Nell-1), TGF-β1, FGF2, have been observed to play a role in premature fusion of calvarial suture [58-61]. Vice versa, players associated with craniosynostosis have also been studied to understand their potential capacity in bone healing. For example, Nell-1 is a secreted protein identified from premature fused sutures. Along with demineralized bone matrix carrier, Nell-1 is found to improve bone healing in a critical-sized femoral segmental defect in rats [62]. Twist1 which is associated with premature synostosis of cranial sutures in both mice and human, has been suggested to inhibit osteoblast differentiation *in vitro* [63,64] and cause reduced bone formation *in vivo* [65]. Thus, molecules and cells identified in premature fusion of sutures might be potential candidates to assist bone repair.

1.2.4 Bone Marrow

Besides differences between dura mater, periosteum and sutures, long bone and calvarial bone differ in terms of bone marrow amount. Long bones, by virtue of their larger bone volume and elongated structure contain a well-defined marrow cavity that serves as the major site for hematopoiesis whereas calvarial bones by virtue of their smaller and flatter structure do not contain much bone marrow. The close association of marrow tissue with skeletal tissue may play a pivotal role in regulating each other's activities. For example, ectopic subcutaneous transplantation of marrow tissue in rats result in functional marrow tissue encased in a shell of bone [66] whereas ectopic bone formation in subcutaneous and intramuscular sites often results in the formation of an accompanying marrow cavity [67]. While ectopic bone in the renal capsule but do so without any bone marrow formation [68,69]. In contrast, calvarial tissues do not exhibit this close association as transplantation of mouse fetal calvarial-derived skeletal cells to the renal capsule forms ectopic bone but without any accompanying bone marrow [68,69]. Likely candidates that may be responsible for this marrow and skeletal tissue association include cell-to-cell interactions between long bone-derived skeletal cells and marrow-derived hematopoetic stem cells (HSCs). These cells reside together in locations known as stem cell niches where the immediate microenvironment consists of various biochemical, neuronal, mechanical cues which arise as a result of cell-to-cell and cell-to-matrix interactions, allowing stem cells to self-renew as well as respond to external stimuli such as injury [70]. For example, osteoblasts [71] and mesenchymal stromal cells [72] are known to regulate HSC numbers and self-renewal, respectively. However, the effect that HSCs may have on skeletal cells along with their net effect on bone healing is uncertain. Studying the nature of these interactions as well as the potential impact on fracture healing is an interesting concept that warrants further study.

Calvarial bones and long bones are surrounded by different structures including dura mater, periosteum, sutures and bone marrow, each of which has a profound impact on the proliferation and differentiation of bone cells as a result of cell-to-cell interactions including paracrine signaling. Understanding the effects of these interactions on calvarial bone formation and repair will be helpful for personalizing therapies based on the anatomical location where an injury is sustained.

1.3 AN OVERVIEW OF FRACTURE REPAIR IN CALVARIAL BONE AND LONG BONE

The developmental and structural differences between calvarial bones and long bones as discussed in preceding sections directly influence their biological healing process after fracture. Fracture repair is a coordinated response that consists of the pathways involved in normal embryonic development as well as the participation of bone cells, immune cells, extracellular matrix, etc [73]. Based on histological observations in both patients and animal models, the endochondral bone fracture healing process is usually divided into four stages: inflammation, soft callus formation, hard callus formation and bone remodeling stages [74]. Although calvarial bone and long bone share similarities during fracture repair process, calvarial bone regeneration is still unique, such as it does not require a cartilaginous template and involvement of different surrounding tissue. We generally classify calvarial bone repair into inflammation, bone remodeling and bone formation stages for the following discussion.

1.3.1 The Inflammation Stage During Calvarial Bone and Long Bone Healing

The inflammatory response after bone fracture shares similar events and signaling pathways with non-skeletal injuries. Despite the considerable controversies that exist regarding to the role of inflammation in fracture repair, it has received increasing attention not only for its role in host defense against infection but also in bone regeneration and repair [75,76].

Hematoma formation and intense cell infiltration are the major features which are similarly observed during the first few days after calvarial fracture and long bone fracture. Inflammatory cells (platelets, macrophages, lymphocytes, monocytes, granulocytes) infiltrate the fracture hematoma, secreting cytokines and growth factors to initiate the healing cascade. Inflammatory cytokines such as IL-1, IL-6, and TNF-α that originate from macrophage and mesenchymal cells show increased levels right after fracture in both long bone and calvarial bone healing [77,78]. These cytokines are highly involved in the inflammatory response and also play a role in promoting angiogenesis, recruiting fibrogenic cells to the fracture site and stimulating extracellular matrix synthesis. Similar to inflammatory cytokines, growth factors such as TGF-β, PDGF, BMP-2, -4, -5, -6, and GDF-8 also show increased expression at this stage. These factors facilitate cellular (inflammatory cell and mesenchymal stem cell) invasion in a positive feedback loop, which is essential for initiating soft callus formation and controlling cellular proliferation.

Differences also exist in the inflammatory stage between calvarial bone and long bone, such as dura mater reaction, hematoma property and gene expression profiles. A unique characteristic during the inflammatory phase of calvarial fracture healing is the early and essential involvement of the dura mater. An increase in dura mater cellularity is observed during this stage, which may be beneficial for healing response given that this tissue is a rich source of osteoprogenitors. Another unique part is the influence or consideration of hematoma during

fracture healing. Hematoma is critical for fracture healing and removal of fracture hematoma will lead to delayed healing [79]. However surgeons are more cautious when treating hematoma occurs in traumatic head injury, the effect of hematoma in calvarial bone healing is still not yet clear [80]. Furthermore, gene expression profiles also vary among injury sites and injured tissue types. For example, serum level of IL6 was higher and serum level of RANKL/OPG was lower in patients with a concomitant head injury and fracture compared to patients with fractures only (femur, clavicle, tibia). As differences in the expression profiles of RANKL, OPG, and IL-6 were observed, altered fracture repair outcome can occur between patients with these two different fractures [81,82]. It suggests that in situation where a head trauma exists, the body prioritizes to protect the central nervous system from infection by eliciting a greater-than-normal inflammatory response, which may come at the expense of bone repair.

Various studies have explored the effect of modulating fracture-induced inflammation for obtaining desirable bone healing outcomes, including manipulating expression of inflammatory cytokine, chemokine, and growth factors (IL1, IL-6, IL-18, TNF-α, Complement 3, TGF-β, VEGF, stromal cell-derived factor). However, the same inflammatory mediator might have different roles in regulating repair in calvarial bone and long bone. For example, Toll-like receptor4 (TLR4) is a member of transmembrane receptor family that activate the innate immune response by recognizing conserved molecular patterns of microbial products as well as endogenous ligands. TLR4 has been reported to have a profound role in mediating innate immune response and skeletal tissue homeostasis [83]. We previously reported a rapid calvarial healing in $TLR4^{-/-}$ mice histomorphometrically and radiographically, accompanied by an increase in dura mater cellularity and inflammatory cytokine expression at the early inflammatory stage [78]. In contrast, a recent study showed that individuals with mutated TLR4 are

associated with long bone non-unions [84]. However, this may be attributed to impaired recognition and elimination of pathogens in the wound site instead of innate differences between calvarial and long bone since sterile calvarial defects were employed. Thus, elucidating the role of inflammation in long bone and calvarial bone healing will be useful in determining whether immunomodulatory drugs may be used for bone repair.

1.3.2 Bone Formation and Bone Remodeling Stages during Calvarial Bone and Long Bone Healing

Bone formation stage during calvarial bone and long bone repair employ different cellular mechanisms that directly influence healing patterns. Chondrocytes and fibroblasts are the most active cell types during the soft callus formation phase of long bone fracture healing [85]. Mesenchymal progenitors infiltrate the defect, differentiate into chondrocytes, and subsequently synthesize a cartilaginous matrix. This cartilage replaces the hematoma and forms a soft callus template in the soft callus formation stage. With mineralization of extracellular bone matrix, soft callus is gradually replaced by woven bone. During calvarial bone healing, osteoblasts and fibroblasts are the most active cell types during the bone formation stage. These osteoprogenitor cells can originate from multiple locations including the bone marrow, periosteum, dura mater and nearby soft tissue [86]. Typical large, cubic, mononucleated osteoblasts are visible at the defect site as early as day 7 after calvarial fracture [78]. The mineralized extracellular matrix is mainly secreted by mature osteoblasts. Woven bone matrix will mineralize and be gradually replaced by lamellar bone. Although calvarial bone and long bone ultilize different ossification modes, some similarity exists in the gene expression profiles during this stage. For example, the expression of inflammatory cytokines that are active during the inflammatory stage begins to decline during

the bone formation stage, while multiple growth factors including TGF-β2, p3, GDF-5, and BMP-2, 3, 4, 5, and 6 show increased expression. Osteoblast, chondrocyte and fibroblast proliferation will be regulated by all the growth factors mentioned above. Angiogenic factors such as angiopoietins, VEGFs, BMPs, FGF-1, and TGF-β stimulate vascular endothelial cells and trigger angiogenesis invasion into newly regenerated bone matrix [87-89].

Bone remodeling stage starts with woven bone generating into cortical and/or trabecular bone configurations. Calvarial bone and long bone share similar histological healing patterns and gene expression profiles during this stage. This stage is characterized by the presence of osteoclasts, which leads to resorption of mineralized bone. Two main cytokines, M-CSF and RANKL (the ligand of NFκB), are critical for the induction of bone resorption. M-CSF plays a role in the differentiation of osteoclast lineage cells from haematopoietic cells. RANKL is expressed by mature osteoblasts and is important in osteoclast differentiation [90,91]. Inflammatory cytokines such as IL-1, IL-6, TNF-a, OPG, and RANKL that show increased expression during inflammation exhibit another peak in expression during bone remodeling, while members of the TGF-β superfamily display diminished expression. Regenerated lamellar bone will eventually re-establish the geometric and functional properties of the fracture site.

As mentioned, commonalities and distinct differences exist in terms of healing process between calvarial and long bone repair. Thus, careful consideration of these factors is necessary when design therapies for long bone and calvarial repair.

1.4 SUMMARY

In summary, calvarial bone is a unique type of bone tissue that is distinct from long bone from various perspectives. In the course of its development, calvarial bone is formed mainly through intramembranous ossification and bypasses the cartilage intermediate stage observed in long bone formation. During fracture healing, a pronounced inflammatory response is elicited to favor protection of the central nervous system over bone repair. Structurally, dura mater and sutures are only found associated with craniofacial bone, which exert profound influences on healing outcome. These factors should be considered, allowing for the development of tailored treatments and interventions for either calvarial or long bone repair.

Inflammation is an integral component of the response to injury and is increasingly recognized as playing an essential role not only in host defense against infection but also in tissue regeneration and repair [75,76]. Traditionally, inflammation has often been negatively associated with pathological bone destruction. However, in recent years, there has been an increased interest in elucidating the positive role of inflammation in bone regeneration and repair. Furthermore, mounting evidences have also suggested that the initial inflammatory stage is among the first events to determine the fracture healing outcome [90]. Toll-like receptor (TLR) is a receptor family, which plays a central role in the induction of sterile inflammatory cascades in response to tissue injury in many settings, including musculoskeletal trauma [91]. The following studies utilized various TLR4-assocaited knock-out (KO) mouse models, as a tool [92] to understand the role of the innate immune system during skull bone healing under clinically relevant settings.

2.0 ACCELERATED CALVARIAL HEALING IN MICE LACKING TOLL-LIKE RECEPTOR 4

2.1 INTRODUCTION

The skeletal and immune systems are interconnected and share multiple signaling pathways [93]. The inflammatory stage of healing that occurs immediately after fracture is non-specific and shares signaling pathways with non-skeletal injuries like skin wound healing. Bone components exposed by long bone fracture possessed immunologic properties that play an important role in the induction of local, but not systemic, inflammation [94,95]. Inflammation promotes cell proliferation and migration into the fracture site, triggering a healing cascade within damaged bone [85]. Inflammation has a well-established role in promoting long bone regeneration. The use of nonsteroidal anti-inflammatory drugs is contra-indicated in patients with bone injuries [96]. Fracture repair is significantly delayed in COX-$2^{-/-}$ mice, suggesting that efforts to blunt inflammation may be deleterious to fracture healing [97]. However, other studies have observed accelerated fracture repair in the absence of an adaptive immune system [98]. The role of the inflammatory response in bone regeneration is more complex than originally envisioned and is not fully understood.

Toll-like receptors (TLRs) play an essential role in innate recognition of microbial products and are critical activators of the innate immune response. More than ten TLRs have

been shown to recognize distinct microbial products, such as microbial membrane lipids or nucleic acids. Another unique role of TLRs is to sense cellular stress or tissue damage by responding to endogenous ligands released from necrotic cells and damaged tissues [99]. Direct TLR signaling inhibits RANKL-mediated osteoclast differentiation, while TLR activation has also been shown to enhance osteoclast differentiation by inducing RANKL and TNF-α expression in osteoblasts [100]. Thus, the role of TLRs in bone healing remains unclear and deserves further investigation [101-103].

Toll-like receptor 4 (TLR4), a cell surface TLR, plays a unique role in sensing tissue damage. TLR4 signaling is activated in response to tissue injury, resulting in the induction of a sterile inflammatory cascade [83]. TLR4 has also been implicated in regulating the systemic inflammatory response following bilateral femoral fracture [104]. Whether TLR4 plays a role in the local inflammatory response to calvarial defects and the impacts of this response on healing remains unknown.

In the current study, we hypothesized that TLR4 activation affects the healing of calvarial defects, and that different gene expression patterns would be observed between wild-type (WT) and Toll-like receptor 4 mutant ($TLR4^{-/-}$) mice during the healing process. To test this hypothesis, we assessed bone healing in small calvarial defects created in WT and $TLR4^{-/-}$ mice using radiographic, histologic and gene expression analyses.

2.2 MATERIALS AND METHODS

2.2.1 Animal Care and Experimental Design

Wild-type C57BL-6J mice (Jackson, Bar Harbor, ME) and TLR4$^{-/-}$ mice (from an ongoing breeding colony housed at the University of Pittsburgh) between 10 and 12 weeks of age (20-30 g) were used in this study. Mice were randomly chosen for radiographic, histological, or RT-PCR analyses. All mice were maintained in the Rangos Research Center Animal Facility, Children's Hospital of University of Pittsburgh with a 12:12 h light-dark cycle and free access to standard laboratory food and water. All procedures were carried out in accordance with the regulations regarding the care and use of experimental animals published by the National Institutes of Health and were approved by the Institutional Animal Care and Use Committee of the University of Pittsburgh.

2.2.2 Calvarial Defects Models

Mice were anesthetized by inhalation with isoflurane (4% for induction, 2% for maintenance, Abbott Laboratories, Chicago). The scalps were depilated and cleaned prior to surgery. Under sterile conditions, the calvariae were exposed by midline scalp incision and the periosteum covering the entire parietal bone was stripped off. A circular parietal defect was made using a 1.8 mm outer diameter trephine (Fine Science Tools, Foster City, CA). The calvariae were irrigated with PBS during surgery. Following creation of the defect, the scalp was reapproximated and closed with 4-0 Vicryl resorbable sutures and 1 mg/kg ketoprofen (Fort Dodge Animal Health, Fort Dodge, IA) was administered as an analgesic immediately after surgery. All animals were

euthanized by CO_2 overdose followed by cervical dislocation at designated time points postoperatively.

2.2.3 Histologic Analyses

Between three and five mice from each group were euthanized on untreated day 0 and postoperative days 1, 4, 7, 14, 21 and 28. Calvariae and surrounding soft tissues (e.g., skin, brain) were harvested by cutting the skull bones anteriorly across the middle of the frontal bones and posteriorly through middle of the interparietal bone. The samples were fixed in 10% neutral buffered formalin for 24-48 h and were decalcified overnight in Cal-Ex decalcifer (Fisher Scientific, Hampton, N.H.) prior to being dehydrated through a series of alcohols and embedded in paraffin. Paraffin-embedded specimens were sectioned through the coronal plane at a thickness of 5 µm. Three regions of each defect, 50 µm apart, were cut and placed on slides (for a total of approximately 30 slides per animal). Slides were stained with Harris' hematoxylin & eosin (Surgipath Medical Industries, Richmond, IL) for conventional, qualitative bright-field light microscopy.

Histomorphometric analysis was performed to quantify the two-dimensional area of new bone formation. Healing data was calculated based on three to five slides per animal. Microscopic images of the histologic sections under 100X were analyzed using Northern Eclipse software (Empix Imagine, Inc., Mississauga, Ontario, Canada). New bone area was calculated as the sum of the areas of each bone section, including within the defect and on both sides of calvarial. Data were expressed as mean +/- SEM.

Russell-Movat pentachrome staining (American MasterTech, CA) was performed to further differentiate the following tissues within the defect: hematoma/fibrin (intense red), elastic

fibers (black), cartilage (deep green), granulation/ fibrous tissue (green or light blue) formation and degradation, newly-formed woven bone (yellow) and lamellar bone (red). All specimens were examined at 25 X, 50 X, 100 X and 200 X magnifications.

Immunohistochemistry stain: Sections were deparaffinized with xylenes and rehydrated through serial of EtOH dilutions to distilled H_2O. Following the manufacturer's instructions, sections were incubated in primary goat polyclonal anti-OPN (Santa Cruz Biotechnology, Santa Cruz, CA) as a marker of osteogenic differentiation suspended at a 1:250 dilution in 2% normal horse serum (Vector Laboratories, Burlingame, CA) for 30 min at room temperature, secondary antibody (biotinylated anti-goat, made in horse, BA-9500, Vector Laboratories, Inc. CA, USA) diluted at 1:250 for 30mins at room temperature, and with Streptavidin-HRP (R&D systems, Gaithersburg, MD) at dilution 1:500 for 30mins at room temperature. Color was developed by application of DAB kit (Vector Laboratories, Burlingame, CA). Sections were dehydrated and mounted prior to examination at 25 X, 50 X, 100 X, and 200 X magnifications.

2.2.4 Radiographic Analysis

Ten animals from each group were euthanized 28 days after surgery and calvariae were harvested and fixed in 10% neutral buffered formalin for 24-48 hours. Radiographs were obtained using a Faxitron MX-20 (Faxitron X-Ray, Lincolnshire, IL) with a 35 Kv exposure and a 45-second exposure time to analyze calvarial healing. The films (Eastman Kodak, Rochester, NY) were developed and scanned using a Microtek 9800 XL scanner (Microtek Lab, Inc., Fontana, CA). The scanned images were imported into Northern Eclipse software (Empix Imagine, Inc., Mississauga, Ontario, Canada). The remaining defect area was measured, and

subtracted from the geometric original defect area (2.54mm^2) to generate the area of newly-formed bone.

2.2.5 mRNA Extraction and Expression Analysis

Five to seven mice from each group per time point were killed at day 0 before surgery and at 3h, days 1, 2, 4, 7, 14, 21, 28 postoperatively. Samples surrounding the initial 1.8 mm defect were collected using a 5.0mm trephine (Fine Science Tools, Foster City, CA), and included blood clots, hematoma, granulation tissue, new bone and surrounding normal bone. Samples were stored at 4°C in RNAlater solutions (Life Technologies, NY) until ready for RNA isolation. The specimens were homogenized in liquid nitrogen using a mortar and pestle, and RNA was extracted from the sample using RNAqueous-Micro Kit (Life technologies, NY) and the manufacturer's protocol. Contaminating genomic DNA was eliminated by treatment with DNAse I (Invitrogen, Life Technologies). Primers used in the study recognize IL-1α, IL-1β, IL-6, TNF-α, BMP-2, BMP-4, TGF-β1, TGF-β2, TGF-β3, VEGF, PDGF, RANK, RANKL and OPG. The housekeeping genes GAPDH and EEF2 were chosen as internal controls. RT-PCR results were analyzed by standard curve analysis. Finally, relative gene expression in WT and TLR4$^{-/-}$ mice was compared at designated time points.

2.2.6 Statistical Analysis

Statistical analyses were performed using SPSS v.20.0 software (SPSS, Inc, Chicago, IL). Mean areas of newly-formed bone collected from histomophometric measurements were compared using a group by time point (2 x 4) two-way ANOVA followed by group by time point (1 x 4)

split plot one-way ANOVAs to compare each group (either WT or TLR4$^{-/-}$) over time. Post-hoc LSD tests for multiple comparisons were used to detemine significant differences among groups and time points. Independent t-tests were performed to compare histomorphometric and radiographic measurements of newly-formed bone area in WT and TLR4$^{-/-}$ mice at each time point.

PCR data violated the assumption of homogeneity of variance, so the data was transformed using a rank transformation. Data were compared using two-way (time x group) ANOVA and are compared according to "early"($\leq$4 days) and "late"(>4 days) time point groups. A *p* value less than or equal to 0.05 was considered significant.

2.3 RESULTS

2.3.1 Histological Analysis

2.3.1.1 Qualitative histologic analysis

Day 0: Similar histological staining was shown in WT and TLR4$^{-/-}$ mice on day 0 using H&E and Pentachrome stain (Figure. 1A, B; Figure. 2A, B).

Day 1-day 4: WT and TLR4$^{-/-}$ mice showed similar histological staining patterns on day 1 and day 4 (Figure. 1C, D; Figure. 2C, D). Hematoma was visible and infiltration by multiple cell types was observed in H&E stained images. The bone defect was filled with hematoma as early as day 1. No changes were observed in the periosteal regions on day 1 (Figure. 1C, D). Evidence of hematoma degradation and a reduction in cellular infiltrate was apparent by day 4. On the

endocortical surface (presumably derived from the dura mater), cells gathered along the perimeter of the defect (Figure. 1E, F). Dural cell layer was thicker and OPN staining intensity were more pronounced in TLR4$^{-/-}$ mice than in WT mice (Figure. 3A, B). No bone formation was evident on day 4.

Day 7-day 14: Larger areas of newly-formed bone were seen in TLR4$^{-/-}$ mice than in WT mice on day 7. Newly-formed cellularized bone matrix, indicated by positive saffron yellow staining (Figure. 2E, F), was observed on the endocortical (dural) side of the calvarial bone lateral to the defect perimeter in both WT and TLR4$^{-/-}$ mice. The thickness of the dural cell layer was diminished relative to day 4, and there was evidence of active bone formation near the dural side of the calvaria. Disorganized loose connective tissue completely filled the bone defect on day 7 (Figure. 1G, H). OPN immunoreactivity was observed along the ectocortical bone surface (periosteal side), along the endocortical bone surface (dural side), within the intercortical region (bone marrow or diploic space), and along the defect margins. OPN immunostaining was more intense in TLR4$^{-/-}$ mice than WT mice (Figure. 3C, D). Typical large, rounded osteoblasts were recognized on the surface of the newly-formed bone in WT and TLR4$^{-/-}$ mice on day 14 (Figure. 3E, F). Regenerated bone was seen along the dural surface of the calvarial bone and along the defect perimeter. Periosteal thickness remained unchanged between days 7 and 14, while the loose connective tissue was thinner and more organized (Figure. 1I, J).

Day 21-day 28: Defects in WT and TLR4$^{-/-}$ mice were histologically similar during this period. On day 21, active bone formation was suggested by the presence of large regions of woven bone matrix at the defect margin in WT and TLR4$^{-/-}$ mice (Figure. 1K, L). Mature OPN-positive osteoblasts were observed on the surfaces of the woven bone. Dural cell layers returned to day1 thickness without OPN positive staining (Figure. 3G, H). On day 28, less OPN positive

staining and less bone formation was detected in both WT and TLR4$^{-/-}$ mice (Figure. 1M, N; Figure. 3I, J). Bone remodeling was evident with acid fuchsin red positive staining (Figure. 2G, H). Periosteum and soft connective tissue became much thinner, more dense, and better organized (Figure. 1M, N).

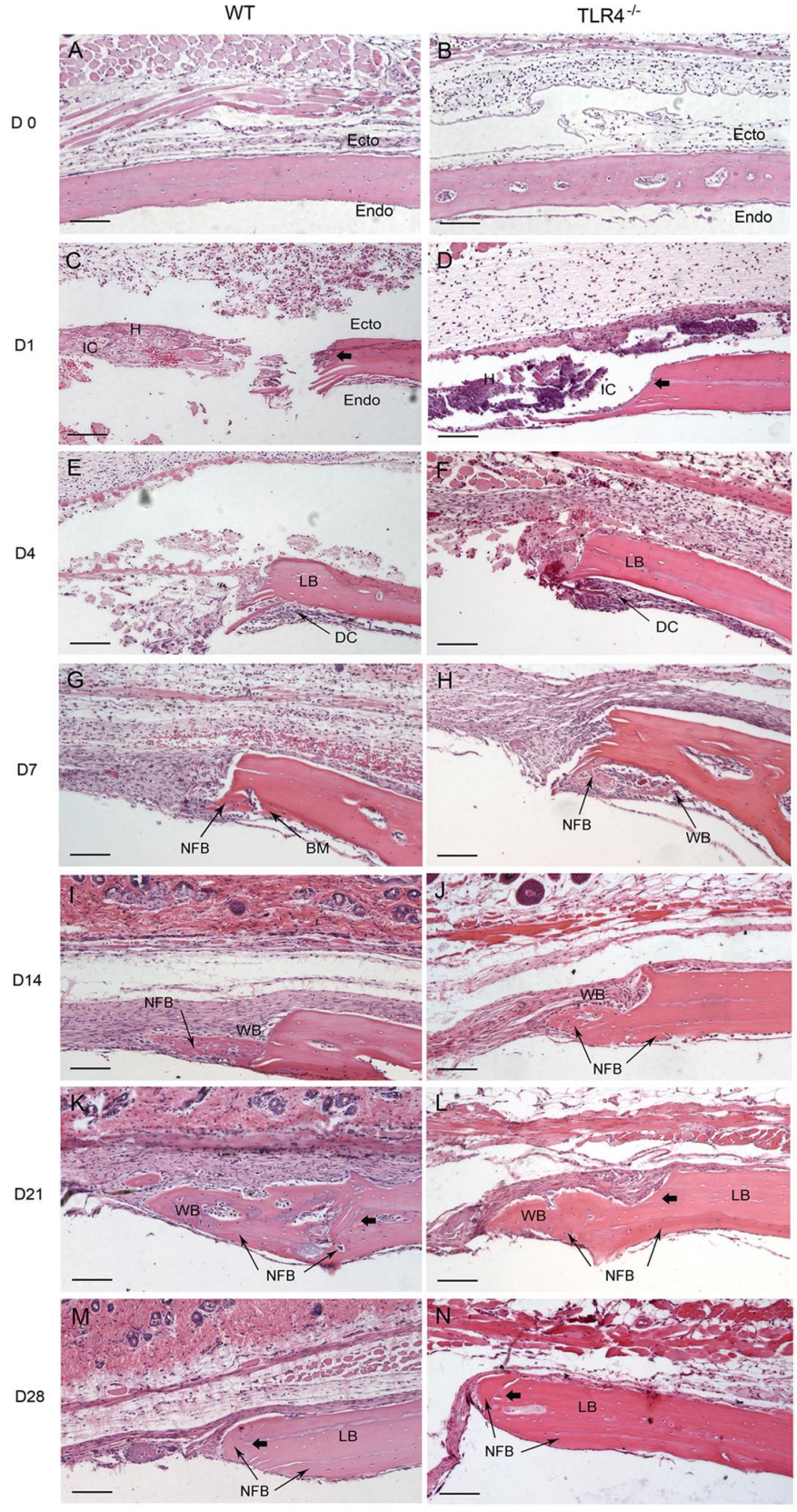
WT
TLR4 -/-
D 0
D1
D4
D7
D14
D21
D28
A
B
C
D
E
F
G
H
I
J
K
L
M
N
Ecto
Endo
H
IC
LB
DC
NFB
BM
WB

Figure 1: Histophotomicrographs for H&E stained tissues at the defect margins at postoperative time points

WT and TLR4$^{-/-}$ mice showed similar histological staining patterns on days 0, 1 and 4, while larger areas of newly-formed bone were seen in TLR4$^{-/-}$ mice than in WT mice on day 7. Newly-formed cellularized bone matrix was observed on the endocortical (dural) side of the calvarial bone lateral to the defect perimeter in both groups since day 7. Active bone formation was suggested by the presence of large regions of woven bone matrix at the defect margin in both groups on days 14 and 21. Defects in WT and TLR4$^{-/-}$ mice were histologically similar since day 21. (scale bar: 100 µm; bolded arrows: defect margin; endo: endocortical surface of calvarial bone; ecto: ectocortical surface of calvarial bone; H: hematoma; IC: infiltrating cells; LB: lamellar bone; WB: woven bone; NFB: newly-formed bone; DC: dural cells)

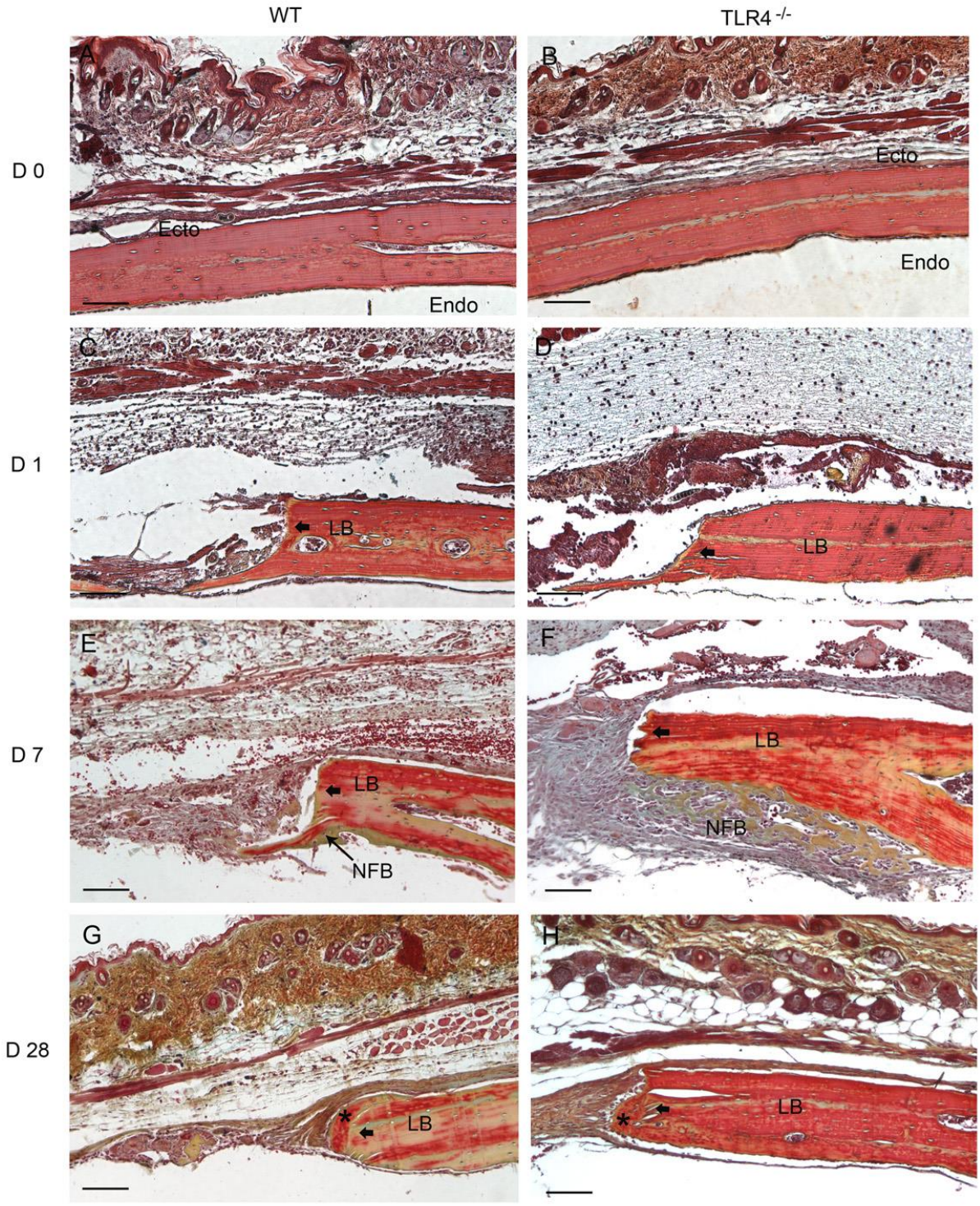

Figure 2: Histophotomicrographs of slides stained with OPN antibodies using immunohistochemistry

OPN staining intensity were more pronounced in TLR4-/- mice than in WT mice on postoperative days 4 and 7. Typical large, rounded osteoblasts were recognized on the surface of the newly-formed bone in both groups on day 14 . On day 28, less OPN positive staining was detected in both WT and $TLR4^{-/-}$ mice. (scale bar: 100 µm; bolded black arrows: defect margin; LB: lamellar bone; WB: woven bone; OPN(+): OPN positive stains; OB: osteoblasts)

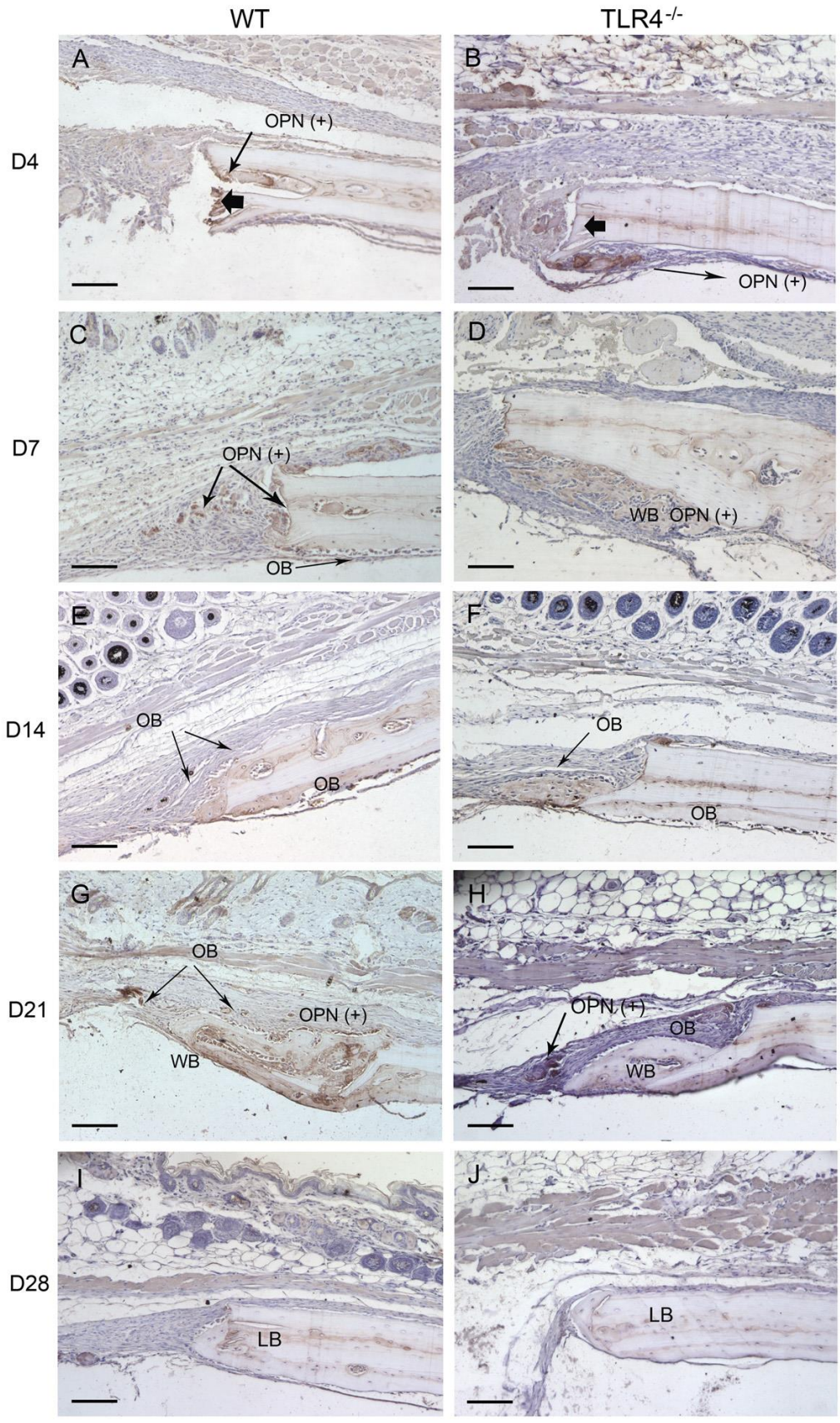
WT
TLR4-/-
D4
D7
D14
D21
D28
A
B
C
D
E
F
G
H
I
J
OPN (+)
OPN (+)
OPN (+)
WB OPN (+)
OB
OB
OB
OB
OB
OPN (+)
WB
OPN (+)
OB
WB
LB
LB

Figure 3: Histophotomicrographs of pentachrome stained tissues in WT and TLR4$^{-/-}$ mice

Similar stains were observed between WT and TLR4$^{-/-}$ mice on day 0 and day 1. An increased amount of newly-formed bone was observed in TLR4$^{-/-}$ mice at day 7, suggesting accelerated healing compared to WT. Lamellar bone (*), which stains positive for acid fuchsin (red) was observed in both groups on day 28, suggesting maturation and remodeling of the newly formed bone matrix. (scale bar: 100 µm; bolded black arrows: defect margin; LB: lamellar bone; NFB: newly-formed bone)

2.3.1.2 Quantitative histologic analysis

No obvious bone formation was observed in either group before day 7. Two-way ANOVA comparing mean newly-formed bone areas showed a significant group by time point interaction ($F=3.476$; $p<0.05$) and significant group ($F=5.946$; $p<0.05$) and time point ($F=14.728$; $p<0.05$) effects. One-way ANOVA showed no significant differences in bone healing between days 21 and 28 in WT mice, or between days 14, 21, and 28 in TLR4$^{-/-}$ mice ($p>0.05$). Independent T-tests showed significant differences in newly-formed bone areas between WT and TLR4$^{-/-}$ mice on both days 7 and 14 ($p<0.05$, Figure. 4). Larger newly-formed bone areas were observed in TLR4$^{-/-}$ mice on days 7 and 14, although comparable levels of bone healing were observed in both groups at other time points ($p>0.05$; Figure. 4).

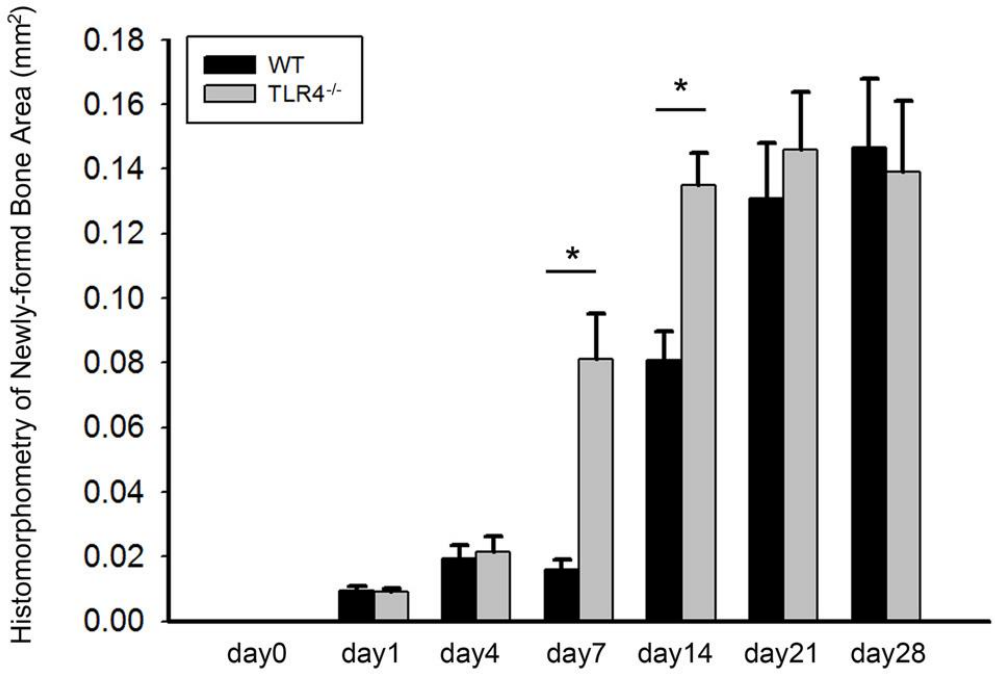

Figure 4: Graph showing newly-formed bone areas measured from H&E stained histology slides

No obvious bone healing was seen before day 7. Significant differences in bone healing areas were observed between WT and TLR4$^{-/-}$ mice on days 7 and 14 postoperatively. Newly-formed bone areas were not significantly different after day 21 in WT mice or after day 14 in TLR4$^{-/-}$ mice (mean +/- SEM ; *p<0.05).

2.3.2 Radiographic Analysis

Mineralized tissue was observed on day 28 radiographs in WT and TLR4$^{-/-}$ mice, although healing remained incomplete during the 28 days of observation. Calculation of newly-formed bone area as determined by radiography revealed healing percentages of 33.14% and 26.83% (data not shown) in WT and TLR4$^{-/-}$ mice, respectively. Independent T-test showed no significant difference in bone healing area between WT (0.9378+/-0.1131mm^2; 33.14% healing) and TLR4$^{-/-}$ (0.6814+/-0.209mm^2; 26.83% healing) mice on day 28 (p>0.05, Figure. 5).

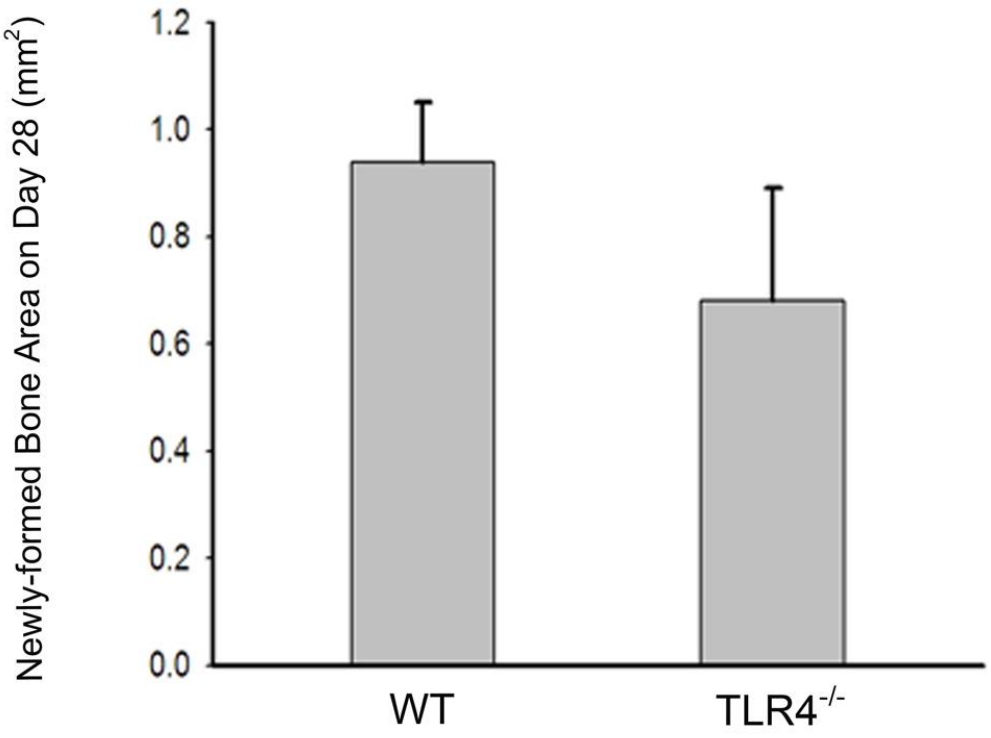

Figure 5: Graph showing similar amounts of radiographically opaque tissue observed on day 28 in both groups

Independent t-test showed no significant differences between the calvarial healing of WT and TLR4$^{-/-}$ mice at this time point. Out of 20 mice tested, none showed complete healing during the 28 days of observation. (mean +/-SEM; n=10 each).

2.3.3 Gene Expression

Baseline expression of 14 genes (IL-1α, IL-1β, Il-6, TNF-α, BMP2, BMP4, TGF-β1, TGF-β2, TGF-β3, VEGF, PDGF, RANK, RANKL, and OPG) were measured by quantitative RT-PCR using day 0 untreated samples. Expression of IL-1β and VEGF was significantly different between the two groups.IL-1β (24.52 +/-16.79 copy in WT; 5.30+/-1.46 copy in TLR4$^{-/-}$) and

RANKL (6.90e-3 +/-4.10e-3 copy in WT;1.80e-3+/-5.00e-4 copy in TLR4$^{-/-}$) expression were higher in WT mice, and VEGF (32.42+/-15.90 copy in WT; 92.39+/-1.64 copy in TLR4$^{-/-}$) expression was higher in TLR4$^{-/-}$ mice on day 0 (Figure. 6).

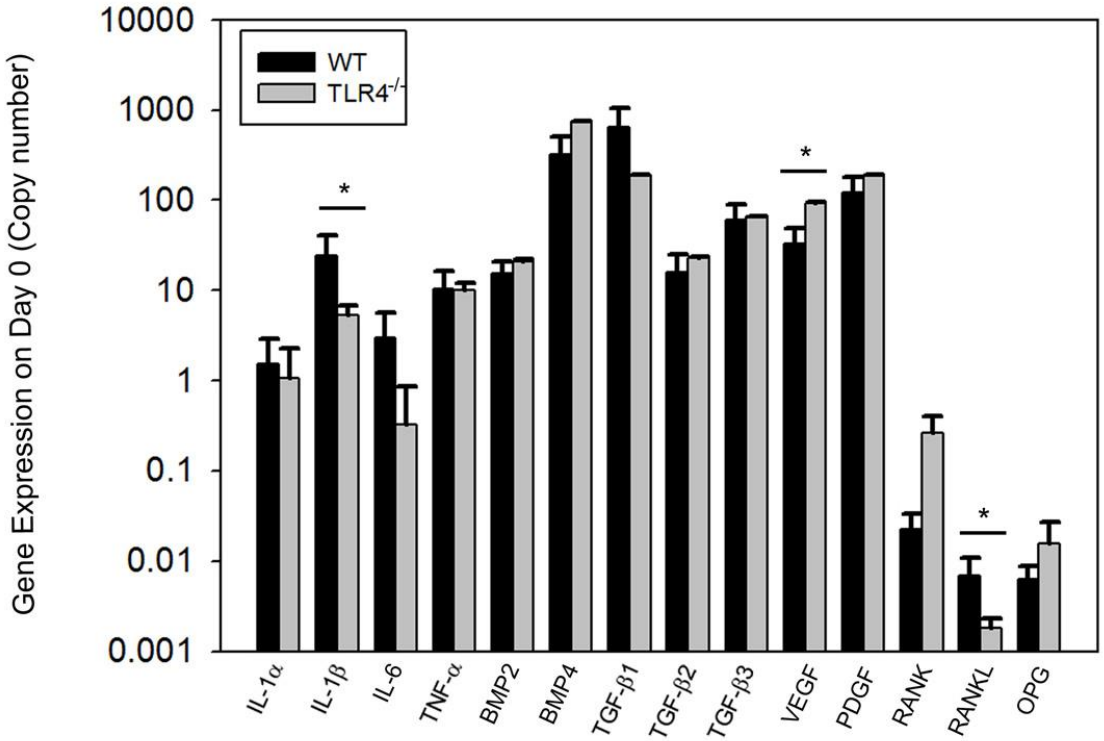

Figure 6: Graph showing quantitative gene expression on day 0 (untreated control) bone tissue

Siginificant differences were identified in the expression of IL-1β,VEGF and RANKL between the two groups. IL-1β and RANKL expression were higher in WT mice and VEGF expression was higher in TLR4$^{-/-}$ mice on day 0 (mean +/-SEM; n=5 to 7; *p<0.05).

Changes in gene expression at designated time points were determined by relative RT-PCR. The gene expression patterns for IL-1α, IL-1β and TNF-α expression were similar in both groups. Expression of these cytokines increased after surgery, remained stable for a few days and then was upregulated on day 14 and day 21 postoperatively. Significantly higher expression of

IL-1β was detected by two-way ANOVA analysis at both early (F=8.414, $p<0.05$) and late (F=26.17, $p<0.001$) time points in TLR4$^{-/-}$ than in WT mice. TNF-α expression was significantly higher at early time points in TLR4$^{-/-}$ mice compared to WT mice (F=6.451, $p<0.05$) (Figure. 7A, B, D). IL-6 exhibited a different expression pattern in TLR4$^{-/-}$ mice, and showed significantly higher fold change expression than in WT mice at early time points postoperatively (F=6.685, $p<0.05$) (Figure. 7C).

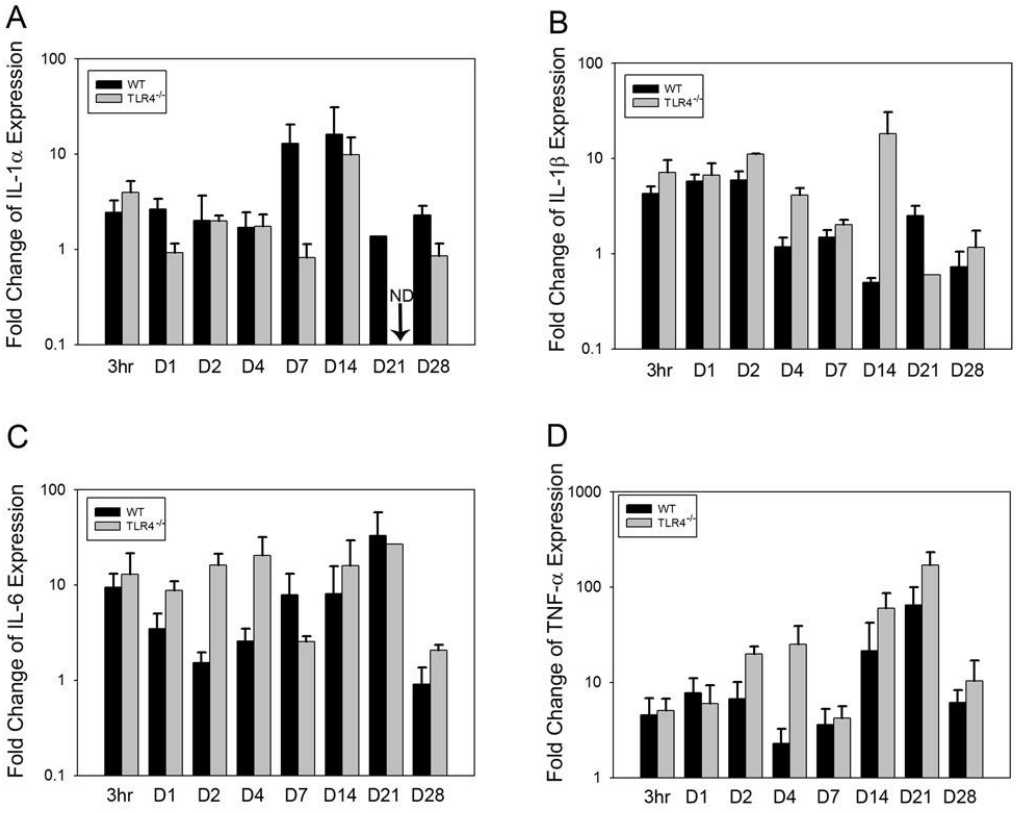

Figure 7: Graph showing relative fold change expression of inflammatory cytokines for WT and TLR4$^{-/-}$ mice

The fold change patterns in IL-1α, IL-1β, and TNF-α expression were similar in both groups. IL-6 had a different expression pattern in TLR4$^{-/-}$ mice compared to WT mice at early time points (mean fold change over day 0; ND, not detectable; mean +/-SEM; n=5 to 7).

BMP2 expression increased slightly after surgery in both groups, peaking at day 14 (3.28+/-1.02 fold in WT;1.59+/-0.81 fold in TLR4$^{-/-}$) and declining thereafter. No significant difference in BMP2 expression was observed between the two groups (Figure. 8A). BMP4 expression was similar in both groups, increasing slightly until day 21 (87.06+/-72.08 fold in WT; 128.27+/-80.39 fold in TLR4$^{-/-}$) and declining at day 28 (18.24+/-13.53 fold in WT; 2.56+/-1.77 fold in TLR4$^{-/-}$). No significant difference in BMP4 expression was observed between the two groups (Figure. 8B).

Significant differences of TGF-β1 were observed in TLR4$^{-/-}$ mice compared to WT mice at early time points ($F=22.636$, $p<0.001$) (Figure. 8C). No significant differences were detected in the expression of TGF-β2 between groups (Figure. 8D). A similar pattern in TGF-β3 expression was observed in both groups. Expression remained stable between 3h and day 7, and achieved a peak in expression at day 14 (12.69+/-3.55 fold in WT; 26.42+/-10.58 fold in TLR4$^{-/-}$). While the pattern of TGF-β3 expression was similar between the two groups, significantlly higher expression of TGF-β3 was observed in TLR4$^{-/-}$ mice than in WT mice ($F=15.283$, $p<0.001$)(Figure. 8E). The fold change expression patterns of VEGF and PDGF in WT and TLR4$^{-/-}$ mice were similar. Expression of VEGF in WT and TLR4$^{-/-}$ remained relatively constant until it was upregulated at day 14 (7.90+/-5.25 fold in WT;1.17+/-0.02 fold in TLR4$^{-/-}$), and began to decrease thereafter. Significantly lower expression of VEGF was detected in TLR4$^{-/-}$ mice than in WT mice ($F=31.258$, $p<0.001$). PDGF expression was stable in both WT and TLR4$^{-/-}$ mice at all time points. Significantly higher expression of PDGF was observed in TLR4$^{-/-}$ mice compared to WT mice at early time points ($F=4.157$, $p<0.05$) (Figure. 8F, G).

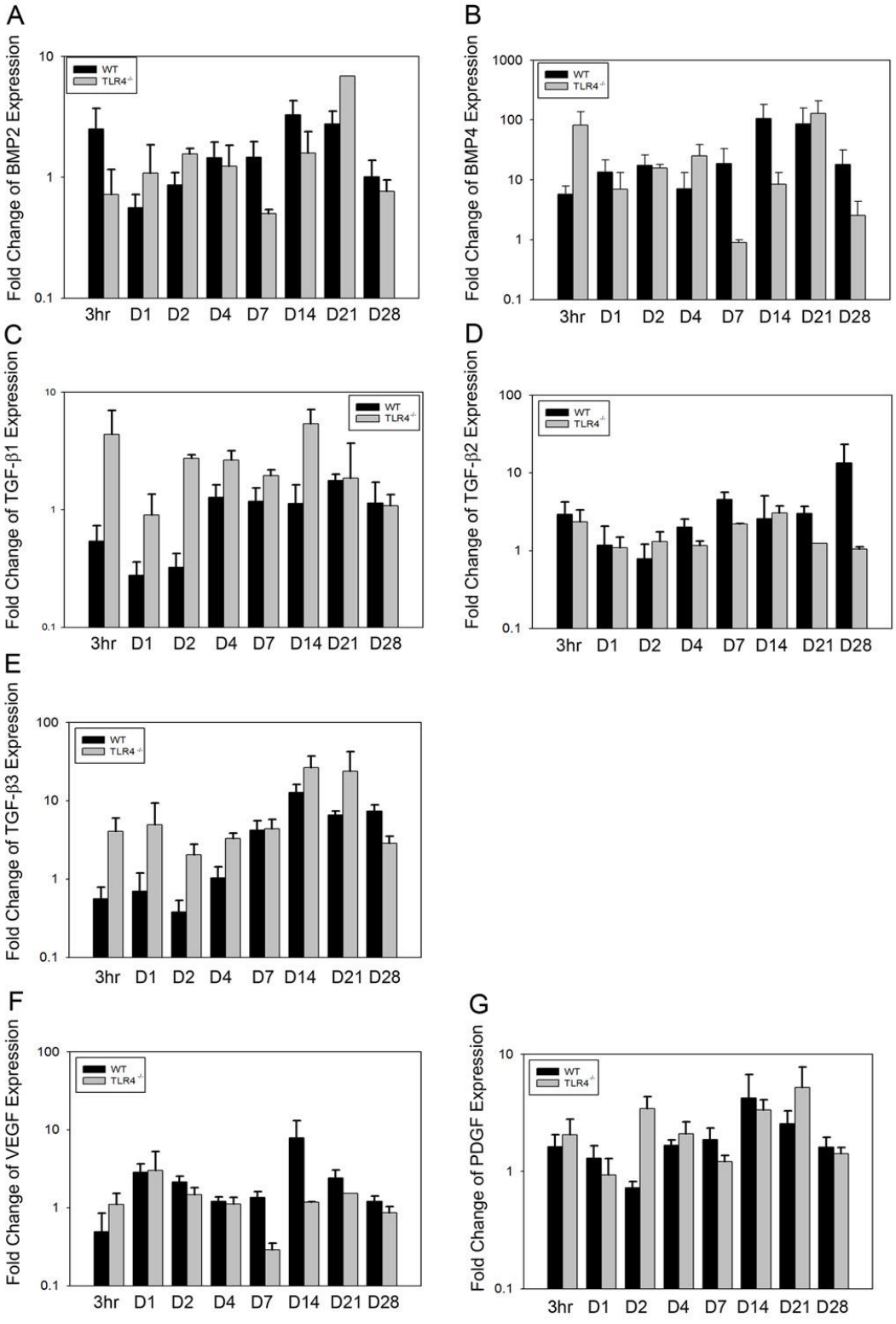
A
Fold Change of BMP2 Expression
10
1
0.1
WT
TLR4-/-
3hr D1 D2 D4 D7 D14 D21 D28
B
Fold Change of BMP4 Expression
1000
100
10
1
0.1
WT
TLR4-/-
3hr D1 D2 D4 D7 D14 D21 D28
C
Fold Change of TGF-β1 Expression
10
1
0.1
WT
TLR4-/-
3hr D1 D2 D4 D7 D14 D21 D28
D
Fold Change of TGF-β2 Expression
100
10
1
0.1
WT
TLR4-/-
3hr D1 D2 D4 D7 D14 D21 D28
E
Fold Change of TGF-β3 Expression
100
10
1
0.1
WT
TLR4-/-
3hr D1 D2 D4 D7 D14 D21 D28
F
Fold Change of VEGF Expression
100
10
1
0.1
WT
TLR4-/-
3hr D1 D2 D4 D7 D14 D21 D28
G
Fold Change of PDGF Expression
10
1
0.1
WT
TLR4-/-
3hr D1 D2 D4 D7 D14 D21 D28

Figure 8: Graph showing relative fold change expression of growth factors for WT and TLR4$^{-/-}$ mice

Similar expression patterns of BMP2, BMP4, TGF-β2, VEGF, and PDGF were observed between the two groups. Higher expression levels of TGF-β1 and TGF-β3 were detected in TLR4$^{-/-}$ mice than in WT mice at early time points (mean +/-SEM; mean fold change over day 0; ND, not detectable; n=5 to 7).

High expression level of RANK was detected on day 14 in WT mice (16.50+/-15.94 fold), while expression level in TLR4$^{-/-}$ was similar at all time points. Fold change expression of RANK in TLR4$^{-/-}$ was significantly lower than in WT mice at both early ($F=4.453$, $p<0.05$) and late time points ($F=6.522$, $p<0.05$) (Figure. 9A). Expression patterns of RANKL and OPG were relatively stable in WT mice. In TLR4$^{-/-}$ mice, both RANKL and OPG were slightly increased at early time points (≤4 days) and decreased at day 7. Expression level of RANKL was significantly higher in TLR4$^{-/-}$ mice at early time points ($F=4.199$, $p<0.05$) and significantly lower at late time points compared to WT mice ($F=56.217$, $p<0.001$). Fold change expression of OPG in TLR4$^{-/-}$ was significantly lower than in WT mice at late time points ($F=83.961$, $p<0.001$). (Figure. 9B, 9C).

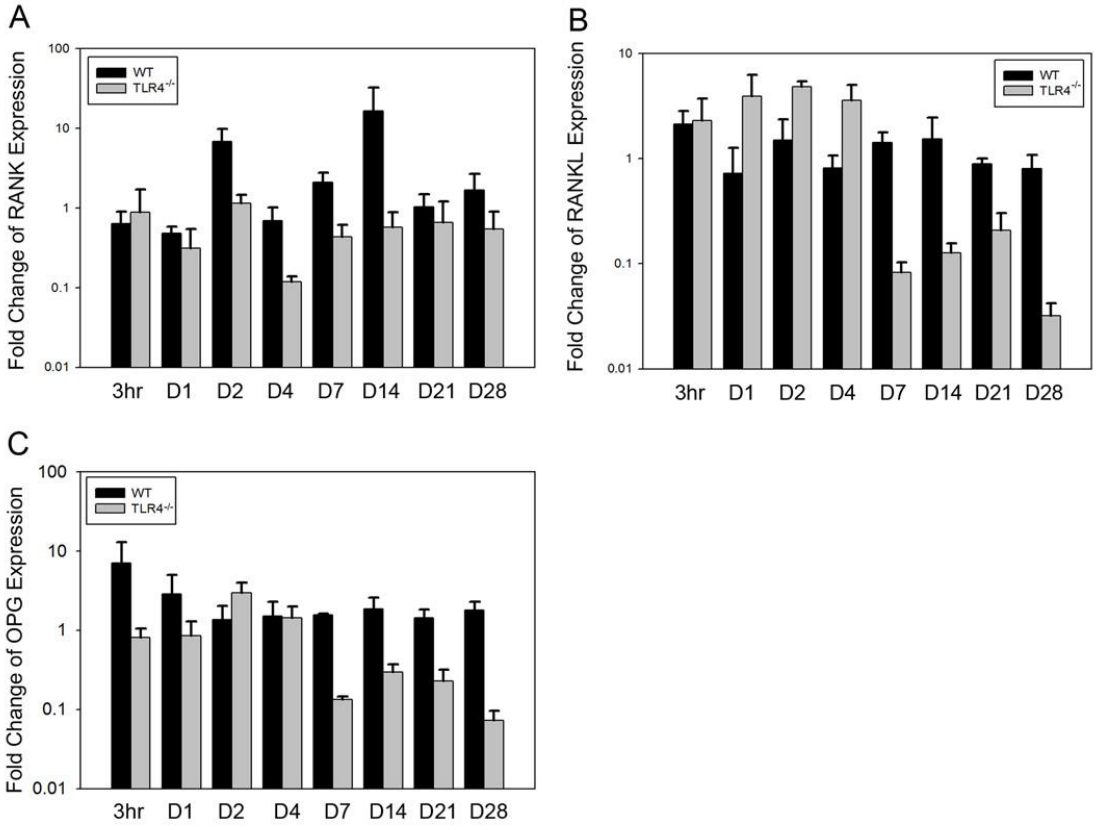

Figure 9: Graph showing relative fold change expression of RANK, RANKL and OPG for WT and TLR4$^{-/-}$ mice

Expression levels of RANK, RANKL and OPG were realtively constant in WT at all time points. Greater variation of the three genes was detected in TLR4$^{-/-}$ (mean +/-SEM; n=5 to 7).

2.4 DISCUSSION

Inflammation has a complex role in fracture repair, although the underlying mechanisms remain unclear [105-107]. TLR4 is a member of a highly conserved receptor family and is a critical activator of the innate immune response after tissue injury. TLR4 signaling has been shown to regulate

both the immune response and bone metabolism during long-bone fracture healing. Here, we tested the hypothesis that TLR4 activation limits the healing of calvarial defects.

In this study, a smaller than "critical-size" calvarial defect model was used, which by definition, would be expected to heal spontaneously over the duration of the observation. However, none of our 1.8mm diameter defects healed complete during 28 days of observation. The maximum healing was approximately 30% of the original defect area, which is consistent with previous observations by Gosain et al., who observed 27-35% healing of critical-size defects at 4 weeks [108]. Importantly, we found that no significant healing occurred after 21 days in this model. Pentachrome staining of day 28 defects supports this observation. The newly-formed woven bone adjacent to the defect perimeter stained with acid fuchsin red, suggesting that bone remodeling had already taken place by day 28. OPN reactivity suggests that bone formation, which was highly active around day 21 in WT mice and day 14 in $TLR4^{-/-}$ mice, became less active and less OPN-positive staining was observed. Thus, there may exist a temporal window for mature calvarial healing even in defects smaller than "critical-size". The molecular signaling involved in the cessation of bone formation within such bone defects need to be further characterized.

Although no significant difference in total calvarial healing was observed between groups radiographically or histologically on post-operative day 28, accelerated healing was observed in $TLR4^{-/-}$ mice. By day 4, a thicker dural cell layer and more dense OPN positive stains were evident in $TLR4^{-/-}$ mice. By day 7, a quantity of newly-formed woven bone was seen on the endocortical calvarial surface in $TLR4^{-/-}$ mice. Quantitative histomorphometry data was consistent with the histological findings mentioned above. Two-way ANOVA comparing mean newly-formed bone areas showed a significant group by time point interaction, suggesting that

the WT and TLR4$^{-/-}$ mice healed differently over time. It showed significantly larger area of new bone in TLR4$^{-/-}$ mice on day 7 and day 14. Similarly, improved bone healing has been reported for long bone fracture healing in mice lacking an adaptive immune system. Specifically, in RAG1$^{-/-}$ mice (recombination activating gene 1 knockout), increased bone formation and biomechanical strength at early time points was associated with reduced pro-inflammatory cytokine expression and increased expression of the anti-inflammatory cytokine, IL-10 [98]. Those observations suggest that the suppression of the adaptive immune system might maximize the regenerative and minimize the destructive effects of inflammation which may promote fracture repair [98]. In our model, bone healing was obviously accelerated in TLR4$^{-/-}$ mice, although the total bone healing achieved was comparable between two groups. Whether accelerated calvarial healing effect is due to the suppression of TLR4-mediated inflammatory response requires further exploration.

Gene expression analysis showed that expression of inflammatory cytokines, generally, was elevated 3 hour post-operatively, and a second spike in inflammatory gene expression was detected around day 14 in both groups. Greater variation was detected in the expression of growth factors after surgery. These findings are consistent with the gene expression patterns described in long bone fracture models [74,109]. Of greater interest, we found that IL-1β, IL6 and TNF-α,TGF-β1, TGF-β3 and PDGF were more highly expressed at earlier time points in TLR4$^{-/-}$ mice. We speculated that accelerated bone healing observed in TLR4$^{-/-}$ mice might, at least in part, be due to earlier and higher expression of these genes [110-112].

The inflammatory cytokines IL-1β, IL-6 and TNF-α have complex effects on bone regeneration. IL-1β can stimulate osteoblasts and bone matrix formation, but also suppress the differentiation of mMSCs [113]. In vivo studies in IL1α, IL1β, and IL1α/β mutant mice have

shown impaired osteoclast development to result in increased bone density and femoral bone mass within these animal models [114]. IL-6 has been shown to both promote and inhibit osteoclastogenesis [115,116]. An in vivo study determined that the absense of IL-6 promoted inflammatory calvarial bone loss in a mouse model[117]. Although IL-$6^{-/-}$ mice showed reduced osteoclastogenesis and impaired callus strength at the early time points after surgery, similar long bone healing outcomes were observed in comparison with WT mice after 3 weeks [118]. Therefore, the role of IL-6 in osteoclastogenesis has been more elucidated [117,118]. Further studies are needed to understand the impact of TLR4-mediated inflammatory and related inflammatory cytokines expression on calvarial bone repair.

RANK, OPG and RANKL are important mediators of remodeling during bone formation and bone regeneration. TLR signaling inhibits RANKL-mediated osteoclastogenesis, although TLR activation can also promote osteoclastogenesis by inducing RANK and TNF-α expression in osteoblasts[100]. In the present study, significant differences were apparent in the expression of RANK, OPG and RANKL between $TLR4^{-/-}$ and WT mice. Expression of RANKL was significantly higher in $TLR4^{-/-}$ mice compared to WT mice at early time points. RANK, RANKL and OPG all showed significantly lower expression in $TLR4^{-/-}$ mice than in WT mice at late time points. During long bone regeneration, upregulated RANKL at primary long bone formation stage is associated with mineralized cartilage resorption and bone formation, and downregulated expression indicated bone remodeling. Early high expression levels in $TLR4^{-/-}$ mice suggest early and high resorption activity of osteoclasts. The differential expression of these three genes might explain the observed accelerated bone formation and early bone remodeling in $TLR4^{-/-}$ mice. It remains unclear whether differenes in RANK, RANKL and OPG expression are directly linked to the absence of TLR4 signaling.

Conclusion: The present study revealed accelerated bone formation and bone remodeling in absence of TLR4 signaling pathway. This phenotype is also associated with changes of local inflammatory cytokines and osteoclastogenic factors expression. Further work is required to determine whether regenerative effects of inflammation mediated by absence of TLR4 may lead to accelerated skull bone repair.

3.0 DENDRITIC CELL-EXPRESSING TLR4-MEDIATED MYD88 SIGNALING IS DETRIMENTAL TO CALVARIAL BONE HEALING

3.1 INTRODUCTION

Craniofacial skeletal injuries have made a tremendous economical, biological and social impact, with over 2 million head injuries and an estimated 592,000 surgeries annually in the United States[1,7]. Clinical management of craniofacial trauma remains highly challenging, thus, various efforts have been undertaken to develop and improve existing therapies for craniofacial reconstruction. Among these efforts, harnessing and modulating inflammation to facilitate bone regeneration has become a promising strategy [119]. The inflammatory response is characterized by local activation of the innate immune system and is increasingly recognized for its essential role not only in host defense against infection but also in tissue regeneration and repair [75,76]. The inflammatory response following wound injury is critical for the initiation of healing cascades, serving to recruit inflammatory and progenitor cells as well as to promote angiogenesis [90]. Mounting evidence indicates that the wound-induced inflammatory response is among the earliest events to determine the quality [120] of the healing response in models of ischemia-reperfusion injury, traumatic tissue injury, and musculoskeletal injury [90,121,122]. As a result, efforts have been made to improve therapeutic strategies for skull repair, particularly under conditions in which healing is impaired or inefficient, either by enhancing the regenerative

effects or by inhibiting the destructive effects of inflammation. Therefore, understanding the molecular mechanisms behind inflammation and skeletal regeneration should provide an avenue for intervention after skeletal trauma, allowing the inflammatory response to be modulated with precision to augment bone healing [90].

Toll-like receptors (TLRs) are important mediators of the immune response that recognize a wide range of pathogen-associated molecular patterns (PAMPs) and damage-associated molecular patterns (DAMPs) in response to infection, injury, stress, and cellular necrosis [123]. In addition to their roles in host defense against microbial infection, TLRs are also involved in tissue fibrosis, tissue homeostasis, and wound healing in the neuronal, digestive, cardiovascular, and musculoskeletal systems, through multiple mechanisms including limiting the extent of initial tissue injury or stimulating the repair cascade [123]. Myeloid differentiation primary response gene 88 (MyD88) and TIR-domain-containing adapter-inducing interferon-β (TRIF) are the two main adaptor proteins of TLR signaling that mediate downstream pathways including NF-κB, IFN regulatory factor-1, and MAP kinases [123]. While most TLRs often utilize only the MyD88 pathway, TLR4 is unique in that it also utilizes the TRIF pathway [124].

Distinction has been made in the contribution of MyD88- and TRIF-mediated signaling pathways to TLR4-driven responses to injury. TLR4 signaling through different pathways can have either damaging or protective effects depending on tissue, mode of injury, or mode of activation. For example, studies have demonstrated that MyD88 signaling contributes to ischemic brain damage[125-127], and hind limb ischemia[128], whereas TRIF-mediated signaling exerts a neuroprotective effect against cerebral ischemia[129]. Conversely, in models of cardiac and pulmonary injury, radiation-induced lung injury[130], and intestinal ischemia[131], MyD88-dependent signaling has protective effects. In short, the functional consequences of TLR activation on tissue

homeostasis and regeneration are strongly dependent upon organ setting, mode of activation, and mode of injury. As such, understanding the mechanistic aspects of TLR signal transduction during bone healing will be crucial for appreciating their contributions to tissue regeneration at the cellular level.

Studies have shown an essential involvement of TLRs in skeletal homeostasis, however specific cellular contribution is unknown. Multiple cell types are involved in injury-stimulated bone regeneration [105], such as inflammatory cells (platelets, macrophages, lymphocytes, and granulocytes) which migrate into the fracture hematoma and regulate inflammation as well as tissue regeneration [132]. For example, dendritic cells regulate the highly pathogen-specific adaptive immune responses and are critical in the development of immunologic memory and tolerance [133]. Macrophages infiltrate into the wound bed within 48-96 hours after injury, participating in the inflammatory response and debridement process via phagocytosis activity and reactive radical release. As TLR expression was primarily found in immune cells, such as macrophage and dendritic cells [134-136], understanding how lineage-specific TLR activation in regulating inflammation and skeletal homeostasis upon injuries may provide insight into the mechanisms of inflammation in bone regeneration and repair under various clinical settings.

Studies have showed an essential role of TLR activation in inflammatory-induced bone destruction, however their direct influence on calvarial bone healing has not yet been thoroughly investigated. In a previous study (chapter 2), we showed accelerated bone healing with higher expression of osteoclastogenesis gene, RANKL, in TLR4 KO ($TLR4^{-/-}$) mice compared to wild-type (WT) mice within a calvarial defect model [78]. Given that TLRs are implicated in inflammation-asssociated bone regeneration and disease [137-139], we employed KO mouse models for TLR2 and TLR4 and their intracellular mediators (MyD88 and TRIF). In addition, since

enhanced osteoclastogenesis was implicated in TLR4$^{-/-}$ mice in our previous findings [78] and osteoclasts are generated from myeloid and dendritic cells, we used cell-specific KO mouse models in which TLR4 expression was deleted in myeloid cells (Lyz-TLR4$^{-/-}$) and dendritic cells (CD11c-TLR4$^{-/-}$) separately as a means to study the cellular influences on calvarial bone healing. We hypothesized that a similar faster healing response would be observed in these KO mice models. The data presented here demonstrate an accelerated healing response in TLR4-deficient mice (TLR4$^{-/-}$, Lyz-TLR4$^{-/-}$ and CD11c-TLR4$^{-/-}$) at post-operative day 7 and enhanced bone healing in MyD88$^{-/-}$ and CD11c-TLR4$^{-/-}$ mice at day 28. This suggests a detrimental role of dendritic cell-expressing TLR4-mediated MyD88 signaling in calvarial bone healing.

3.2 MATERIALS AND METHODS

3.2.1 Mouse Strains and Derivation

WT mice were obtained from the Jackson® Laboratory (Bar Harbor, Maine). TLR4$^{-/-}$, TLR2 KO (TLR2$^{-/-}$), myeloid lineage-specific TLR4 KO (Lyz-TLR4$^{-/-}$), dendritic-specific TLR4 KO (CD11c-TLR4$^{-/-}$), MyD88$^{-/-}$, and TRIF$^{-/-}$ mice mentioned in this study were generated from an ongoing breeding colony at the University of Pittsburgh as described [134,140]. Female mice from all strains, between 10 and 12 weeks of age and 20-30 g weight were used in this study. All mice were maintained in the Rangos Research Center Animal Facility at Children's Hospital of Pittsburgh of UPMC with a 12:12 hour light-dark cycle and free access to standard laboratory food and water. All procedures were carried out in accordance with regulations regarding the

care and use of experimental animals published by the National Institutes of Health and was approved by the University of Pittsburgh Institutional Animal Use and Care Committee.

3.2.2 Surgical Procedure

Mice were anesthetized with isoflurane (2% by inhalation) and their scalps were shaved and cleaned with Betadine. Under sterile conditions, a 1.8 mm circular bone defect was created in the skull parietal bone using a 1.8 mm outer diameter trephine as previously described [78]. 1 mg/kg ketoprofen (Fort Dodge Animal Health, Fort Dodge, IA) was administered as an analgesic immediately and two days after surgery. Mice were euthanized via CO_2 asphyxiation followed by cervical dislocation at post-operative day 7 and day 28.

3.2.3 Live Micro-computed Tomographic (μCT) Analyses

Calvarial defect healing was analyzed using a live high-resolution μCT system (Inveon microCT, Siemens, Germany). At postoperative days 7, 14, and 28, bone healing of WT, TLR4$^{-/-}$, TLR2$^{-/-}$, Lyz-TLR4$^{-/-}$, CD11c-TLR4$^{-/-}$, MyD88$^{-/-}$, and TRIF$^{-/-}$ mice (average 10 mice per group) were analyzed using live-μCT with a fixed isotropic voxel size of 62.4 μm. 3D images were reconstructed using Amira 5.4 3D software (FEI Visualization Sciences Group, Burlington, MA). Quantitative data were analyzed with OsiriX software with a global fixed threshold -330 and a region of interest (ROI) of 0.4mm^2×20.9 mm was defined. Standard μCT measurements (regenerated bone volume (BV) = BV within ROI at day 7, 14 and 28 – BV at day 0) were calculated for each sample using OsiriX software.

3.2.4 Histology and Histomorphometric Analysis

All mice were euthanized on post-operative day 28. WT, TLR4$^{-/-}$, Lyz-TLR4$^{-/-}$, and CD11c-TLR4$^{-/-}$ mice were also euthanized at post-operative day 7. Calvariae and surrounding soft tissues (e.g., skin, brain) were harvested, and fixed in 4% neutral buffered paraformaldehyde for 24 hours, and decalcified in 10% EDTA prior to dehydration through a series of alcohols and embedment in paraffin. Paraffin-embedded specimens were sectioned through the coronal plane at a thickness of 5-6 μm. Slides were stained with Harris' hematoxylin & eosin (H&E) (Surgipath Medical Industries, Richmond, IL) for conventional, qualitative bright-field light microscopy. All specimens were examined at 25 X, 100 X, 200 X, and 400 X magnifications.

Russell-Movat pentachrome staining (American MasterTech, CA) was performed to further differentiate the following tissues within the defect: hematoma/fibrin (intense red), elastic fibers (black), and granulation/fibrous tissue (green or light blue), newly-formed woven bone (yellow) and lamellar bone (red) formation and degradation. All specimens were examined at 25 X, 50 X, 100 X and 200 X magnifications.

Histomorphometric analysis was performed to quantify the two-dimensional area of new bone formation using a Leica MZ12 Stereo Zoom microscope and Northern Eclipse (v5.0) image analysis software (Empix Imagine, Inc., Mississauga, Ontario, Canada). Healing data were calculated based on three to five slides per animal. New bone area was calculated as the sum of the areas of each bone section, including within the defect and on both the endocortical and endocotical sides of calvarial bone.

3.2.5 Statistical Analyses

Statistical analyses were performed using SPSS v.20.0 software (SPSS, Inc, Chicago, IL). Newly-regenerated bone volumes collected from μCT analysis were compared using a group by time point (7 x 3) two-way ANOVA followed by group by time point (7 x 1) split plot one-way ANOVA and *Post-hoc* LSD tests to compare each group over time. Mean areas of newly-formed bone calculated from histomorphometric measurements were analyzed using one-way ANOVA and *post-hoc* LSD tests for multiple comparisons at each time point.

3.3 RESULTS

3.3.1 Enhanced Calvarial Bone Healing in CD11c-TLR4$^{-/-}$ and MyD88$^{-/-}$ mice at Day 28

While no group showed complete bone healing of the 1.8 mm diameter defect within 28 days, mineralized tissue was observed around the defect margins of TLR4$^{-/-}$, Lyz-TLR4$^{-/-}$, and CD11c-TLR4$^{-/-}$ mice at day 7, suggesting a faster healing response (Fig.10A). Improved overall healing of calvarial defects was observed in CD11c-TLR4$^{-/-}$ mice and MyD88$^{-/-}$ mice compared to WT control mice at day 28 (Fig.10A). Detailed regenerated BV data from μCT measurements of all groups at different time points is shown in Fig.10B. The greatest difference in bone healing was observed at day 7 (Fig.11C). Differences in healing were less pronounced at day 28 (Fig.11E). Two-way ANOVA of BV analyses showed that significant differences were detected within time interactions (day 7, day 14, and day 28, $p<0.001$), and within group interactions (all seven experimental groups, $p<0.001$), while no significant difference was detected within group by

time interactions. At post-operative day 7, one-way ANOVA analyses showed that BV measurements were significantly larger in the TLR4$^{-/-}$ (0.141±0.019 mm^3, p<0.05), Lyz-TLR4$^{-/-}$ (0.179±0.029 mm^3, p<0.001) and CD11c-TLR4$^{-/-}$ (0.183±0.021 mm^3, p<0.001) groups than the WT group. At day 14, BV measurements were significantly larger in TLR4$^{-/-}$ (0.223±0.035 mm^3, p<0.05), Lyz-TLR4$^{-/-}$ (0.231±0.032 mm^3, p<0.05), CD11c-TLR4$^{-/-}$ (0.254±0.021 mm^3, p<0.05) and MyD88$^{-/-}$ groups (0.227±0.062, p<0.05) compared to WT group. At post-operative day 28, BV measurements were significantly larger in CD11c-TLR4$^{-/-}$ (0.43±0.025, p<0.05) and MyD88$^{-/-}$ groups (0.369±0.046, p<0.05) compared to the WT group (0.232±0.036 mm^3) (Fig.11C-11E).

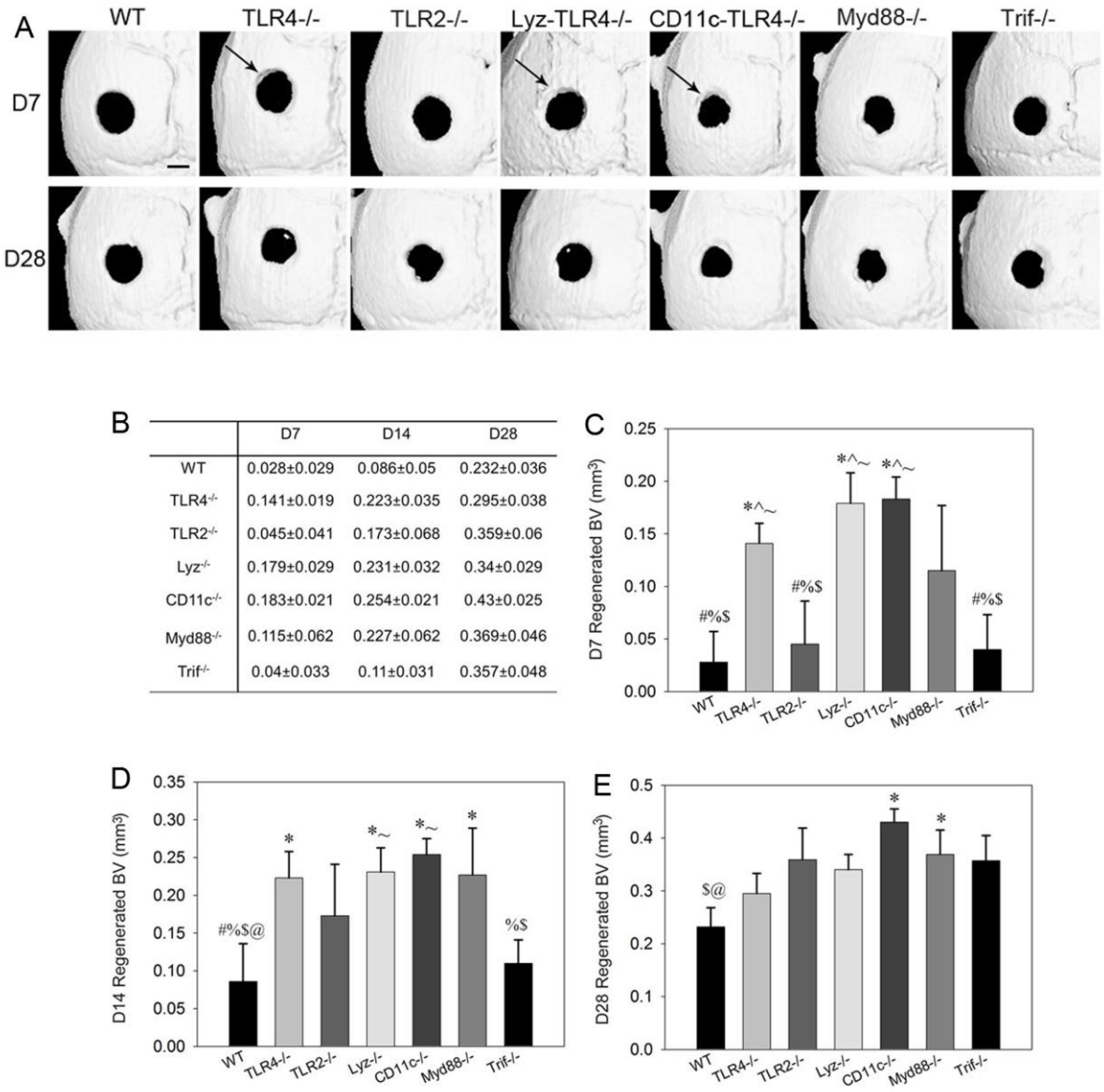

	D7	D14	D28
WT	0.028±0.029	0.086±0.05	0.232±0.036
TLR4$^{-/-}$	0.141±0.019	0.223±0.035	0.295±0.038
TLR2$^{-/-}$	0.045±0.041	0.173±0.068	0.359±0.06
Lyz$^{-/-}$	0.179±0.029	0.231±0.032	0.34±0.029
CD11c$^{-/-}$	0.183±0.021	0.254±0.021	0.43±0.025
Myd88$^{-/-}$	0.115±0.062	0.227±0.062	0.369±0.046
Trif$^{-/-}$	0.04±0.033	0.11±0.031	0.357±0.048

Figure 10: Live μCT analyses of all mouse groups

(A) Representative 3D reconstructions of calvarial defects in the transverse plane at postoperative days 7 and 28. Faster healing was evident in TLR4$^{-/-}$, Lyz-TLR4$^{-/-}$, and CD11c-TLR4$^{-/-}$ mice as indicated by mineralized tissue around the defect edges on day 7. Smaller defect areas are shown in CD11c-TLR4$^{-/-}$ and MyD88$^{-/-}$ mice compared to WT mice on day 28. (B) Table shows the regenerated BV measurements based on μCT analyses. (C-E) Two-way ANOVA analyses of regenerated BV-based μCT measurements showed no significant differences within groups (all mouse groups) by time interactions (day 7, day 14, and day 28). One-way ANOVA analyses showed that BVs were significantly larger in TLR4$^{-/-}$, Lyz-TLR4$^{-/-}$, and CD11c-TLR4$^{-/-}$ groups than the WT group at day 7; TLR4$^{-/-}$, Lyz-

TLR4$^{-/-}$, CD11c-TLR4$^{-/-}$, and MyD88$^{-/-}$ groups than the WT group at day 14; and CD11c-TLR4$^{-/-}$ and MyD88$^{-/-}$ groups compared to WT group on day 28. More detailed comparisons among groups at different time points are shown in Fig.2. (Scale: 500 μm; BV: bone volume within region of interest (ROI); mean ± SEM; p<0.05 * compared to WT; # compared to TLR4$^{-/-}$; ^ compared to TLR2$^{-/-}$; % compared to Lyz-TLR4$^{-/-}$; $ compared to CD11c-TLR4$^{-/-}$; ~ compared to TRIF$^{-/-}$; @ compared to MyD88$^{-/-}$)

3.3.2 Faster Intramembranous Bone Formation in TLR4$^{-/-}$, Lyz-TLR4$^{-/-}$ and CD11c-TLR4$^{-/-}$ Mice

Disorganized connective tissue completely filled the bone defect on day 7. Cellularized newly-regenerated woven bone, indicated by positive saffron yellow staining, was observed mainly on the endocortical side of the calvarial bone lateral to the defect perimeter in all groups (Fig.11A). Typical large, rounded osteoblasts were recognized on the surface of the newly-formed woven bone of the three KO mice groups (Fig.11A). Pentachrome staining showed larger areas of newly-formed bone in TLR4$^{-/-}$, Lyz-TLR4$^{-/-}$, and CD11c-TLR4$^{-/-}$ mice compared to WT mice on day 7 (Fig.11A). One-way ANOVA analyses showed significantly larger areas of newly-regenerated bone area in TLR4$^{-/-}$, Lyz-TLR4$^{-/-}$, and CD11c-TLR4$^{-/-}$ mice compared to WT mice on day 7 (p<0.05, Fig.11B). No significant differneces in newly-regenerated bone areas were observed among TLR4$^{-/-}$, Lyz-TLR4$^{-/-}$ and CD11c-TLR4$^{-/-}$ groups.

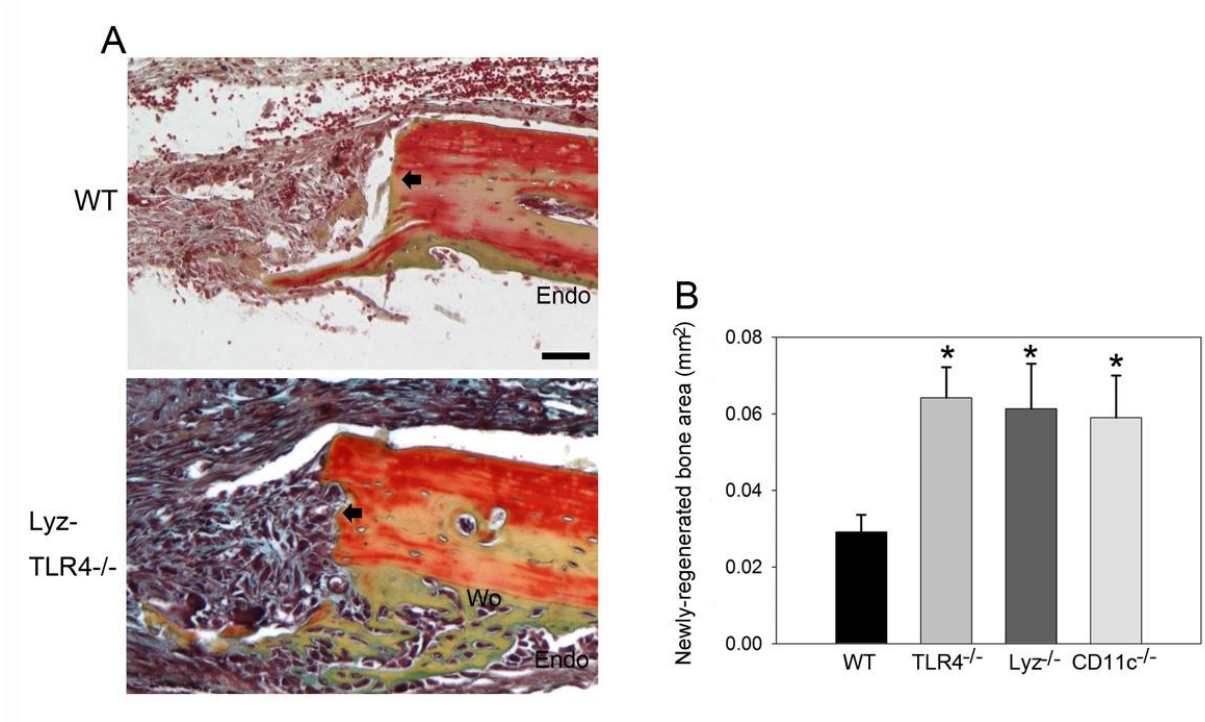

Figure 11: Histology and histomorphometric analyses of calvarial bone repair at post-operative day 7

(A) Representative pentachrome-stained images of WT and Lyz-TLR4$^{-/-}$ mice on day 7. We used pentachrome-stained images of Lyz-TLR4$^{-/-}$ mice to represent TLR4$^{-/-}$ and CD11c-TLR4$^{-/-}$ groups (H&E stained images not shown). Larger areas of woven bone, indicated by saffron yellow staining, and more infiltration osteoblasts were observed in TLR4$^{-/-}$, Lyz-TLR4$^{-/-}$ and CD11c-TLR4$^{-/-}$ mice compared to WT mice. (B) Histomorphometric analysis revealed larger areas of newly-regenerated bone in the three KO mice groups compared to the WT group. Comparable healing was observed in the three KO groups on day 7. (Scale bar: 50 μm; bolded arrow indicated defect margin; Endo: endocortical side; Wo: woven bone; mean ± SEM; * p<0.05 compared to WT).

All groups showed similar histological healing patterns and complete bone healing was not observed on post-operative day 28 (Fig.12, H&E stained images not shown). Periosteum and soft connective tissue became much thinner, more dense, and better organized on day 28. Regenerated bone was seen along the dural surface of the calvarial bone and along the defect perimeter. Typical rounded osteoblasts were less-recognized on the newly-formed bone surface compared to day 7. All groups showed bone remodeling as indicated with acid fuchsin red-

positive staining (Fig.12A). One-way ANOVA analyses showed no significance of newly-regenerated bone areas in all groups (Fig.12B).

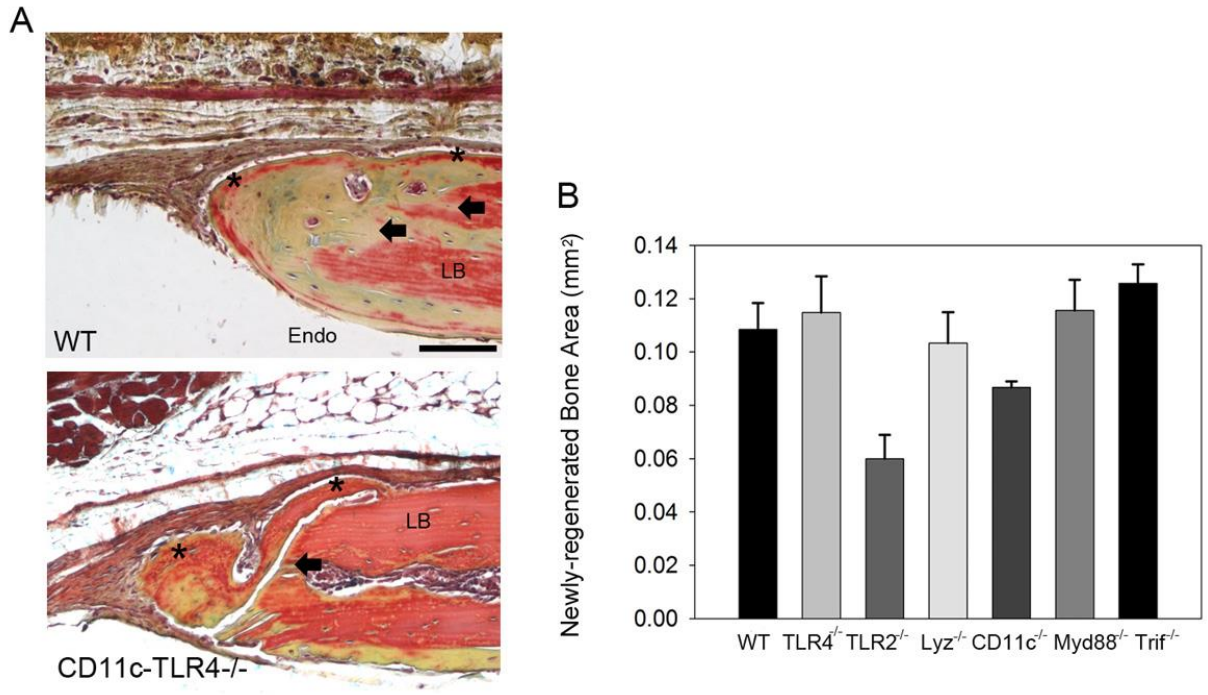

Figure 12: Histology and histomorphometric analyses of calvarial bone repair at post-operative day 28

(A) Representative pentachrome-stained images. Similar healing was observed among all KO groups at day 28; thus, CD11c-TLR4$^{-/-}$ mice were used to represent the rest of the KO mice. Periosteum and soft connective tissue became much thinner, denser, and better organized. Regenerated bone was seen along the dural surfaces of the calvarial bone and along the defect perimeter. Lamellar bone (*), which stains positive for acid fuchsin (red), was observed in both groups on day 28, suggesting maturation and remodeling of the newly formed bone matrix. (B) Histomorphometric analysis revealed comparable newly-regenerated bone area among all groups on day 28. (scale bar: 50 μm; bolded black arrows: defect margin; Endo: endocortical side; LB: lamellar bone).

3.4 DISCUSSION

TLRs are critical activators of the innate immune response and are attractive therapeutic targets for inflammation-modulated tissue regeneration [75,76]. The role of inflammation on long bone healing has been extensively investigated; however, its impact within craniofacial settings is not well understood. Here, we examined the calvarial bone healing in mice lacking important mediators of TLR signaling pathways, aiming to understand the role of TLR signaling on calvarial defect healing. Remarkably, we found that dendritic cell-expressing TLR4 might be detrimental to bone healing through MyD88 pathway, suggesting a regulatory role of these TLR pathway mediators in calvarial fracture repair.

Studies have suggested important roles of TLR4/MyD88 and TLR2/MyD88 signaling pathways in regulating inflammation and bone metabolism in various osteolytic diseases [141-144], however their involvement in non-compromised fracture healing process has not been investigated. In this study, we observed the calvarial bone healing process in $TLR2^{-/-}$, $TLR4^{-/-}$, $MyD88^{-/-}$, and $TRIF^{-/-}$ mice. The fact that we did not observe differences of bone healing in $TLR2^{-/-}$ and $TLR4^{-/-}$ mice compared to WT mice at day 28, may be attributed to the ability of TLRs to reciprocally compensate for each other's loss of gene function[145,146]. For example, in a mouse cecal ligation puncture-sepsis model, TLR4 was overexpressed in $TLR2^{-/-}$ mice compared to that in WT mice. Although $TLR2^{-/-}$ and $TLR4^{-/-}$ mice presented lower renal inflammatory cytokine expression, only $MyD88^{-/-}$ mice were fully protected from damage caused by sepsis[145]. MyD88 is an important adaptor protein for the majority of TLR signaling. Therefore, loss of MyD88 function has a large impact on the downstream TLR signaling pathways including the immune response against pathogens and tissue regeneration after injury [147,148]. The functional consequence of MyD88 signal loss may vary substantially depending on the organ setting and

mode of injury. For example, MyD88-deficient mice present with detrimental phenotypes including delayed wound healing phenotype, impaired epithelial regeneration, and decreased radiation survival in multiple mouse models of injury, but present advantageous phenotypes including decreased fibrosis and protection against cardiac hypertrophy after myocardial infraction [149-153]. In our study, we showed that MyD88 has a detrimental role in bone regeneration because enhanced bone healing was observed in MyD88$^{-/-}$ mice and not TRIF$^{-/-}$ mice compared to WT mice on day 28; thus, the accelerated bone healing phenotype observed within this model might not be TLR4/TRIF or TLR3/TRIF signaling dependent, but is instead mediated via MyD88-dependent pathway.

In our previous study (chapter 2), enhanced osteoclastogenesis was implicated in accelerated skull healing in TLR4$^{-/-}$ mice. We showed a faster bone healing response based on histological analysis with upregulated expression of RANKL in TLR4$^{-/-}$ mice compared to WT mice [78]. Since both myeloid and dendritic cells give rise to osteoclasts, we further dissectted the role of TLR4 signaling in these cells to understand their role in calvarial bone healing. To specifically knockout TLR4 expression in myeloid cells (Lyz-TLR4$^{-/-}$) and dendritic cells (CD11c-TLR4$^{-/-}$), the Cre-*loxP* technique was used in conjunction with lysozyme (*lyz*) and CD11c (*cd11c*) promoters, respectively. One limitation is that, while *lyz* is highly expressed in all myeloid cells, depletion of TLR4 in this model might also occur in a small population of CD11c+ dendritic cells. Previous studies have shown that this effect is negligible [134,154]. Therefore, our myeloid and dendritic cell-specific knockouts enabled us to extend our previous findings with global TLR4$^{-/-}$ mice, so that we can better understand the unique effect that TLR4 signaling has on bone regeneration and repair.

In the current study, μCT data further support our previous histomorphometric findings[78] showing TLR4$^{-/-}$, Lyz-TLR4$^{-/-}$, and CD11c-TLR4$^{-/-}$ mice all exhibited accelerated bone healing phenotypes (Figure 11). Although TLR4 deficiency in both myeloid cells and dendritic cells contribute to a faster healing response, only the latter showed enhanced healing at a later time point (day 28). Previous studies suggested that dendritic cells differentiate into osteoclasts under the appropriate inflammatory conditions and may contribute to inflammation-induced osteoclastogeneis, however, how deficient dendritic cells mediate fracture repair is unknown [155,156]. It was recently revealed that immature dendritic cells (iDC) had an increased ability to form osteoclast-like multinucleated giant cells when compared to myeloid derived-monocytes in an inflammatory environment [157,158]. We propose that the differences observed in healing in this study may be attributed to 1) differential osteoclastogenesis of macrophages and dendritic cells induced by TLR4 activation, or 2) different spatiotemporal-dependent roles of macrophages and dendritic cells expressing TLR4 during the four stages of bone repair. Further study is required to fully elucidate the relationship between TLR4 activation in macrophage and dendritic cells with osteoclastogenesis during bone healing.

In summary, we have demonstrated that TLR signaling components affect calvarial bone healing, establishing a link between the skeletal and immune systems during craniofacial fracture repair. The differential healing responses we observed in KO mouse models, suggests that the dendritic cell-expressing TLR4-mediated MyD88 signaling pathway might be detrimental for calvarial defect healing. However, further work is required to explore the changes in gene expression and cellular infiltration over time during the healing process, which will benefit our understanding of the role of TLR-mediated inflammation in bone regeneration.

4.0 TLR4 INACTIVATION IN MYELOID CELLS IMPROVE BONE HEALING THROUGH ENHANCED OSTEOCLASTOGENESIS

4.1 INTRODUCTION

Skeletal development and tissue regeneration utilize many similar molecular mechanisms, some of which lie dormant and only activate in response to injury. Inflammation, an integral component of the injury response, is involved not only in the host defense against infectious pathogens but also in tissue repair and regeneration, dynamically balancing its tissue-destructive and tissue-constructive properties [75,76]. For decades, osteoimmunology has overwhelmingly focused on investigating osteoclasts and metabolic bone disease as they relate to pathologic bone resorption. Recently, interest has increased in elucidating the positive interactions between the immune and skeletal systems during the fracture healing process. This is an important consideration for bone repair and reconstructive therapies, especially when the injury site is unduly compromised by trauma and/or infection. Therefore, studies have conducted to explore the modulation of fracture-induced inflammation for obtaining desirable bone healing outcomes. These studies include modulating the expression of inflammatory cytokines, chemokines, and growth factors (IL1, IL-6, IL-18, TNF-α, Complement 3, TGF-β, VEGF, stromal cell-derived factor); controlling cellular proliferation, infiltration, and activity (macrophage, lymphocytes, bone cells, various stem cells); and using pharmacologic approaches (cytokine-specific

antagonists, corticosteroids, non-steroidal anti-inflammatory drugs) [119]. Such studies have increased our understanding of the relationship between immunity and skeletal regeneration, which provides evidence and experience for future clinical translation.

Toll-like receptors (TLRs) are a family of transmembrane receptors that activate the innate immune response by recognizing conserved molecular patterns of microbial products as well as endogenous ligands [123]. TLR activation results in intracellular signaling cascades that are mediated by two main adaptor proteins – Myeloid differentiation primary response gene 88 (MyD88), and TIR-domain-containing adapter-inducing interferon-β (TRIF). While most TLRs utilize only the MyD88 pathway, TLR4 is unique in that it can also utilize the TRIF pathway. TLR4 signaling is of particular interest in regenerative biology due to its pronounced impact on healing in diverse models of injury and sterile inflammatory disease [159,160]. It can recognize a wide range of pathogen-associated molecular patterns (PAMPs) as well as damage-associated molecular patterns (DAMPs) including bacterial lipopolysaccharide (LPS)[161] and endogenous molecules such as fibrinogen [162], fibronectin [163], heat shock proteins 60 and 70 [164], β-Defensin 2 [165], and high mobility group protein B1 (HMGB1) [166].

TLR4 is mainly expressed in immune cells, such as monocytes/macrophages, dendritic cells, T cells and B cells, as well as bone cells, such as osteoblasts and osteoclasts. While the expression of different TLRs vary with different stages of osteoclast differentiation, expression of TLR2 and TLR4 expression have been reported within all osteoclast-lineage cells [167]. Understanding how TLR4 signaling regulates the inflammatory response and osteoclast differentiation after fracture may provide insight into mechanisms of bone remodeling and regeneration as a result of skeletal diseases or trauma. Studies have shown that TLR4 activation can either promote or inhibit osteoclastogenesis under different clinical settings[168-170]. For

example, TLR4 signaling is involved in osteoclast development during osteoporosis, and is critical for LPS-stimulated inhibition of osteogenic differentiation through inducing RANKL and TNF-α in osteoblasts [101,102,171,172,173]. Conversely, direct TLR signaling has also been show to inhibit RANKL-mediated osteoclast differentiation *in vitro*, via maintaining the phagocytic pro-inflammatory activity of osteoclast precursors as well as inhibiting their differentiation into non-inflammatory mature osteoclasts [100,174]. The fact that TLR stimulation acts as a potent negative regulator of osteoclastogenesis contradicts with the observation that TLR activation is associated with excessive bone resorption in many inflammatory bone diseases [102,151,152]. Thus, these contradictory results hint that TLRs may have a dual role of regulating the balance between immune response and bone metabolism under various settings.

In our previous study, accelerated bone healing with higher expression of RANKL was observed in TLR4 knockout mice ($TLR4^{-/-}$) within a non-compromised calvarial defect model [78]. Based on this data, we proposed that TLR4 depletion would enhance osteoclastogenesis, ultimately leading to accelerated calvarial bone healing. To test this hypothesis, we utilized a cell-specific $TLR4^{-/-}$ mouse model (Lyz-$TLR4^{-/-}$) in which TLR4 expression was deleted in myeloid cells, as osteoclasts are derived from myeloid-lineage cells. In this study, Lyz-$TLR4^{-/-}$ mice showed a faster healing phenotype similar to $TLR4^{-/-}$ mice basing on histomorphometric and μCT analyses. Increased infiltration of osteoclasts were also similarly observed in both $TLR4^{-/-}$ and Lyz-$TLR4^{-/-}$ mice. Although similarities in osteoclastogenesis were observed between both TLR4 deficient mice, higher expression of BMP2, TGF-β1, IL-β, and TLR2 was also observed in $TLR4^{-/-}$ mice compared to WT and Lyz-$TLR4^{-/-}$ mice, suggesting involvement of other mechanisms for the faster bone healing response observed in $TLR4^{-/-}$ mice. Our data show that TLR4 inactivation in myeloid cells enhanced osteoclastogenesis differentiation and

exhibited faster bone healing in a calvarial defect model. Our data, together with previous work linking TLR4 with bone destruction in inflammatory disease, highlights a potential role for TLR4 as an important immune mediator that modulates osteoclastogenic differentiation in various clinical settings.

4.2 MATERIALS AND METHODS

4.2.1 Mouse Strains and Generation of Myeloid-specific TLR4$^{-/-}$ Mice

Wild-type (WT) (C57BL-6J, The Jackson® Laboratory, Bar Harbor, Maine), TLR4$^{-/-}$, Lyz-TLR4$^{-/-}$, and TLR4$^{loxp/loxp}$ female mice between 10 and 16 weeks of age and 20-30 g were utilized in this study. Myeloid lineage-specific TLR4 knockout (KO) mice (TLR4$^{flox/-,\ lyz\ cre}$ or Lyz-TLR4$^{-/-}$) were developed by breeding TLR4$^{loxp/-;\ Lyz\text{-}cre}$ mice with TLR4$^{loxp/loxp}$ mice [134]. Tail snips of offspring were collected at 21 days of age for genotyping using polymerase chain reaction (PCR). As TLR4$^{-/-}$ mice are viable without baseline abnormalities, we anticipated no baseline phenotypic variation in the mice with TLR4 deleted from specific cell types. Mice were randomly chosen for analyses. All procedures were carried out in accordance with regulations regarding for the care and use of experimental animals published by the National Institutes of Health and was approved by University of Pittsburgh Institutional Animal Use and Care Committee.

4.2.2 Surgical Procedure

Mice (WT, $TLR4^{-/-}$, Lyz-$TLR4^{-/-}$, and $TLR4^{loxp/loxp}$) were anesthetized with isoflurane (4% by inhalation) and 1.8 mm diameter defects were created on mouse parietal bones as previously described [78]. 1 mg/kg ketoprofen (Fort Dodge Animal Health, Fort Dodge, IA) was administered as an analgesic immediately and for two days after surgery. All mice were euthanized via CO_2 overdose followed by cervical dislocation at designated time points. $TLR4^{-/-}$ mice and Lyz-$TLR4^{-/-}$ mice were designated experimental groups and WT and $TLR4^{flox/flox}$ mice were designated control groups.

4.2.3 μCT Analyses

An average of ten mice from each group (WT, $TLR4^{-/-}$, Lyz-$TLR4^{-/-}$, and $TLR4^{loxp/loxp}$) were euthanized at seven and 28 days after surgery. The skulls were dissected and stored in 4% paraformaldehyde overnight and later stored in 70% ethanol. The calvarial defect healing process was analyzed in three-dimensions (3D) using a high-resolution μCT system with a fixed isotropic voxel size of 15 μm. 3D images were reconstructed using Amira software (FEI Visualization Sciences Group, Burlington, MA) and OsiriX software. Quantitative data was analyzed by OsiriX software with a global fixed threshold -330 and a region of interest (ROI of $0.4mm^2 \times 20.9$ mm) was defined. Standard μCT measurements (regenerated bone volume (BV) = BV within the ROI at day 7, and 28– BV at day 0) were calculated for each sample using OsiriX software.

4.2.4 Histology and Histomorphometric Analyses

An average of four mice from each group (WT, TLR4$^{-/-}$, and Lyz-TLR4$^{-/-}$) were euthanized at day 0 and postoperative days one, four, seven, and 28. Calvariae and surrounding soft tissues (e.g., skin, brain) were harvested and fixed in 4% paraformaldehyde for 24 hours. Samples were decalcified in 10% EDTA prior to being dehydrated through a series of ethanol and embedded in paraffin.[78] Paraffin-embedded specimens were sectioned through the coronal plane at a thickness of 5-6 μm. Slides were stained with Harris' hematoxylin & eosin (H&E, Surgipath Medical Industries, Richmond, IL) for conventional, qualitative bright-field light microscopy.

Russell-Movat pentachrome staining (American MasterTech, CA) was performed to further differentiate the following tissues within the defect: hematoma/fibrin (intense red), elastic fibers (black), newly-formed woven bone (yellow), and lamellar bone (red).

Tartrate-resistant acid phosphatase (TRAP) stain: Sectioned slides were first incubated in phosphate buffered saline (pH=5) at 37°C for five minutes, then incubated in TRAP buffer (PH=5), containing 0.1 M acetate buffer, 0.3 M sodium tartrate, 10 mg/ml Naphthol AS-MX phosphate, 100 μl Triton X-100, and 0.3 mg/ml Fast Red Violet LB salt for one hour at 37°C. Sections were counterstained with 0.02% fast green (Sigma-Aldrich Corp, St. Louis, MO) before mounting in cytoseal^{TM}280 (Fisher Scientific, Pittsburgh, PA). Osteoclasts were detected as TRAP-positive cells.

Histomorphometric analyses were performed to quantify cellular infiltration and two-dimensional areas of new bone formation using a Leica MZ12 microscope (Leica Microsystems Ltd. Switzerland) and Northern Eclipse (v5.0) image analysis software (Empix, Imaging, Inc. Cheektowage, NY). Bone healing data was calculated based on three to five slides per animal. New areas of bone formation were visually identified under 100X magnifications. New bone

area was calculated as the sum of the areas of each bone section, including within the defect and on both sides of the calvaria. The sum totals of newly formed bone areas were averaged by the number of slides per animal. Osteoblasts were calculated as the total number of osteoblasts per osteoblast-lining bone surface under 100X magnification. Osteoclasts were calculated as the total number of osteoclasts per field under 200X magnification. Data was expressed as mean +/- SEM. All measurements were taken by researchers blinded to group identity.

4.2.5 Immunohistochemistry Analyses

Sections from WT, TLR4$^{-/-}$, and Lyz-TLR4$^{-/-}$ mice were deparaffinized with xylenes and rehydrated through a series of ethanol to distilled H_2O. Antigen retrieval was performed on all samples using a Universal Antigen Retrieval Kit (R&D Systems, Minneapolis, MN). Following the manufacturer's instructions, sections were incubated in 10% blocking serum for one hour at room temperature. Sections were then incubated in primary antibodies, which were suspended at a 1:100~1:250 dilution in 10% blocking serum overnight at 4°C. Sections were incubated in HRP-conjugated secondary antibody (dilution 1:100~1:250) for 30 minutes at room temperature. Color was developed by application of DAB kit (Vector Laboratories, Burlingame, CA). Horse and goat blocking serum came from Vector Laboratories. (Burlingame, CA). Primary antibodies were anti-OPN as a marker of osteogenic differentiation, anti-F4/80 as a marker for M0 macrophages, and anti-Arginase1 as a marker for M2 macrophages (Santa Cruz Biotechnology, Santa Cruz, CA; Abcam, Cambridge, MA). Secondary antibodies were anti-goat horse IgG or anti-rabbit goat IgG (Vector Laboratories, Inc. CA). Sections were dehydrated and mounted prior to examination at 25X, 50X, 100X, 200X, and 400X magnifications.

4.2.6 mRNA Extraction and Expression Analyses

An average of five mice from each group (WT, TLR4$^{-/-}$, and Lyz-TLR4$^{-/-}$) were euthanized at day 0 before surgery and at three hours on days 1 and 4 after surgery. Samples surrounding the initial 1.8 mm defect were collected using a 5.0mm outer diameter trephine (Fine Science Tools, Foster City, CA), including blood clots, hematoma, granulation tissue, new bones, and surrounding normal bones. Samples were stored at 4°C in RNAlater solutions (Life Technologies, NY) until ready for RNA isolation. The specimens were homogenized and RNA was extracted from the sample using RNAqueous-Micro Kit (Life technologies, NY) according to the manufacturer's protocol. Primers used in the study recognized IL-1β, IL-6, IL-4, IL-10, BMP-2, TGF-β1, Runx2, Osterix, RANKL, OPG, iNOS, Arginase, and TLR2. The housekeeping gene GAPDH was chosen as an internal control. RT-PCR results were calculated by standard curve analysis. The relative amount of target gene was normalized to the expression of neomycin resistance gene. Finally, relative fold change in expression of target gene to GAPDH in WT, TLR4$^{-/-}$, and Lyz-TLR4$^{-/-}$ mice was compared at designated time points.

4.2.7 *In Vitro* Bone Marrow-derived Osteoclast Differentiation Assay

Femora and tibiae were excised from seven- to 10-week-old female mice (WT, TLR4$^{-/-}$, and Lyz-TLR4$^{-/-}$). The soft tissue and connective tissue were carefully removed and the ends of the bones were cut off. Bone marrow was flushed out using a 5mL syringe into a 50mL tube with DMEM media (Life technology, NY). Bone marrow suspension was centrifuged at 1000 rpm, 4℃ for five minutes. The supernatant was removed and the cells were suspended in the DMEM media containing 10% fetal bovine serum (FBS), 1% penicillin/streptomycin, and 10ng/ml M-

CSF. The cell suspension was seeded onto a 6-cm cell culture dish. Sixteen hours after seeding, unattached cells were collected and seeded with DMEM containing 10% FBS, 1% penicillin/streptomycin, and 30ng/ml M-CSF (Life Technologies, Carlsbad, CA) at 10^5 cells/well on a 24-well plate. Three days after seeding, the media was changed to fresh DMEM containing 10% FBS, 1% penicillin/streptomycin, 30ng/ml M-CSF (Life Technologies, Carlsbad, CA), and 50ng/ml RANKL (Life Technologies, Carlsbad, CA).

ALP and TRAP Staining: At day 5 and day 7 after osteoclast differentiation culture, cells were fixed with 10% buffered paraformaldehyde solution. Fixed cells were stained with TRAP and ALP double-stain kit (Takaba, Clontech Laboratories, CA) according to the manufacturer's protocol. After staining, TRAP-positive cells and ALP-positive cells were quantified under 100X magnification.

4.2.8 Statistical Analyses

Statistical analyses were performed using SPSS v.20.0 software (SPSS, Inc, Chicago, IL). Data (Mean BV calculation from μCT analyses, mean areas of newly-formed bone, N.Ob/BS and N.Oc/BA collected from histomorphometric measurements and numbers of ALP (+) and TRAP (+) cells from *in vitro* cultures) were compared using one-way ANOVA followed by *post-hoc* LSD test. A *p* value less than or equal to 0.05 was considered significant.

4.3 RESULTS

4.3.1 Accelerated Intramembranous Bone Formation in TLR4$^{-/-}$ and Lyz-TLR4$^{-/-}$ Mice

In order to characterize the bone healing process, µCT was performed on four groups of mice (WT, TLR4$^{-/-}$, Lyz-TLR4$^{-/-}$ and TLR4$^{loxp/loxp}$ at postoperative days 7 and 28. Representative 3D reconstructed images are shown in Fig.13. No group showed complete bone healing within 28 days of observation. Areas of mineralized tissue were observed in TLR4$^{-/-}$ and Lyz-TLR4$^{-/-}$ mice, while no obvious new bone formation was evident in WT and TLR4$^{loxp/loxp}$ mice at day7 (Fig. 13A). Significantly larger BV was found in TLR4$^{-/-}$ and Lyz-TLR4$^{-/-}$ mice compared to WT mice on day 7 (Fig. 13B). No significant difference in bone healing based on µCT was found between WT and TLR4$^{loxp/loxp}$ mice at all time points.

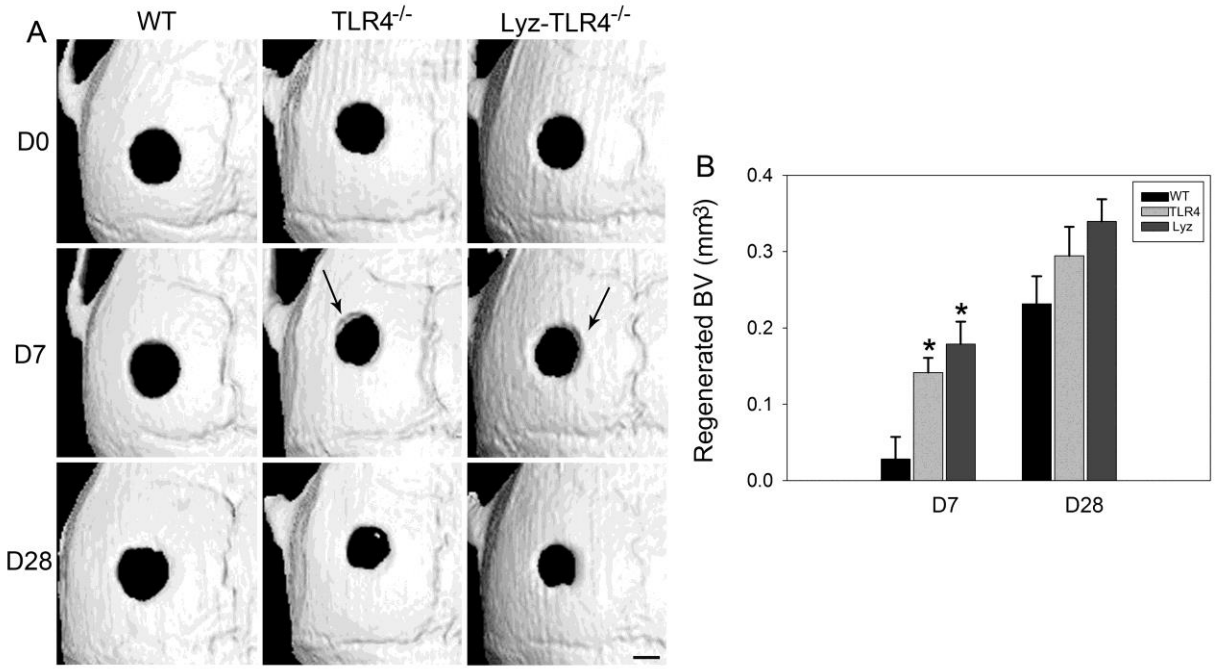

Figure 13: µCT analyses

(A) Representative 3D reconstructions of calvarial defects in the transverse plane at postoperative days 0, 7, and 28 of WT, TLR4$^{-/-}$, and Lyz-TLR4$^{-/-}$ mice. Faster healing was evident in TLR4$^{-/-}$ and Lyz-TLR4$^{-/-}$ mice, as indicated by more mineralized tissue around the defect edges at day 7 (arrows). Similar bone healing was shown among the three groups on day 28. (B) Statistical analyses of bone volume (BV) measurements at different time points. Significantly larger BV was found in TLR4$^{-/-}$ and Lyz-TLR4$^{-/-}$ mice relative to WT mice at day 7, while no significant differences were seen among the three groups at day 28. No significant difference in BV between TLR4$^{-/-}$ and Lyz-TLR4$^{-/-}$ mice was seen at both days 7 and 28. (Scale: 500 μm, $p<0.05$, * compared to WT mice).

To further demonstrate the accelerated healing response in TLR4$^{-/-}$ and Lyz-TLR4$^{-/-}$ mice, H&E staining, pentachrome staining, and IHC staining for osteopontin (OPN) were performed. Histological healing patterns at day 7 demonstrated larger areas of newly-formed woven bone at the endocortical side of cavalria bone in TLR4$^{-/-}$ and Lyz-TLR4$^{-/-}$ mice compared to WT mice, accompanied by active osteoblast infiltration, and enhanced OPN staining (Fig. 14A and Fig.15A). On day 28, similar histological characteristics were seen among the three groups. Although woven bone matrix was still evident, mature lamellar bone was present on the ectocortical and endocortical calvarial sides in all groups on day 28 (Fig. 14B). Histomorphometric measurements showed significantly larger areas of newly-formed bone and significantly more infiltrated osteblasts in the TLR4$^{-/-}$ and Lyz-TLR4$^{-/-}$ mice compared to WT mice at day7 (Fig. 14C and Fig. 15B). No significant difference in new bone areas or osteoblast numbers was found between TLR4$^{-/-}$ and Lyz-TLR4$^{-/-}$ mice on day7 (Fig. 14C and Fig. 15B) and among the three groups on day 28 (Fig. 14D).

Levels of osteogenic gene expression (BMP2, TGF-β1, RUNX2, and Osterix) from WT, TLR4$^{-/-}$, and Lyz-TLR4$^{-/-}$ mice were compared at 0 hour, 3 hours, day 1, and day 4. No significant differences in expression levels were detected at zero hour (data not shown). Elevated expression of these four genes was observed in TLR4$^{-/-}$ after surgery, while no significant change

in gene expression was observed in WT and Lyz-TLR4$^{-/-}$ mice, (Fig.15C). BMP2 and TGF-β1 expression exhibited a significantly higher fold change in TLR4$^{-/-}$ mice than in WT and Lyz-TLR4$^{-/-}$ mice at day 1 post surgery. No difference in expression level of RUNX2 and Osterix were observed among the three groups at all time points.

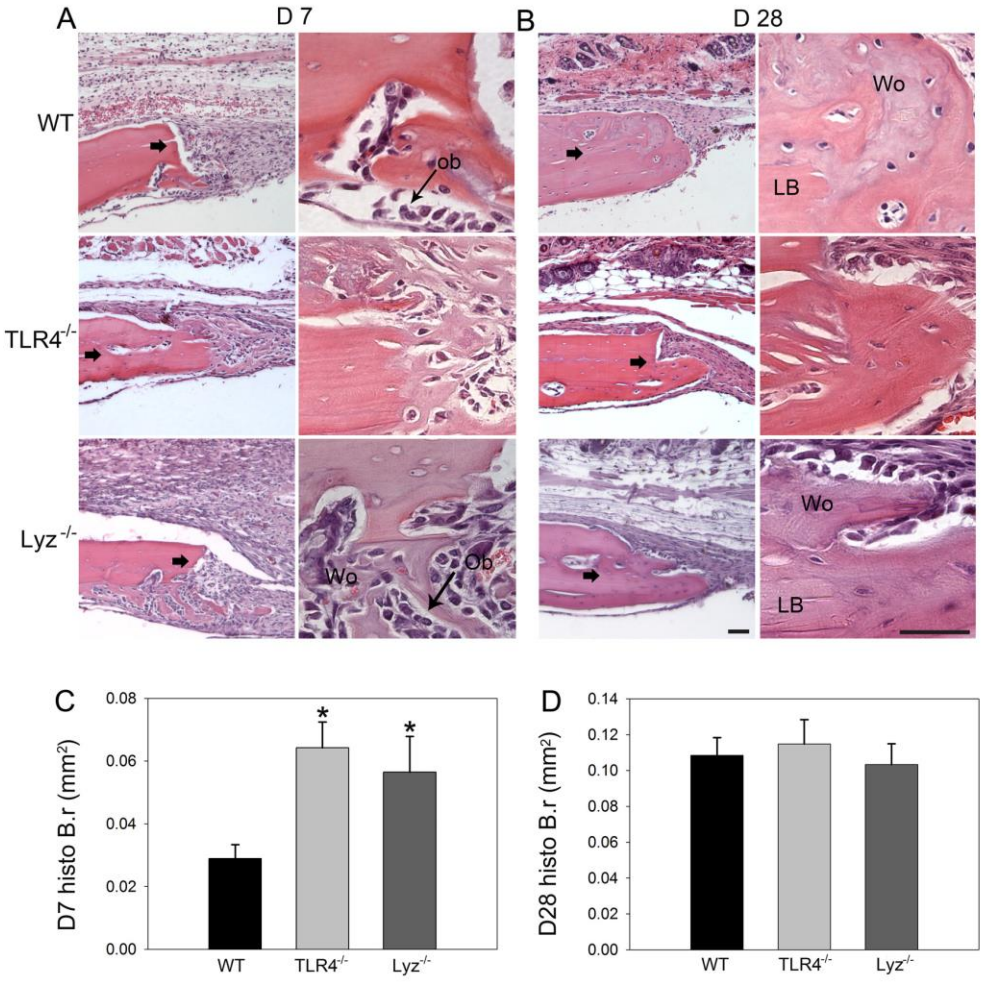

Figure 14: Accelerated intramembranous bone formation in TLR4$^{-/-}$ and Lyz-TLR4$^{-/-}$ mice

(A) Representative H&E-stained images at day 7. Disorganized loose connective tissue completely filled the bone defect on day 7 in all groups. Larger area of newly-formed cellularized woven bone was observed in TLR4$^{-/-}$ mice and Lyz-TLR4$^{-/-}$ mice compared to WT mice. (B) Similar histological healing pattern was observed in all groups and no groups showed complete bone healing at day 28. (C-D) One-way ANOVA showed significantly large areas of bone formation in TLR4$^{-/-}$ and Lyz-TLR4$^{-/-}$ mice compared to WT mice. No significant difference was detected in

bone formation among three groups on day 28. (Scale bar: 50 μm; bolded arrow: defect margin; Ob: osteoblast; Wo; woven bone; LB: lamellar bone; $p<0.05$, * vs. WT).

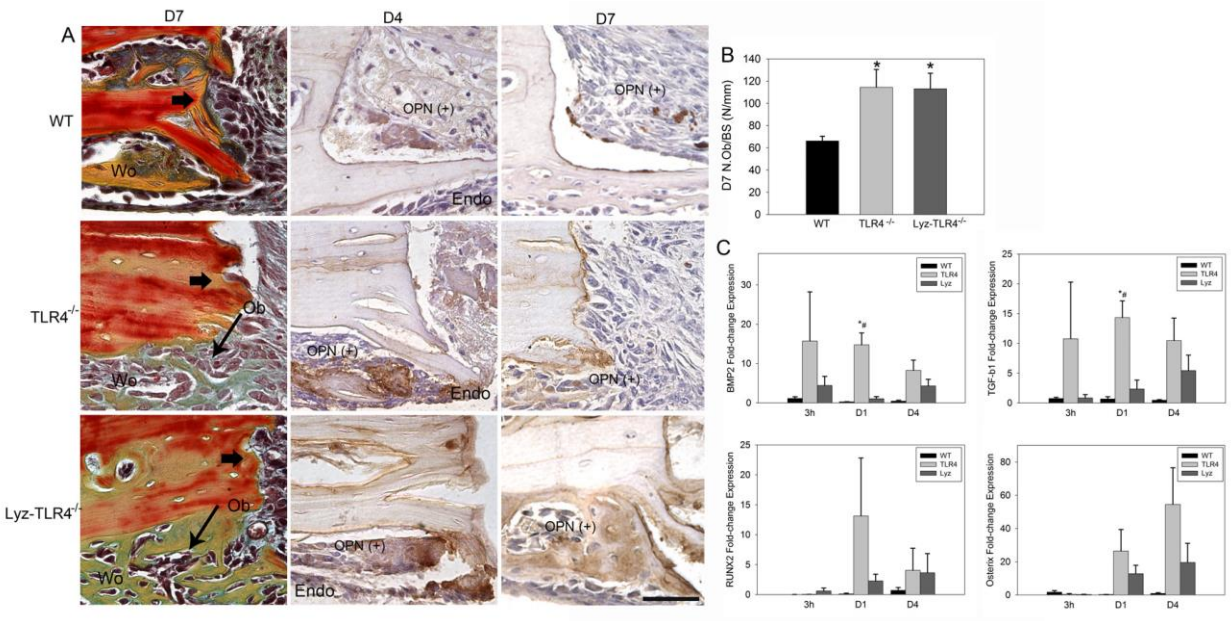

Figure 15 : Enhanced osteogenesis in TLR4$^{-/-}$ and Lyz-TLR4$^{-/-}$ mice

(A) Representative pentachrome-stained and anti-OPN-stained images. One or two layers of bone surface-lining osteoblasts were observed on the endocortical side of calvarial bone in WT mice. More infiltrated osteoblasts, larger areas of newly-formed woven bone matrix (yellow in pentachrome staining), and more intense OPN staining were evident in both TLR4$^{-/-}$ and Lyz-TLR4$^{-/-}$ mice than in WT mice. (B) One-way ANOVA showed significantly more osteoblasts in TLR4$^{-/-}$ and Lyz-TLR4$^{-/-}$ mice compared to WT mice. (C) Elevated expression of BMP2, TGF-β1, RUNX2, and Osterix were evident in TLR4$^{-/-}$ mice after surgery, while remaining relatively unchanged in WT mice. Significantly higher fold change in expressions of BMP2 and TGF-β1 were observed in TLR4$^{-/-}$ mice than in WT and Lyz-TLR4$^{-/-}$ mice at day 1. No significant differences in expressions of RUNX2 and Osterix were found among the three groups at all time points. (Scale bar: 50 μm; bolded arrow: defect margin; Ob: osteoblast; Wo; woven bone; Endo: endocortical side; $p<0.05$, * vs. WT, # vs. Lyz).

4.3.2 TLR4 Inactivation Enhanced Osteoclastogenesis *In Vitro* and *In Vivo*

In order to gain better understanding of osteoclast infiltration and tissue resorption during the early phase of the fracture healing process, TRAP staining of paraffin-embedded slides of WT, TLR4$^{-/-}$, and Lyz-TLR4$^{-/-}$ mice was performed on day 7. TRAP (+) osteoclasts were evident at the defect margin and newly-regenerated woven bone in all groups at day 7 (Fig. 16A). More intense TRAP (+) staining and significantly more osteoclasts were detected in Lyz-TLR4$^{-/-}$ mice relative to WT mice (Fig. 16A and Fig.16B). The number of osteoclasts did not significantly differ between TLR4$^{-/-}$ mice and Lyz-TLR4$^{-/-}$ mice at day 7 (Fig. 16B).

Levels of osteoclastogenic gene expression (RANKL and OPG) from WT, TLR4$^{-/-}$, and Lyz-TLR4$^{-/-}$ mice were compared at 0 hour, 3 hours, day 1 and day 4. No significant differences in expression levels were detected at 0 hour (data not shown). WT mice did not exhibit obvious changes in expression of RANKL or OPG, while TLR4$^{-/-}$ and Lyz-TLR4$^{-/-}$ mice both showed increased expression of RANKL and OPG after surgery (Fig. 16C-16D). A significantly higher expression of RANKL was found in TLR4$^{-/-}$ mice compared to WT mice at day 4, and a higher expression of OPG was found in TLR4$^{-/-}$ mice compared to WT mice at day 1. No significant difference in expression level of RANKL and OPG was detected between TLR4$^{-/-}$ and Lyz-TLR4$^{-/-}$ mice at all time points (Fig. 16C-16D).

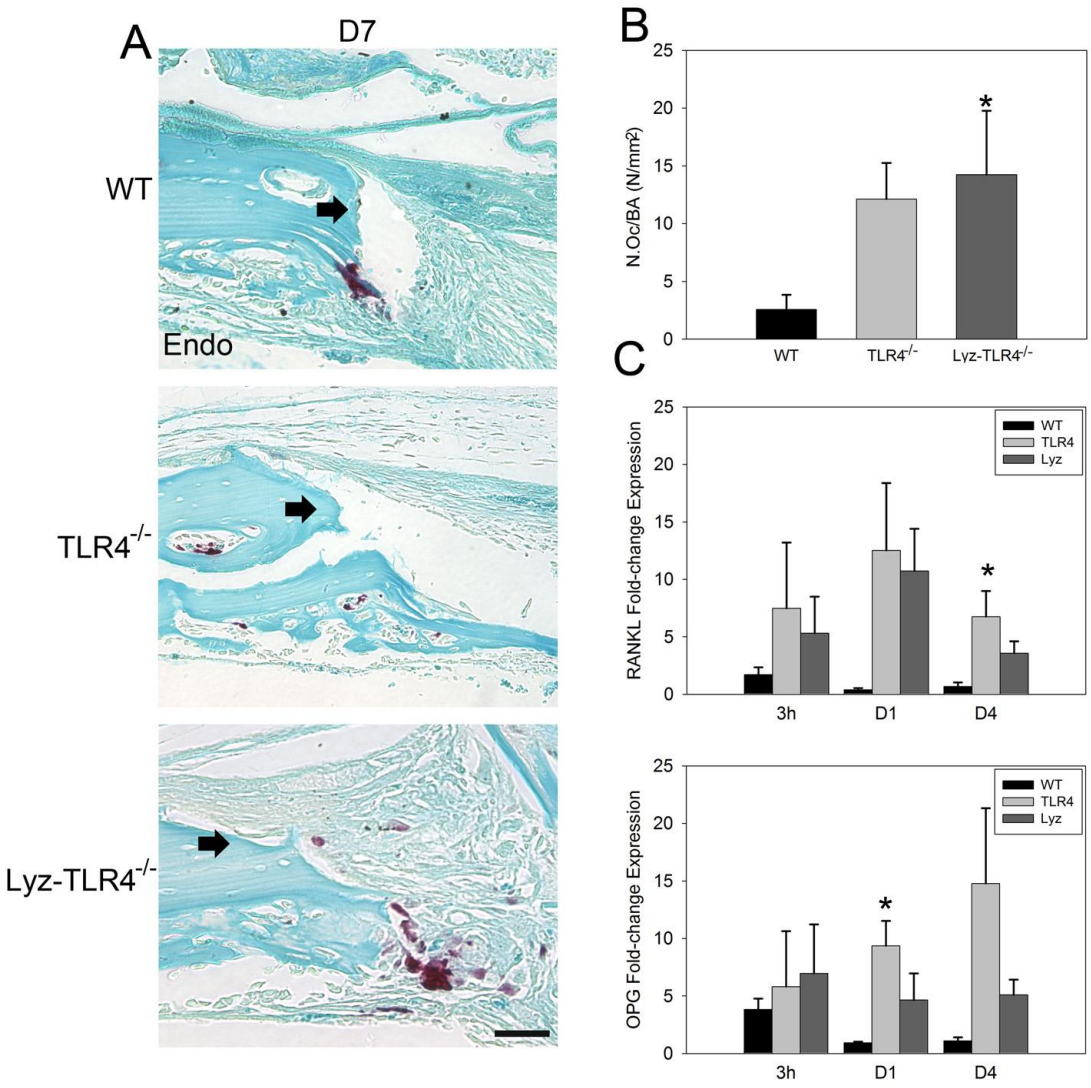

Figure 16: Enhanced osteoclastogenesis in TLR4-deficient mice

(A) Representative TRAP-stained images at day 7. TRAP (+) osteoclasts were evident at the defect margin and the bone marrow space. More intense TRAP (+) staining was shown in Lyz-TLR4$^{-/-}$ mice compared to WT mice. This observation was consistent with TRAP (+) osteoclast counts shown in (B). No significant difference in numbers of TRAP(+) osteoclast was shown between TLR4$^{-/-}$ mice and Lyz-TLR4$^{-/-}$ mice at day 7. (C) Similar expression patterns of RANKL and OPG were shown between TLR4$^{-/-}$ and Lyz-TLR4$^{-/-}$ mice, while fold change in expression of these two genes remained relatively unchanged in WT mice after surgery. No differences were found in expression levels of RANKL or OPG between TLR4$^{-/-}$ and Lyz-TLR4$^{-/-}$. (Scale: 50 μm; bolded arrow: defect margin; Endo: endocortical side; $p<0.05$, * compared to WT mice).

To better understand the capacity of osteoclast differentiation and resorption activity of WT, TLR4$^{-/-}$, and Lyz-TLR4$^{-/-}$ mice, TRAP and ALP double staining was performed on the bone marrow-derived primary cells obtained from the three groups. More red, TRAP (+), cells were observed in the TLR4$^{-/-}$ culture group on both day 5 and day 7 compared to the WT and Lyz-TLR4$^{-/-}$ groups. Similar ALP-positive staining was observed among the three groups at both time points (Fig. 17A-17C). Consistent with observations from *in vitro* staining, significantly more TRAP (+) cells were seen in the TLR4$^{-/-}$ group compared to the WT and Lyz-TLR4$^{-/-}$ groups on both day 5 and day 7. No significant differences in ALP (+) cell numbers were seen among all three groups (Fig. 17B).

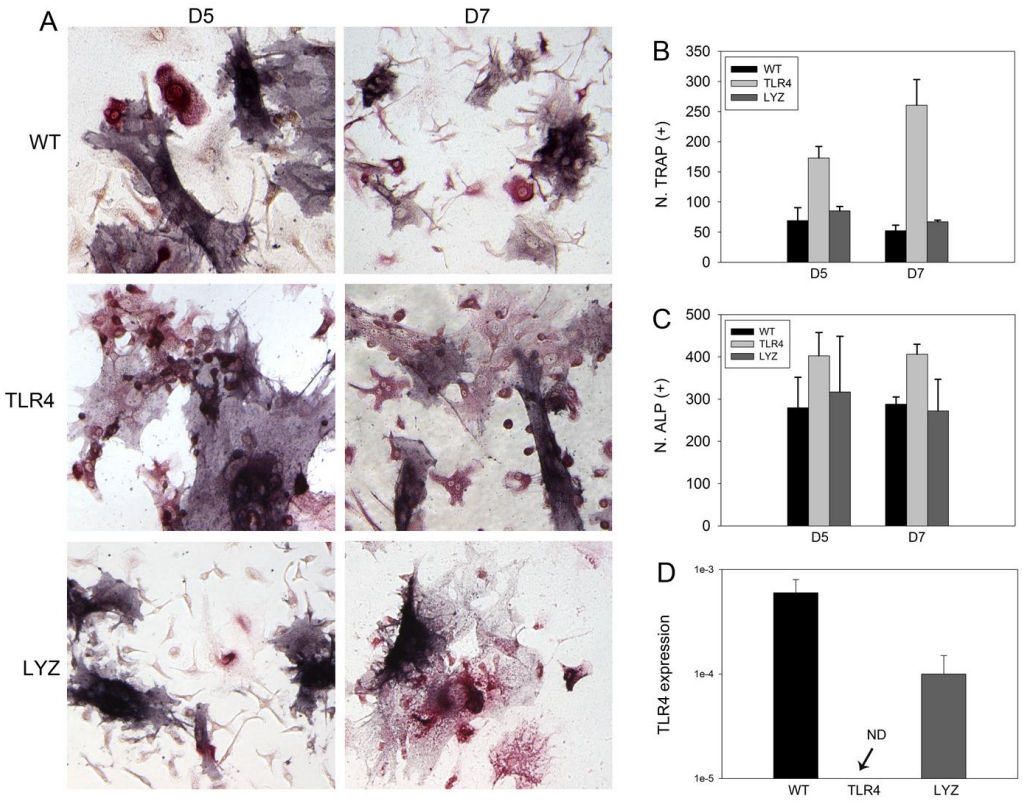

Figure 17 *in vitro* osteoclast differentiation analysis

(A) Representative TRAP-stained images at day 5 and day 7. More TRAP (+) cells were observed in TLR4$^{-/-}$ mice compared to the other two groups. This observation was consistent with TRAP (+) osteoclast counts shown in (B).

(C) Comparable ALP (+) cells were shown among all three groups. (D) TLR4 expression was not detected in TLR4$^{-/-}$ culture group.

4.3.3 Inflammatory Response during the Healing Process in the Absence of TLR4

In order to better understand the inflammatory response during early fracture healing, anti-F4/80 and anti-Arginase1 IHC staining and inflammatory cytokine expression (IL-1β, IL-6, IL-4, IL-10, iNOS, Arginase, and TLR2) were analyzed. At day 1, similar intense staining of anti-F4/80 indicating infiltration of M0 macrophages, and anti-Arginase1 staining indicating M2 macrophages were evident in all groups (Fig. 18A). At days 4 and 7, no obvious anti-F4/80 or anti-Arginase1 positive staining was observed in all groups (data not shown). Inflammatory gene expression from WT, TLR4$^{-/-}$, and Lyz-TLR4$^{-/-}$ mice was detected at 0 hour, 3 hour, day 1 and day 4 (Fig. 18B). No significant differences in expression levels were detected at 0 hour (data not shown). TLR4$^{-/-}$ mice exhibit significantly higher expression of IL-1β at day 1, and significantly higher expression of TLR2 at 3h and day 1 compared to WT and Lyz-TLR4$^{-/-}$ mice (Fig. 18B). IL-6 presented the highest expression levels at three hours, and declined in expression at later time points in all groups (Fig. 18B). No difference in expression level of iNOS and arginase was detected among all groups (Fig. 18B). Neither IL-4 nor IL-10 expression were detected at all time points (Data not shown)

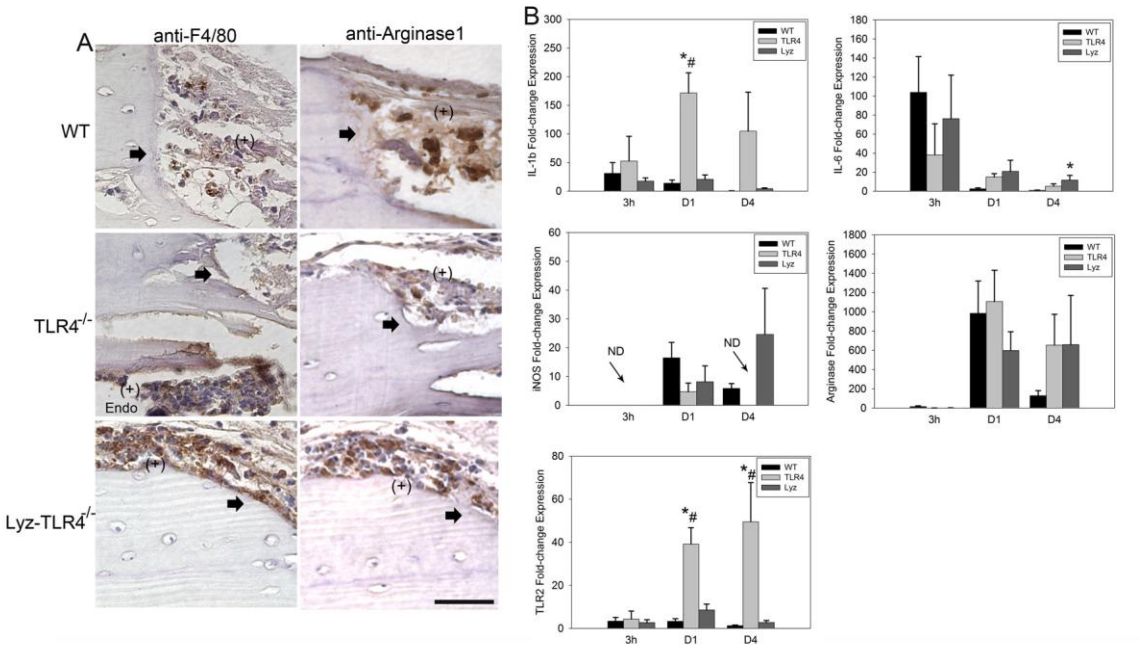

Figure 18: Unshifted balance of inflammatory response in TLR4-deficient mice

(A) Representative anti-F4/80 and anti-Arginase1 stained images at day 1. Similar anti-F4/80 staining and anti-Arginase1 staining, suggesting M0 and M2 macrophage infiltration, was observed in WT, TLR4$^{-/-}$, and Lyz-TLR4$^{-/-}$ mice at day 1. (B) Fold change in expression of inflammatory cytokines from WT, TLR4$^{-/-}$, and Lyz-TLR4$^{-/-}$ mice at three hours, day 1 and day 4. Significantly higher expression of IL-β was detected in TLR4$^{-/-}$ mice compared to WT and Lyz-TLR4$^{-/-}$ mice at day 1. Significantly higher expression of IL-6 was shown in Lyz-TLR4$^{-/-}$ mice compared to WT mice at day 4. Significantly higher expression of TLR2 was observed in TLR4$^{-/-}$ mice compared to Lyz-TLR4-/- and WT mice at day 1 and day 4. No significant difference was found in expression levels of iNOS and Arginase in all groups. Neither IL-4 nor IL-10 expression was detected at all time points. (Scale: 50 μm; bolded arrow: defect margin; Endo: endocortical side; ND: not detected; p<0.05, *compared to WT mice, # compared to Lyz-TLR4$^{-/-}$ mice).

4.4 DISCUSSION

The aim of this study was to investigate the effect of TLR4 depletion on osteoclastogenesis and its impact on bone healing. We found that depletion of TLR4 from osteoclast precursors resulted in enhanced osteoclastogenesis and accelerated bone healing in a calvarial defect model, suggesting an important role of TLR4 in regulating osteoclastogenic differentiation.

Since TLR4 has been reported to have a profound role in mediating innate immune response and skeletal tissue homeostasis, we aimed to test the effect of TLR4 deletion on both osteoclastogenesis differentiation and macrophage polarization in this study. Previous studies have used the cathepsin K (*Ctsk*) or Tartrate-resistant acid phosphatase (*TRAP*) promotors, which are expressed in mature osteoclasts or osteoclast precursors and osteoclasts respectively, to generate osteoclast-specific KO animal model [175]. However these two osteoclast-specific animal models do not target macrophage lineage differentiation. As lysozyme is predominantly synthesized in myelomonocytic lineage [176], we utilized a calvarial defect model of myeloid lineage-specific TLR4$^{-/-}$ mice (Lyz-TLR4$^{-/-}$ mice), in which Cre under lysozyme (*lyz*) promoter enables inducible recombinase expression in osteoclast and macrophage precursors, in order to test the early development and differentiation of osteoclast/macrophage after calvarial fracture.

Consistent with our hypothesis, accelerated bone healing and increased infiltration of osteoclasts were observed in Lyz-TLR4$^{-/-}$ and TLR4$^{-/-}$ mice. Although the differences in RANKL expression observed between Lyz-TLR4$^{-/-}$ and WT mice were not statistically significant, the increased RANKL expression pattern for Lyz-TLR4$^{-/-}$ mice was similar to TLR4$^{-/-}$ mice, while RANKL expression remained relatively unchanged in WT mice after surgery. Previous studies showed that enhanced osteoclast activity is the main driving force for chronic inflammation-

stimulated bone destruction[101,102,171,172,173], however, in our non-compromised calvarial defect model it initiates an earlier bone repair cascade. Collectively, these data suggest that TLRs may act as a "switch," directing precursors towards differentiation into either inflammatory cells or bone-resorbing osteoclasts. This regulatory role of TLR4 in osteoclastogenesis might be due to the fact that TLR4 can signal through two adaptor proteins, MyD88 and TRIF. This unique property of TLR4 has also been reported in other animal models. For example, TLR4 signaling through the MyD88-dependent pathway contributes to ischemic brain damage [125-127], whereas TRIF-mediated signaling exerts a neuroprotective effect against cerebral ischemia [129]. Thus, the functional consequences of TLR4 activation on tissue regeneration might depend upon its activation through different signaling pathways. In addition, studies have also suggested that TLR activation in osteoclast precursors maintains their phagocytic activity and inhibits their differentiation into non-inflammatory mature osteoclasts, whereas TLR activation on mature osteoclasts increases their survival rate [167]. In light of these findings, TLR4 may be involved in regulating the balance between immune response and bone metabolism at different stages of differentiation by utilizing different down stream pathways.

Although TLR4$^{-/-}$ mice and Lyz-TLR4$^{-/-}$ mice present similar healing phenotypes, the mechanisms through which this occurs may be different. Despite similar accelerated bone healing observed in both TLR4$^{-/-}$ and Lyz-TLR4$^{-/-}$ mice, higher expression of osteogenic genes (BMP-2 and TGF-β1) and inflammatory cytokine (IL-1β) were only observed in TLR4$^{-/-}$ mice. Thus, enhanced osteogenesis and inflammatory cytokine expression might also contribute to the accelerated healing observed in TLR4$^{-/-}$ mice. Traditionally, inflammation has often been negatively associated with pathological bone destruction. However, in recent years, there has been an increased interest in elucidating the positive role of inflammation in bone regeneration

and repair. The impact of inflammation on healing is complex, however, and may be either beneficial or detrimental to repair.[75,76,177] In general, key inflammatory molecules, such as IL-1, IL-6 and TNF-α, have well-established roles in modulating the proliferation and differentiation of skeletal cells during the fracture healing process [74]. Specifically, IL-1β has been shown to present high expression levels during the osteogenic phases of fracture repair, suggesting its involvement in promoting osteoblast proliferation and differentiation [178]. In addition, administration of IL-1β lead to increased cartilage to callus formation at early time points after long bone fracture, while mice lacking IL-1β did not exhibit obvious changes in long bone fracture healing [113]. These observations were in agreement with our findings showing that increased IL-1β expression was associated with accelerated bone healing observed in TLR4$^{-/-}$ mice.

In addition, TLRs can act reciprocally to compensate for each other's loss of gene function [134,135,145,146] which is consistent with our results showing higher TLR2 expression in TLR4$^{-/-}$ mice compared to WT mice and Lyz-TLR4$^{-/-}$ mice at all time points. Similar to TLR4, TLR2 can recognize signals from both bacterial infection and tissue damage. Studies have shown a role for TLR2 in pathogen-associated bone destruction and impaired wound healing [144,179,180]. In addition, it is implicated that TLR2 activation is essential for recruiting neutrophils following injury [181], and neutrophils, which infiltrate into fracture hematoma, produce several macrophage chemoattactants, triggering macrophage infiltration [182,183]. However, there are no studies that show a direct influence for TLR2 with regards to fracture healing. Whether up-regulated TLR2 expression is partially responsible for the faster healing phenotype observed in TLR4$^{-/-}$ mice requires further studies.

Macrophages are highly involved in regulating inflammation, and also play an integral role in tissue regeneration. Within the first 3 days of injury, macrophages infiltrate into the wound bed, participating in the inflammatory response and debridement process via phagocytosis activity and reactive radical release. Lee *et al.* showed that macrophage activation and polarization influence kidney injury and repair [184]. Depletion of M1 macrophages decreased kidney damage whereas depletion of M2 macrophages increased kidney damage [184]. Macrophage polarization is known to be associated with TLR signaling in acute kidney injury. By deleting a macrophage-specific inhibitor of TLR signaling known as IL-1 receptor-associated kinase-M, polarization towards an anti-inflammatory M2 phenotype is prevented, resulting in up to two-thirds loss of kidney mass and interstitial scarring [185]. Since macrophages are derived from myeloid cells, we examined their differentiation and polarization after the calvarial defect in Lyz-TLR4$^{-/-}$ mice. We observed similar infiltration levels of M0 and M2 macrophages in WT, TLR4$^{-/-}$ and Lyz-TLR4$^{-/-}$ mice at day 1, consistent with the expression levels of iNOS, which is expressed by M1 macrophage, and expression level of arginase, which is expressed by M2 macrophage, based on RT-PCR results. Together, depletion of TLR4 expression in myeloid cells did not seem to change macrophage-lineage differentiation or macrophage polarization in this calvarial defect model. However, more evidence related to the differentiation and phagocytic activity of macrophages is needed in order to gain a better understanding of the impact of TLR4 depletion in myeloid cells on macrophage differentiation and inflammatory reaction.

Taken together, our data suggest that TLR4 depletion in myeloid cells enhanced osteoclastogenesis and infiltration into the injury site, resulting in accelerated bone healing in a non-compromised calvarial defect model. Our study shows that TLR4 signaling plays an important regulatory role in enhancing bone destruction and initiating early bone healing via

control of osteoclastogenesis in myeloid cells. This highlights a potential opportunity in which appropriate modulation of the TLR4 signaling pathway can be used to reduce bone destruction in inflammatory bone diseases or enhance early healing in bone defects to improve clinical outcomes.

5.0 TOLL-LIKE RECEPTOR 4 MEDIATES THE REGENERATIVE EFFECTS OF BONE GRAFTS FOR CALVARIAL BONE REPAIR

5.1 INTRODUCTION

Large bone defects are notoriously difficult to repair, presenting a significant risk to patients and an enormous challenge to reconstructive surgeons. Autologous and allogeneic bone remains the graft materials of choice for surgical reconstruction of large bone defects owing to their clinical efficacy and minimal side effects. A clinical demand for bone graft substitutes exists, however, due to the limited availability of donor material. Commercial bone graft substitutes are available within the clinical setting, but are generally considered to possess inferior osteoconductive, osteoinductive, and osteogenic properties when compared to autologous or allogeneic graft [186]. A better undertanding of the biological basis for the superiority of bone graft in promoting tissue repair is needed to improve the design of graft substitutes for the repair of large bone defects.

Autologous bone graft consists of cellular and matrix components which are presumed to facilitate integration with host tissue following transplantation. The cellular component of autologous bone is associated with its superior osteogenic properties and includes osteoblasts, osteoclasts, osteocytes, and supporting stromal cells. The acellular component of bone is derived primarily from the bone extra-cellular matrix (ECM) and its associated biochemical cues which include growth factors and other signaling molecules secreted by bone cells. The acellular

component of bone has osteoconductive and osteoinductive properties, providing architectural support and creating a distinct biochemical environment that supports the formation and maintenance of bone [187,188]. The cellular and acellular components of bone graft possess immunologic properties which are incompletely understood [94,189]. Recent studies have demonstrated that a potent inflammatory response to damaged ECM and necrotic or stressed cellular components is also involved in tissue regeneration, highlighting a potential role for graft-induced inflammation in facilitating fracture healing [190,191]. Although considerable controversy exists regarding the exact role of inflammation during bone healing, inflammation is well recognized as an integral component of the injury response and has received increasing attention for its role in host tissue regeneration and repair [75,76]. The inflammatory response following bone injury is critical for the initiation of healing cascades, serving to recruit inflammatory and progenitor cells and to promote angiogenesis during the remodeling of damaged tissues [93]. A role for inflammation in graft-induced bone regeneration has been suggested, but is still not well understood.

Toll-like receptors (TLRs) play an essential role in innate recognition of microbial products and are critical activators of the innate immune response. Another unique role of TLRs is to sense cellular stress or tissue damage by responding to endogenous ligands released from necrotic cells and damaged tissues in many settings including musculoskeletal trauma [75,172]. TLR expression is primarily detected within macrophages, neutrophils, dendritic cells, and bone cells [159,177,192,193]. TLR4 signaling is of particular interest in regenerative biology due to its pronounced impact on healing in diverse models of injury and sterile inflammatory disease [159,160]. The impact of TLR4 activation on tissue homeostasis and regeneration partially depends upon organ setting and mode of injury. TLR4 signaling has been suggested to mediate bone destruction by inducing

inflammation and osteoclastogenesis [168,194-196]. In a previous study, we showed that calvarial bone healing is accelerated in TLR4 knock-out ($TLR4^{-/-}$) mice and is associated with elevated expression of cytokines and osteoclast differentiation markers [78]. Furthermore, our team has previously presented data suggesting that morselized bone graft induces a TLR4-dependent systemic inflammatory response in a bilateral femoral fracture model [104]. Based upon these observations, we hypothesized that TLR4 signaling is necessary for graft-induced bone formation by mediating the remodeling and integration of bone graft within regenerating calvarial defects. To test this hypothesis, we assessed calvarial bone healing using radiography, live computerized tomography, and histological analyses in WT and $TLR4^{-/-}$ mice engrafted with different fractions of morselized bone-enriched implants.

5.2 MATERIALS AND METHODS

5.2.1 Animal Care and Experimental Design

Wild type (WT) C57BL-6J mice (Jackson, Bar Harbor, ME) and $TLR4^{-/-}$ mice (from an ongoing breeding colony housed at the University of Pittsburgh), between 10 and 12 weeks of age (20-30 g) were utilized in this study. All mice were maintained in the Rangos Research Center Animal Facility, Children's Hospital of University of Pittsburgh with a 12:12 h light-dark cycle and free access to standard laboratory food and water. All procedures were carried out in accordance with the regulations regarding the care and use of experimental animals published by the National Institutes of Health and was approved by the Institutional Animal Use and Care Committee of the University of Pittsburgh.

5.2.2 Preparation of Bone Component Implants

In the current study, four different types of implants derived from morselized bone and PBS solution were implanted into the WT and TLR4$^{-/-}$ mice. The four implants included (1) "BC" group (morselized bone components), (2) "BC+TLR4 inhibitor" group and "BC+TLR4 inhibitor peptide control" group (morselized bone component mixing with TLR4 peptide inhibitor, or with its peptide control), (3) "CE" group (fractionated, cell-enriched portion of morselized bone component), and (4) "ME" group (fractionated, matrix-enriched portion of morselized bone component).

To generate implants, two femora and two tibiae were harvested from one donor WT mouse and were crushed with a mortar and pestle under sterile conditions, while bone marrow was not removed prior to crushing. The "BC" group was generated by resuspending the morselized bone in 1 mL of PBS. The "BC+TLR4 inhibitor" group was generated by resuspending the morselized bone in 1 mL of VIPER TLR4 neutralizing peptide (0.3mg/ml, IMGENEX, CA). To fractionate the "BC" group into its "CE" and "ME" groups, morselized bone resuspended in 1 mL of PBS was flushed through a 70-μm cell strainer (BD Biosciences, Bedford) and centrifuged at 1,200 rpm for 10 min. The resulting cellular pellets were resuspended in 1 mL of PBS to obtain the "CE" group. The remaining bone cortices were resuspended in 1 mL of PBS to derive the "ME" group. Cell counts of the "CE" group per animal showed approximately 6 to 8 × 10^5 nucleated cells per mL. The density of "ME" group was 200 to 300 mg/mL. Fractionated bone suspensions (300 μL) were mixed with 100 μL fibrinogen (10mg/mL) and 2 μL thrombin (Sigma-Aldrich, MO) and were incubated at 37°C for one hour before being implanted in the calvarial defect model. (Fig. 19) Sham controls received

no graft following surgery and vehicle controls were prepared in the absence of bone components.

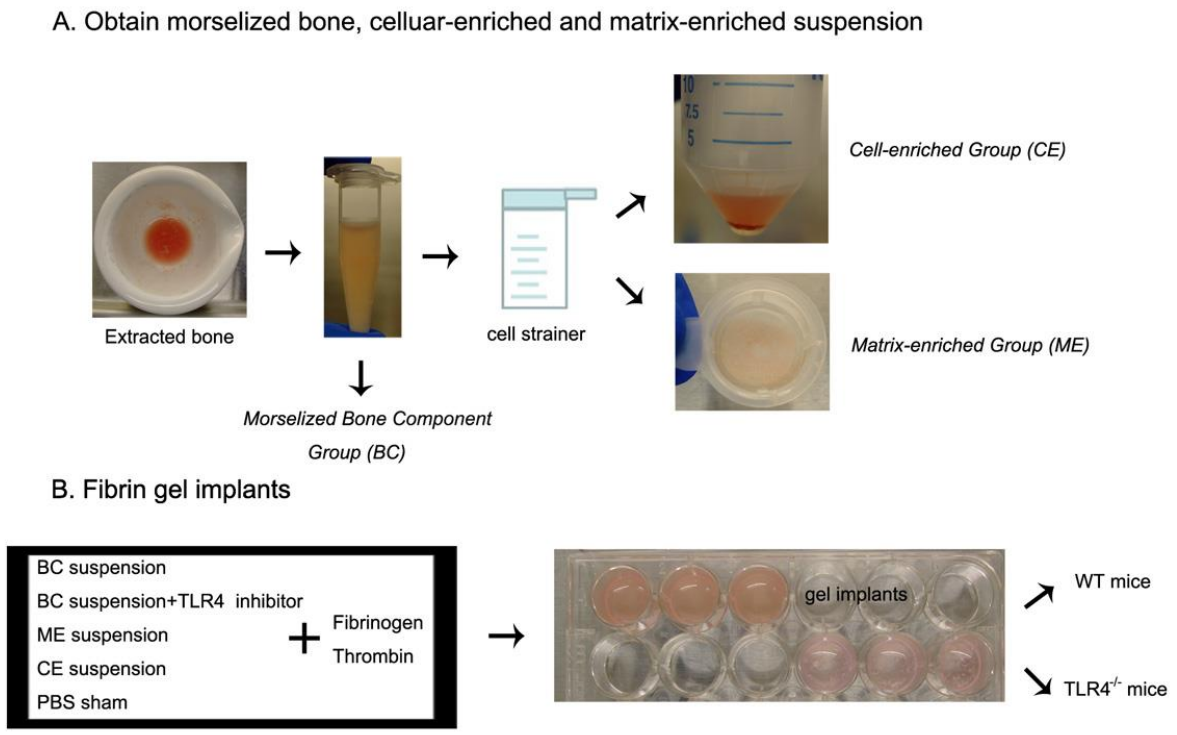

Figure 19: Preparation of bone component implants

(A) Morselized bone (BC), cell-enriched fraction of morselized bone (CE), and matrix-enriched fraction of morselized bone (ME) suspension preparation. (B) Fractionated bone suspensions (300 μL/each group) were mixed with fibrinogen and thrombin, and were incubated at 37°C for one hour before being implanted in the calvarial defect model.

As bone marrow was not removed prior to crushing the donor bones, CE suspension was considered to be rich in bone marrow lineage cells including hematopoietic cells, myelopoietic cells, erythropoietic cells, and mesenchymal stem cells; while ME suspension included mesenchymal stem cells, bone-, adipose-, muscle- residency cells [197-200]. To further characterize the CE and ME suspension, Syto® green-fluorescent nucleic acid staining (Life Technologies,

NY), Propidium Iodide staining (PI staining, Sigma-Aldrich, MO), PicoGreen® dsDNA Reagent and Kits (Life Technologies, NY), Near-infrared fluorescent probe image system (far-red fluorescent pamidronate, FRFP680, Osteosence, VisEn Medical, Bedford, MA) were applied according to manufacturer's instructions.

CE and ME suspension from three donor WT mice was separately diluted with PBS to 1 million cell per mL, and washed with sterilized PBS three times prior to following staining. Suspension was incubated with 5 μM Syto® green dye and 3 μM PI dye in dark at 37℃ for half an hour before observed under fluorescent microscopy. All specimens were imaged at 100X and 200X magnifications. FRFP680 is a fluorescently-labeled bisphosphanate that binds to mineral substrates, and has been utilized as a tool for monitoring bone remodeling and skeletal calcification *in vivo* [201]. To demonstrate the extent of matrix portion in CE and ME portion, three WT mice, between 10 and 12 weeks of age, were administrated FRFP680 at 10 nmol/100 μL by tail vein injection. Baseline tissue autofluorescence was examined in two WT mice with control saline injection. Mice were euthanized at twenty-four hours after FRFP680 administration. Femora and tibiae were harvested and imaged by IVIS imaging system (IVIS® lumina, Xenogen, Cranbury. NJ). CE and ME suspension were later collected as previously described and imaged by IVIS imaging system for fluorescence efficiency. To characterize the extent of dsDNA concentration in CE and ME portion, CE and ME solution from three donor mice were suspended in TE buffer and stained with PicoGreen® dsDNA reagent at room temperature in dark for 10 minutes. Fluorescence intensity was later measured using Synergy H1 Hybrid microplate reader (BioTek, Winooski, VT).

5.2.3 Calvarial Defect Model

A circular parietal defect was made using a 1.8 mm outer diameter trephine (Fine Science Tools, Foster City, CA) as previously described [78] to model craniofacial bone defects that result from trauma, craniofacial reconstruction, or management of tumors. Implants were created using a 5 mm outer diameter trephine (Fine Science Tools, Foster City, CA). Circular implants in the groups outlined above were placed on top of the 1.8mm calvarial defect. After implant placement, the scalp was closed with 4-0 Vicryl resorbable sutures. During surgery, sterile PBS was used for continuous irrigation at the defect site and 1 mg/kg ketoprofen (Fort Dodge Animal Health, Fort Dodge, IA) was administered immediately post-surgery as an analgesic.

5.2.4 Live Micro-computed Tomographic (μCT) and Radiographic Analyses

For characterization of three-dimensional (3D) calvarial defect healing process, bone healing was analyzed using a high-resolution μCT system (Inveon microCT, Siemens, Germany). At postoperative days 0, 7, 14 and 28, "BC" implanted WT and $TLR4^{-/-}$ groups, and "BC+TLR4 inhibitor" implanted WT group (average 7 each) were scanned using live μCT with a fixed isotropic voxel size of 63.8 μm. 3D images were reconstructed using Osirix software and region of interest (ROI) was defined as 4.0 $mm^2 \times 2.09$ mm. Qualitative and quantitative data were analyzed by Osirix software with a global fixed threshold of -330. Standard μCT measurements (bone volume fraction, BV/TV within the ROI; regenerated BV: BV-day0 BV) were calculated for each sample using Osirix software. "CE" and "ME" implanted WT and $TLR4^{-/-}$ mice were also sacrificed on postoperative day 28. Calvariae were harvested and fixed in 4%

paraformaldehyde for 24 hours. Radiographs were obtained using Faxitron MX-20 (Faxitron X-Ray, Lincolnshire, IL) with a 35 Kv exposure and a 45-second exposure time to analyze calvarial healing.

5.2.5 Histological Analyses

H&E and pentachrome staining was performed as described in our previous study [78]. Calvarial samples obtained from each group were harvested, fixed in 4% paraformaldehyde, decalcified in EDTA, dehydrated in a series of graded ethanol (EtOH) solutions and subsequently embedded in paraffin. 5-6 μm thick sections were obtained from paraffin-embedded specimens by sectioning through the coronal plane. Three regions of each circular defect, 50 μm apart, were cut and placed on slides (for a total of approximately 30 slides per animal). Slides were stained with Harris' hematoxylin & eosin (Surgipath Medical Industries, Richmond, IL) and Russell-movat pentachrome staining (American MasterTech, CA) for conventional, qualitative bright-field light microscopy. All specimens were imaged at 50X, 100X, 200X and 400X magnifications.

Immunohistochemical staining was performed as previously described. [78] Sections were deparaffinized with xylene solution and rehydrated through serially graded ethanol (EtOH) solutions. Antibodies were diluted in in 2% normal horse serum (Vector Laboratories, Burlingame, CA) and incubated with sections according to the manufacturer's instructions. Slides were incubated in goat polyclonal anti-F4/80 (Santa Cruz Biotechnology, Santa Cruz, CA; 1:250 dilution), goat polyclonal anti-osteopontin (anti-OPN, Santa Cruz Biotechnology, Santa Cruz, CA; 1:250 dilution), and rabbit polyclonal anti-cathepsin K (Abcam, MA; 1:250 dilution) for 30 minutes at room temperature. Slides were then incubated in biotinylated horse anti-goat secondary antibody (BA-9500, Vector Laboratories, Inc. CA, USA; 1:250 dilution) or

biotinylated goat anti-rabbit secondary antibody (Abcam, MA; 1:250 dilution), followed by Streptavidin-HRP (R&D systems, Gaithersburg, MD; 1:500 dilution). Color was developed by application of DAB kit (Vector Laboratories, Burlingame, CA). Sections were dehydrated and mounted prior to examination at 50 X, 100 X, 200X and 400 X magnifications.

Histomorphometric analysis was used to quantify two-dimensional bone formation using three to five slides per animal. New areas of bone formation were visually identified under 100X magnifications and measured using Northern Eclipse software (Empix Imagine, Inc., Mississauga, Ontario, Canada). Regions of new bone formation included areas at the defect as well as on both endo-and ecto-cranial surfaces of the calvaria within ROI. (Fig. 20) The sums total of newly formed bone areas were averaged by the number of slides per animal.

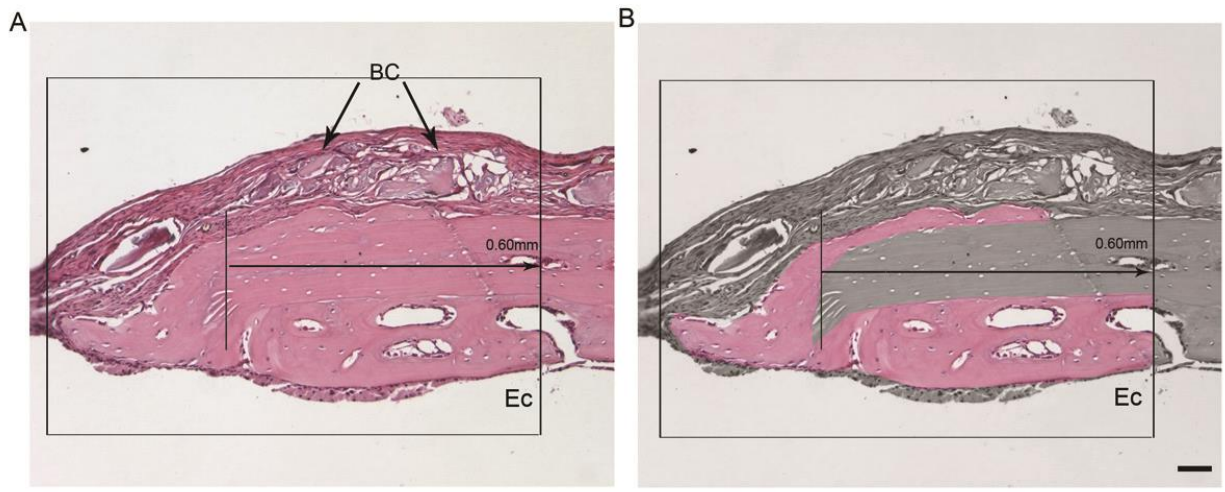

Figure 20: Histomorphometric analysis method

Microscopic images of the histological sections under 100X magnification were analyzed. (A) Representative images showed H&E stained slides at 100X magnification. Rectangle indicated ROI we used for histomorphometric analysis. The defect margin was identified (left vertical line). Since new bone formation occurred on both inside the defect as well as in the outside region surrounding the defect, a second margin was demarcated (right vertical line 0.60 mm away from the defect margin). The distance for this second margin was chosen such that the majority of all new bone formation that occurs outside the defect margin was included for analysis. (B) New areas of bone

formation were identified by visual inspection up to the second margin (shown in color). This region excluded newly regenerated bone from the implanted graft. (Scale bar: 50 μm; Ec: endocortical side)

Anti-cathepsin K staining was used for visualizing the osteoclast infiltration. Cathepsin K-positive cells attaching the bone surface were counted under 200X. Numbers of osteoclasts per total bone surface area (N.OC/BS; n/mm) were calculated. Data were expressed as mean area ± SEM.

5.2.6 Statistical Analysis

Statistical analyses were performed using SPSS v.20.0 software (SPSS, Inc, Chicago, IL). Mean areas of newly-formed bone by time points, numbers of osteoblasts per bone surface area, and numbers of osteoclasts per bone surface areawere compared among groups using One-way ANOVA followed by Post-hoc LSD test. A *p* value less than or equal to 0.05 was considered significant.

5.3 RESULTS

5.3.1 Characterization of BC, CE and ME Implants

Characterization of CE and ME suspensions indicated good separation of grounded bone graft (BC group) into CE and ME portions (Fig.21). Both CE and ME suspensions contained similar percentages of live cells with around 44.5% live cells in CE suspension and 46.6% live cells in ME suspension. The CE suspension contained 22 million cells per mL while the ME suspension

contained 0.32 million cells per mL in the ME suspension (Fig.21A). IVIS imaging results showed that majority of FRFP fluorescent labeling was detected in the ME portion. Fluorescent efficiency in CE portion was similar compared to baseline control group without FRFP administration (Fig.21B). Picogreen® analysis demonstrated that there were average 38038.30 ± 817.95 ng/ml dsDNA in CE portion and average 5590.11 ± 2114.96 ng/ml dsDNA in ME portion (Fig.21C).

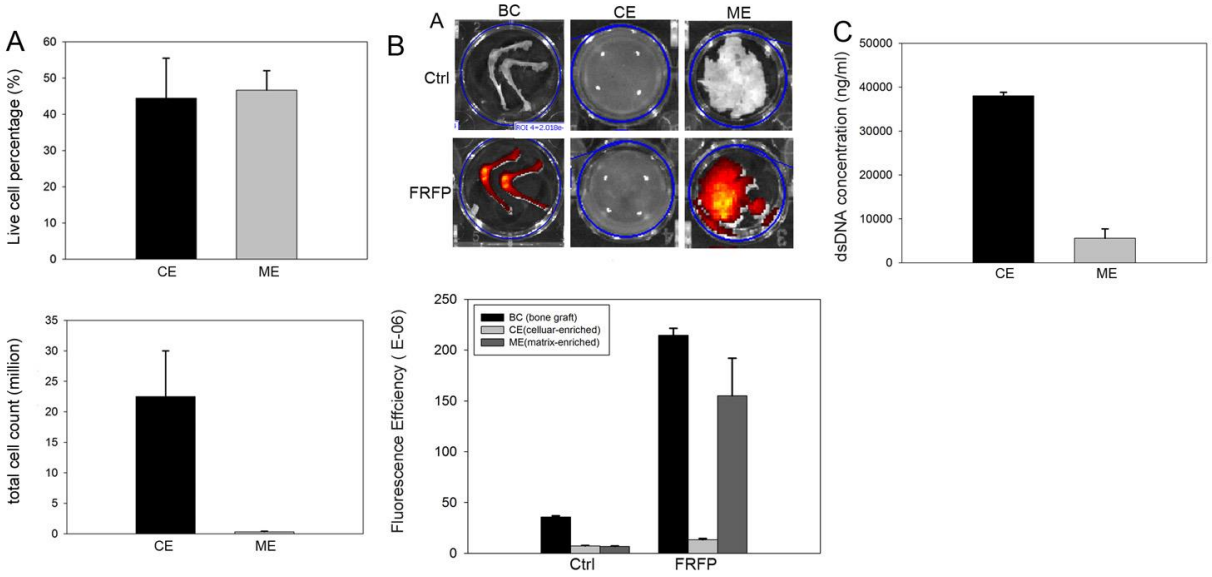

Figure 21: Characterization of implants

(A) Live-dead cell analysis was characterized using Syto®green-fluorescent nucleic acid staining and Propidium Iodide staining. Quantitative analysis from stained images showed there was around 22 million cells (44.5% live cells) in CE solution and 0.32 million cells (46.6% live cells) in ME solution. (B) IVIS images showed FRFP fluorescent labeling in whole BC graft, CE and ME portion. IVIS images demonstrated a comparable fluorescent efficiency between BC graft and ME portion. CE portion showed similar fluorescent efficiency to baseline control group without FRFP fluorescent reagent administration. (C) Picogreen® staining kit was used to determine dsDNA concentration in CE and ME solution. Quantitative results showed that around 38038.30 ± 817.95 ng/ml dsDNA in CE solution and 5590.11 ± 2114.96 ng/ml dsDNA in ME solution.

5.3.2 Delayed Calvarial Healing in Absence of TLR4 Signaling after Bone Graft Implantation

In order to understand the role of TLR4 signaling in bone graft-induced calvarial defect healing, BC (morselized bone component) implants, with and without a TLR4 inhibitor, were placed within calvarial defects of WT mice. BC was implanted in $TLR4^{-/-}$ mice as well. Vehicle controls were included for both WT and $TLR4^{-/-}$ mouse strains. Representative 3D reconstruction images of μCT of three implant groups are shown (Fig. 22A). Qualitative and quantitative analyses of the calvarial defects revealed more mineralized tissue in the BC implanted WT group than either the BC implanted $TLR4^{-/-}$ group or the BC+TLR4 inhibitor implanted WT group. Larger areas of mineralized tissue were visible within the defect and adjacent to the implants in the BC implanted WT group at designated time points compared to the other two groups. Morselized bone graft, however, remained relatively unchanged in $TLR4^{-/-}$ mice or in WT mice when mixed with TLR4 inhibitor (Fig. 22A).

Measurements from μCT analysis revealed that bone volume fraction was significantly larger in the BC WT group (BV/TV: 28.46±6.88%) than in the BC $TLR4^{-/-}$ group (BV/TV: 17.15±1.47%, $p<0.05$) on day28. No significant difference in bone healing was observed between "BC+TLR4 inhibitor" WT group and BC $TLR4^{-/-}$ group on postoperative day 7, day 14 or day 28 (Fig.22B). The BC WT group showed significantly larger volume of regenerated mineralized tissue compared to the WT vehicle control group at postoperative days 14 and 28. No significant differences in regenerated bone volume were observed between BC $TLR4^{-/-}$, BC+TLR4 inhibitor WT and $TLR4^{-/-}$ vehicle control groups (Fig. 22C). No significant difference

in bone volume fraction was observed between BC WT group and BC+TLR4 inhibitor control peptide group (Fig.23)

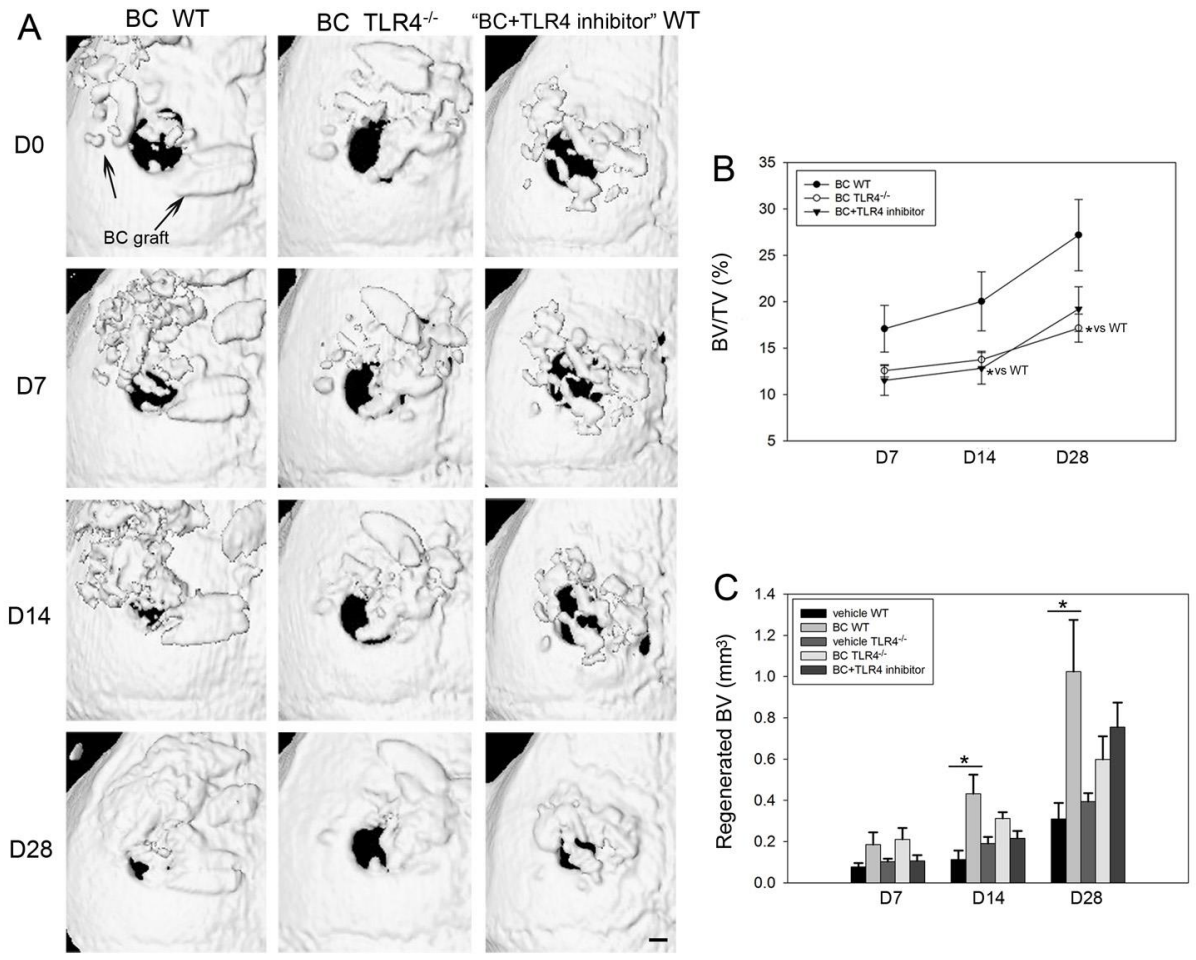

Figure 22: Live μCT analysis of WT and TLR4$^{-/-}$ graft recipients

WT recipients were engrafted with BC in the presence or absence of TLR4 inhibitor, and TLR4$^{-/-}$ recipients were engrafted with BC only. Calvarial bone repair was measured over 28 days using μCT. (A) Representative 3D reconstructions of calvarial defects in the transverse plane at postoperative days 0, 7, 14 and 28. Each group received a similar amount of graft material at day 0. Faster healing was evident in BC implanted WT mice than the other two groups. (B) Quantitative data based on μCT analysis revealed that bone volume fraction (BV/TV) in BC WT mice was larger relative to the other two groups. (C) More regenerated mineralized tissue was observed in the BC WT group than in the WT vehicle control group. Comparable healing was observed in the BC TLR4$^{-/-}$, BC+TLR4

inhibitor WT, and TLR4$^{-/-}$ vehicle control group on day 28. (BC: morselized bone components; scale bar: 500 μm; mean ± SEM; * p<0.05).

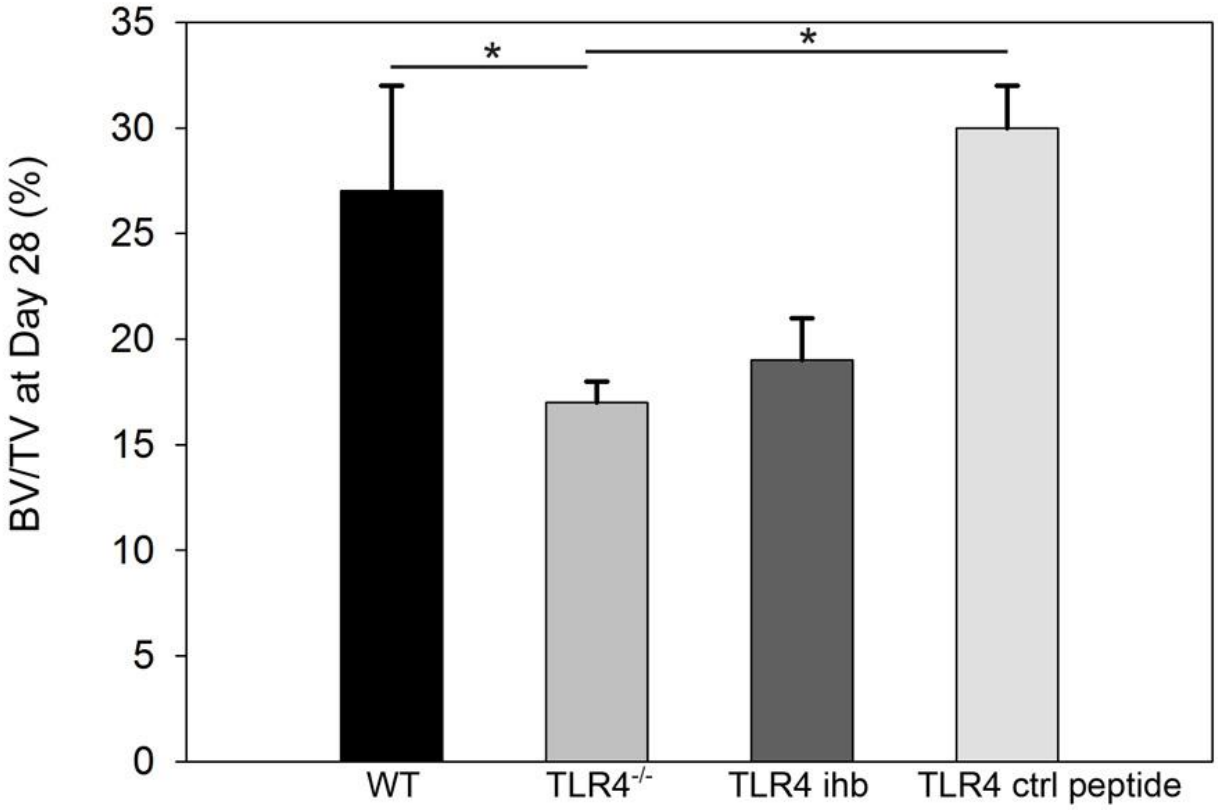

Figure 23: μCT analysis of WT and TLR4$^{-/-}$ graft recipients

Quantitative data based on μCT analysis revealed that bone volume fraction (BV/TV) in BC WT mice and "BC+TLR4 inhibitor peptide control" WT was larger relative to the other two groups. No significant differences were observed between "BC+TLR4 inhibitor" WT and BC TLR4$^{-/-}$, and between BC WT mice and "BC+TLR4 inhibitor peptide control" WT mice. (BC: morselized bone components; mean ± SEM; * p<0.05)

5.3.3 Accelerated Intramembranous Bone Formation and Active Graft-remodeling in WT, but not in TLR4$^{-/-}$ Mice after BC implantation

Histological characterization revealed early evidence of intramembranous bone formation accompanied by greater osteoblast and macrophage infiltration and more intense periosteal and dural cellularity in WT mice compared to TLR4$^{-/-}$ mice after BC implantation (Figs.24, and Fig.25). On day 7, BC WT mice exhibited more pronounced evidence of newly-formed, highly cellularized-woven bone along the endocortical (dural) side of the calvarial bone and along the defect perimeter than observed in control WT mice. Newly-regenerated woven bone was visible in the TLR4$^{-/-}$ control group, while BC TLR4$^{-/-}$ mice showed little-to-no obvious mineralization on day 7 (Fig.24A). Histomorphometric analysis on day 7 showed significantly more bone formation in the BC WT group compared to the WT sham control group and the BC TLR4$^{-/-}$ group, also WT control group compared to TLR4$^{-/-}$ sham group. No significant difference was found between the BC TLR4$^{-/-}$ group and the TLR4$^{-/-}$ sham control group (Fig.24B).

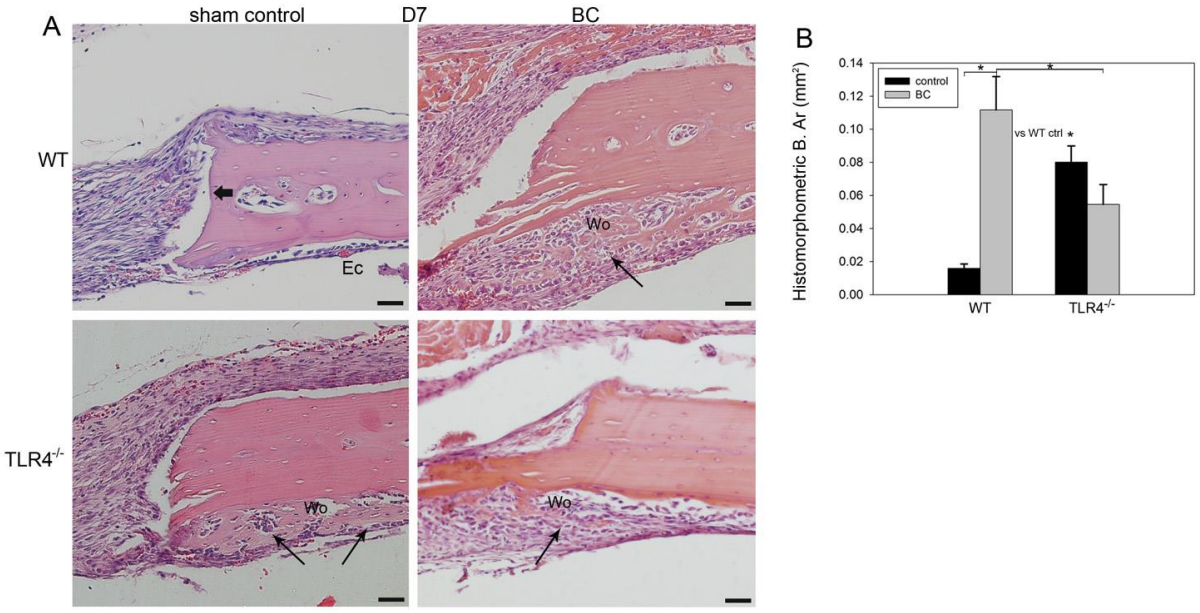

Figure 24: Histology and histomorphometric analysis of calvarial bone repair in WT and TLR4$^{-/-}$ graft recipients at post-operative day 7

(A) Representative H&E stained images of WT or TLR4$^{-/-}$ mice with and without BC implants on day 7. Cellularized woven bone formation was elevated in the BC WT group compared to the other three groups on day 7. (B) Histomorphometric analysis revealed more newly regenerated bone in BC WT mice compared to WT sham control and BC TLR4$^{-/-}$ group, also TLR4$^{-/-}$ sham group compared to WT control group. Comparable healing was observed in the BC TLR4$^{-/-}$ group and TLR4$^{-/-}$ sham control group on day 7. (Scale bar: 50 μm; bolded arrow indicated defect margin; Ec: endocortical side; Wo: woven bone; mean ± SEM; * p<0.05).

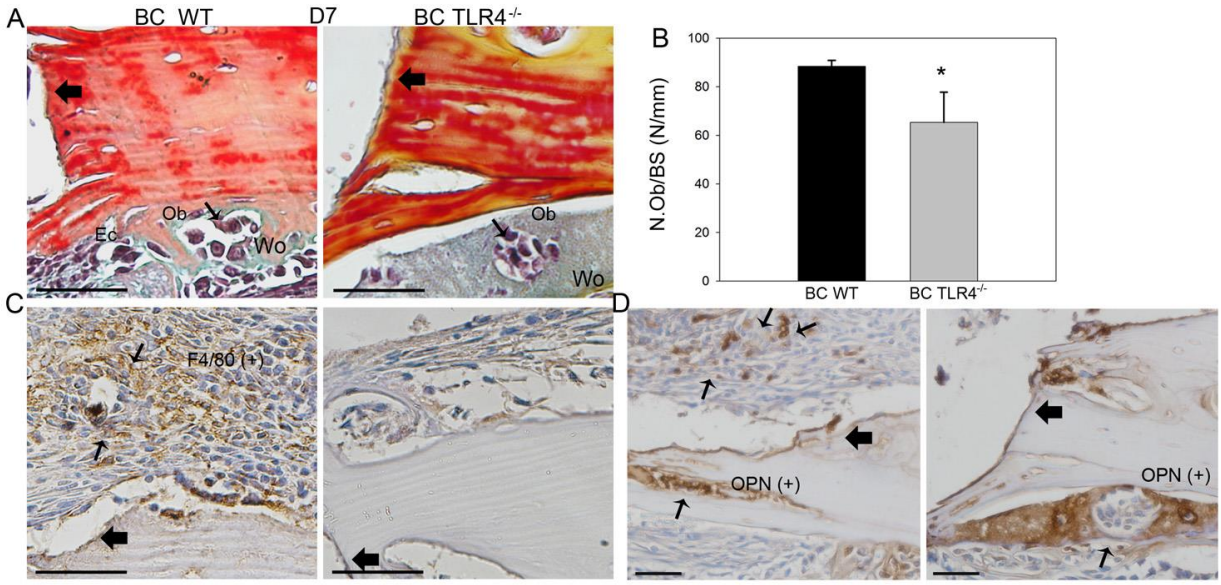

Figure 25: Cell population dynamics in WT and TLR4$^{-/-}$ graft recipients

BC implanted WT mice had more osteoblast and macrophage infiltration versus TLR4$^{-/-}$mice. (A-B) Following pentachrome staining, cuboidal OBs and osteocytes were observed on the endocortical side of the calvarial bone in WT group, whereas fewer OBs with a flatter morphology were observed in the TLR4$^{-/-}$ group in presence of morselized bone components. Larger areas of mineralized woven bone were evident in WT compared to TLR4$^{-/-}$ group. (C) Immunohistochemical staining revealed more intense F4/80 positive macrophage infiltration in the periosteum of BC WT mice compared to BC TLR4$^{-/-}$ mice. (D) Intense OPN staining was evident in both WT and

TLR4$^{-/-}$ mice after engraftment with morselized bone. (Scale bar: 50 μm; bolded arrow indicated defect margin; Ec: endocortical side; Ob: osteoblasts; Wo: woven bone; mean ± SEM; *p<0.05).

To detect osteoblast and macrophage lineage cell infiltration, pentachrome staining, OPN and F4/80 immunohistochemistry staining were performed on day 7 slides in BC WT and BC TLR4$^{-/-}$ mouse groups. On day 7, more bone surface lining mononucleated osteoblasts and woven bone were evident in BC WT group than in BC TLR4$^{-/-}$ group (Fig. 25A). These observations were consistent with the osteoblast count based on pentachrome staining analysis (Fig. 25A, 25B). Positive F4/80 macrophage lineage cells were observed in the BC WT group, especially in the regenerated periosteal region, whereas no obvious F4/80 positive cells were evident in the BC TLR4$^{-/-}$ group on day 7 (Fig.25C). Intense OPN staining was observed in both the BC implanted WT and TLR4$^{-/-}$ groups (Fig.25D).

On day 28, remodeled woven bone matrix and thickened periosteum were observed in all three experimental groups. In addition, Howship's lacunae at the edge of the graft implants and bony union of grafts and recipients were observed in WT group. In contrast, fibrous encapsulation of morselized bone components was observed in TLR4$^{-/-}$ graft recipients (Fig.26A). Histomorphometric measurements of newly regenerated bone area indicated no significant difference among the three groups (Fig.26B; BC WT group: 0.14±0.01mm^2; BC TLR4$^{-/-}$ group: 0.19±0.04 mm^2; BC+TLR4 inhibitor WT group: 0.15±0.02mm^2). More intense OPN staining showing evidence of bone resorption near scalloped edges of the BC grafts (Fig. 27A) and significantly more intense cathepsin K stained osteoclasts were observed in the WT group than in the TLR4$^{-/-}$ group (Fig.27B and 27C).

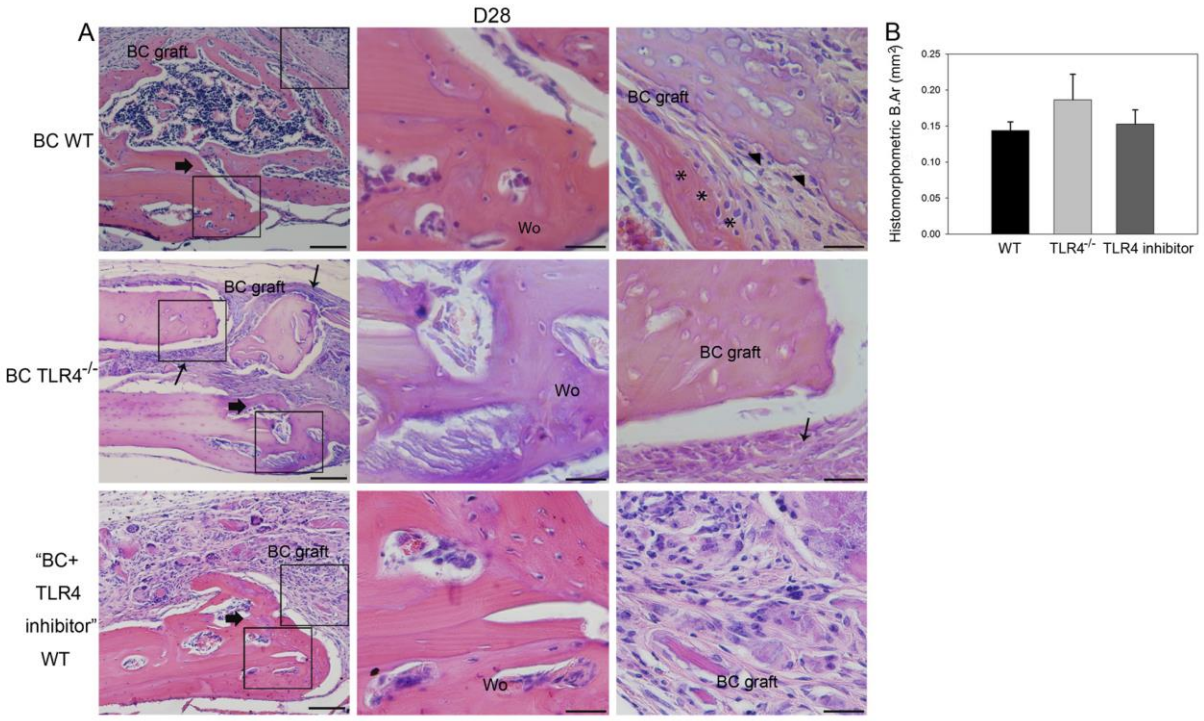

Figure 26: Histology and histomorphometric analysis of calvarial bone repair in WT and TLR4$^{-/-}$ graft recipients at post-operative day 28

(A) Representative H&E stained images of the BC implanted WT, BC implanted TLR4$^{-/-}$ mice and "BC+TLR4 inhibitor" implanted WT groups. Newly-formed woven bone on the outer periphery of the BC implant (*) and Howship's lacunae (arrow heads) were observed in WT mice, suggesting the presence of active remodeling. In TLR4$^{-/-}$ mice, fibrous encapsulation of morselized BC (arrow) was observed with little-to-no signs of remodeling. (B) Histomorphometric analysis revealed similar area of regenerated bone among the three groups on day 28. (Scale bar: 50 μm; bolded arrow indicated defect margin; * indicated newly-regenerated bone on the surface of grafts; BC: morselized bone component implants; Wo: woven bone; B.Ar: bone area; mean ± SEM).

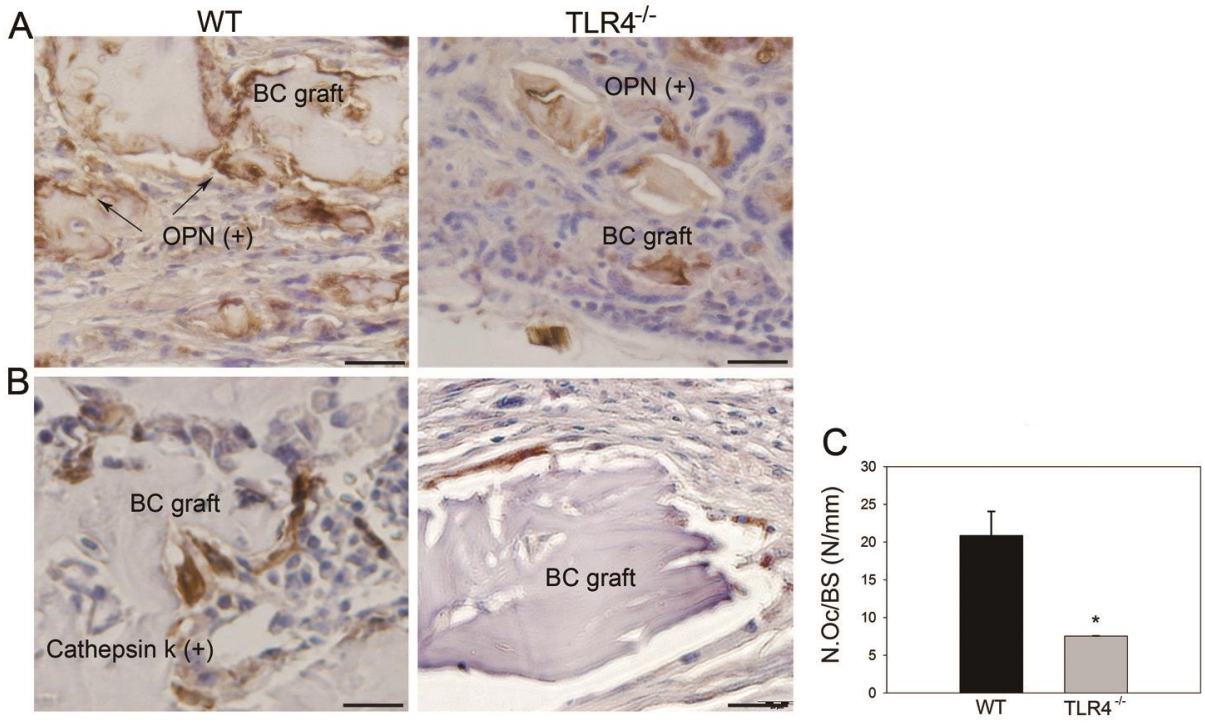

Figure 27: Representative images showing OPN and cathepsin K stained slides of BC implanted WT and TLR4$^{-/-}$ mice on day 28

More intense OPN staining (A) showing evidence of bone resorption near scalloped edges of the grafts, and more intense cathepsin K staining (B) indicating more osteoclast infiltration was observed in WT mice compared to TLR4$^{-/-}$ mice. (C) Histomorphometric analysis revealed significantly more cathepsin K stained osteoclast infiltration in WT mice than TLR4$^{-/-}$ mice. (Scale bar: 50 µm; mean ± SEM; *p<0.05)

5.3.4 The Matrix-enriched Fraction of Morselized Bone Enhanced Calvarial Healing in WT Mice, not in TLR4$^{-/-}$ Mice

In order to determine the impact of bone graft component on calvarial repair, cell-enriched (CE) and matrix-enriched (ME) bone fractions were implanted in the calvarial defects in WT mice. On day 28, an overall more intense reaction of periosteum was shown in the ME group compared to the CE group. Remodeling bone matrix was evident in the soft tissue covering the defect in the

ME group (Fig. 28A). To determine if TLR4 signaling plays a role in matrix-induced calvarial defect healing, the CE and ME implants were similarly placed in calvarial defects in $TLR4^{-/-}$ mice. Histological characterization revealed that CE and ME implant groups presented a similar healing pattern in $TLR4^{-/-}$ mice on postoperative day28. The majority of woven bone formation was evident on the endocortical side of the calvarial bone and adjacent to the original defect in both groups in $TLR4^{-/-}$ mice (Fig. 28B).

Histomorphometric measurements showed significantly more newly-formed bone in the ME group ($0.18\pm0.01mm^2$) compared to CE ($0.13\pm0.02mm^2$, $p<0.05$) and vehicle control ($0.12\pm0.00mm^2$, $p<0.05$, data no shown) groups in WT mice on postoperative day28. No significant difference was shown between CE ($0.18\pm0.00mm^2$) and ME ($0.17\pm0.04\ mm^2$) groups in $TLR4^{-/-}$ mice on day28 (Fig. 28C). Calculation of newly-formed bone area based on radiographic images (Data not shown) on postoperative day28 revealed significantly more new bone formation in the ME group ($1.70\pm0.13mm^2$; 66.79% healing) than in the CE group ($1.01\pm0.11mm^2$, 39.91% healing, $p<0.05$) and the vehicle control group ($0.65\pm0.12mm^2$, 25.59% healing, $p<0.001$, data not shown) in WT mice. CE and ME implanted $TLR4^{-/-}$ mice exhibit comparable bone healing (CE: $0.90\pm0.14mm^2$; 35.43% healing; ME: $1.05\pm0.16mm^2$, 41.34% healing; Fig.28D).

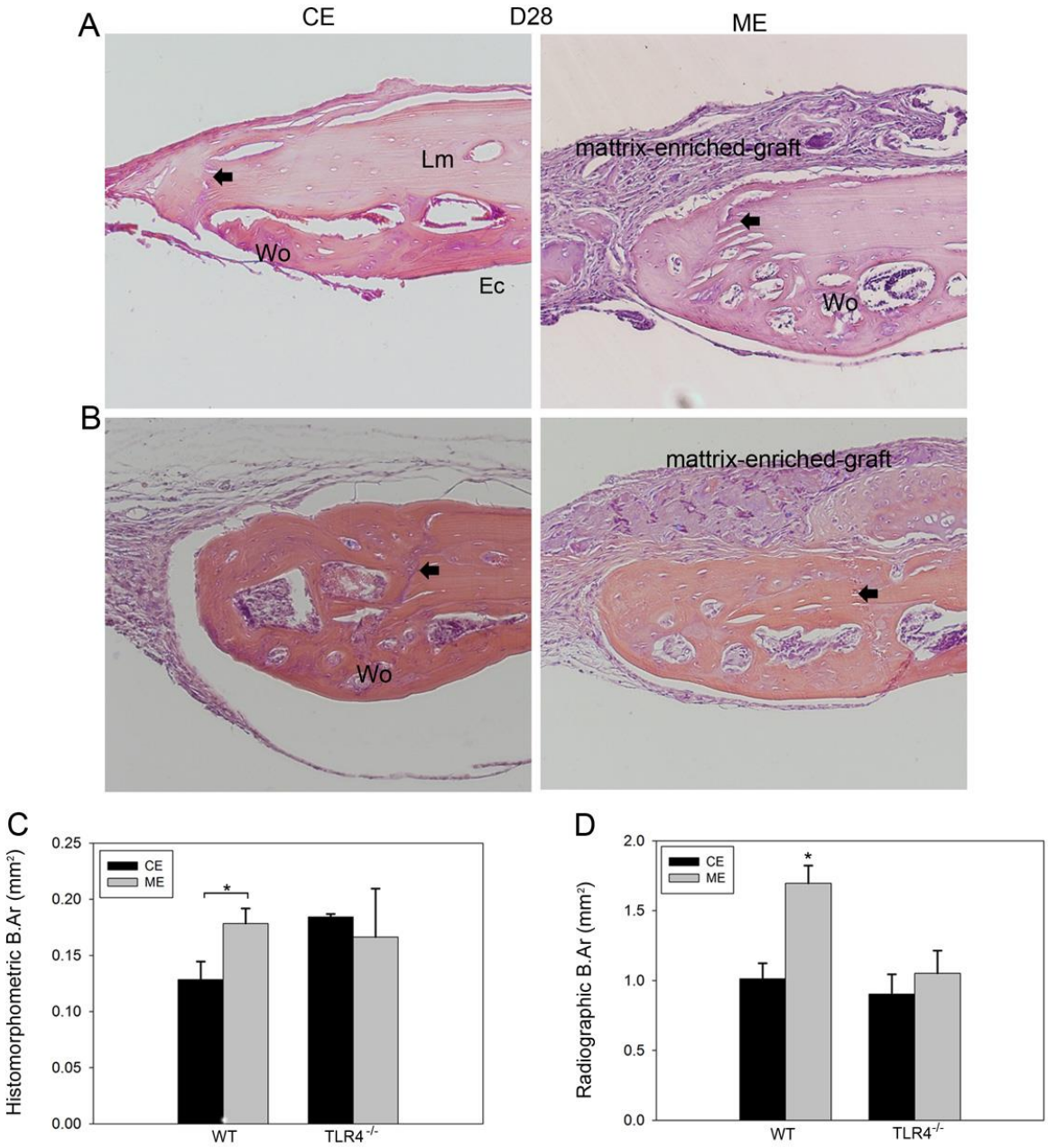

Figure 28: Histology and histomorphometric analysis of WT and TLR4$^{-/-}$ mice engrafted with fractionated bone components at day 28

Representative images showing H&E stained slides of CE and ME implanted WT (A) and TLR4$^{-/-}$ (B) mice on day 28. Notice: larger area of new bone at the endocortical side in ME implanted WT mice than CE group, and a similar healing pattern after ME and CE were implanted in TLR4$^{-/-}$ mice. On day 28, histomorphometric (C) and radiographic (D) analyses revealed more bone formation in the ME group than the CE group in WT mice. No

significant differences in bone formation were observed between CE and ME implanted TLR4$^{-/-}$ mice. (Scale bar: 50 μm; CE: cell-enriched implant; ME: matrix-enriched implant; arrow indicated defect margin; Ec: endocortical side; Wo: woven bone; Lm: lamellar bone; B.Ar: bone area; mean ± SEM; * p<0.05).

5.4 DISCUSSION

Although various engineered materials including ceramics and metal implants have been developed for bone repair, autologous and allogeneic bone implants remain the graft materials of choice for bone reconstruction. The successful integration of implant material with the host requires the implanted bone graft to undergo remodeling and the induction of the healing cascade. The TLR receptors play a unique role in tissue repair by helping to regulate the innate inflammatory response to damage. Here, our data highlight a critical role for TLR4 signaling in graft-mediated calvarial repair.

The impact of inflammation on healing is complex and may be either beneficial or detrimental to repair [202,203]. Recent advances in our understanding of the innate immune response have helped to distinguish between tissue-protective and tissue-destructive inflammatory signaling pathways [90]. In a previous study, accelerated bone healing within a calvarial defect model was observed in TLR4$^{-/-}$ mice, suggesting that TLR4 signaling is detrimental to the normal healing of calvarial bone defects [78]. In contrast to our previous findings, we report here that TLR4 is *required to support graft-induced bone repair* using a calvarial defect model. At day 7 after implantation, WT mice showed more F4/80 positive macrophage lineage cell infiltration, while macrophages were not detected in TLR4$^{-/-}$ mice after bone component implantation. Inflammation promotes cell proliferation and migration into the fracture site to

trigger the repair and healing response within damaged bone [76,90]. In addition, we showed that surgical implantation of morselized bone into damaged soft tissue induced a deleterious, TLR4-dependent, systemic inflammatory response [104]. Together, these data suggest that TLR4 functions differently in our two models of craniofacial bone injury and repair. Specifically, TLR4 function delays normal bone healing, but is essential for graft-induced bone formation. The results we present here suggest that certain molecular signals within bone graft require TLR4 signaling to induce bone healing. Whether allograft or synthetic graft material-assisted healing also need TLR4 signaling, or manipulating TLR4-induced inflammatory response will assist in allograft or biomaterials-mediated bone healing requires better investigation.

BC grafts were obtained from different mice of the same strain (WT, C57BL-6J). Thus, grafts were considered to be allogeneic in source [204-207]. Allogeneic bone is frequently employed as a decellularized graft material, but is generally inferior to autologous bone graft and exhibits inferior remodeling upon implantation. Coating of structural allografts with RANKL and VEGF resulted in marked remodeling, improved vascularization, and enhanced bone repair, however, suggesting an essential role for remodeling in forming bony unions between grafts and host bone tissue [208]. Our results support and extend this finding by suggesting that modulator of the innate immune response (TLR4) is required for graft remodeling and for subsequent bone healing. In our study, engraftment of WT mice with BC grafts resulted in earlier mineralization, more pronounced infiltration of regenerating tissue with osteoblasts, and more F4/80 stained macrophage infiltration relative to $TLR4^{-/-}$ recipients at day 7 (Fig.2, 3). At day 28, implanted grafts in WT recipients showed irregular reversal lines and evidence of remodeling, whereas grafts in $TLR4^{-/-}$ recipients showed relatively smooth margins and no obvious signs of remodeling (Fig.4 and Fig.5). Qualitative and quantitative μCT analyses revealed graft-enhanced

repair in WT mice, but not in TLR4$^{-/-}$ mice. Moreover, inhibition of TLR4 suppressed healing in WT graft recipients, resulting in healing rates similar to those observed in TLR4$^{-/-}$ graft recipients between days 7 and 14. Healing was accelerated in the inhibitor group at later time points, presumably due to a decline in the local concentration of the inhibitor and restoration of TLR4 signaling over time. Because there was little or no evidence of graft remodeling (normally caused by osteoclastic destruction of the bone graft surface) in mice lacking the TLR4 gene, it is likely that TLR4 signaling is needed to induce graft remodeling.

We also sought to determine which fraction of bone graft triggers TLR4-dependent bone healing. It has been argued that the regenerative potential of bone graft is dependent upon the efficient transfer of progenitor cells to the defect site [191,192], although donor cells typically fail to survive beyond hours to weeks [193,194]. In our previous work [78], we used radiographic bone measurement to assess bone repair in a calvarial defect model and observed that 33.14% of the defect had regenerated by day 28 in WT mice, while the current study showed that BC and ME (matrix-enriched) groups achieved 74.80% and 66.79%, respectively (Fig.6). The CE (cell-enriched) implant, in contrast, failed to stimulate bone repair beyond control values. Furthermore, comparable levels of healing were observed in both ME- and CE- engrafted TLR4$^{-/-}$ mice (Fig.6). These combined observations suggest that the matrix-bearing fraction of morselized bone bears primary responsibility for graft-induced bone regeneration and this bone healing effect is also partially TLR4 dependent. Disparities between our findings and those reported in other studies [209,210] may be due to the differences in graft fractionation procedures.

Several points of considerations should be noted in this study including our use of a larger graft and approach for measuring bone formation. Firstly, the graft size was designed to be larger than the defect size to facilitate stable placement of grafts on the top of the calvarial defect

site, thereby ensuring consistency among all recipient mice. Secondly, we employ separate approaches for measuring bone formation (μCT and histolomorphometric analyses). In our μCT analysis, we measured all mineralized tissue within the ROI, thus including both regenerated host new bone and remodeled bone graft. However, in our histomorphometric analysis, only newly-regenerated host bone was measured as some bone grafts remained as tiny pieces which made it challenging to accurately measure remodeled bone grafts (suppl Fig.2). As a result, a slight discrepancy exists between our μCT and histomorphometric analysis (Fig.1B and Fig. 6C). This discrepancy also explains the lack of significant differences among "BC WT", "BC TLR4$^{-/-}$ ", and "BC+TLR4 inhibitor WT" groups in histomorphometric measurements (Fig.4). However, this slight discrepancy in measurement does not alter the key finding of the study.

In summary for this chapter, our results suggest that the healing effect of bone graft was inhibited without TLR4 signaling using a TLR4 gene knockout mouse model or the local delivery of TLR4 peptide inhibitor. These observations together establish an important and novel role of TLR4 in the healing effect driven by bone graft, especially the matrix-enriched fraction. Future work will seek to identify the molecular signals released from bone graft or the ECM component that is recognized by TLR4 and capable of inducing bone remodeling and bone formation.

In my study, I aimed to understand the role of TLR4-associated pathway mediators in calvarial bone healing in the absence and presence of allograft implantation. In the 2nd , 3rd and 4th chapters, the results showed that dendritic cell expression of TLR4-mediated MyD88 signaling was detrimental for calvarial bone healing. In addition, TLR4 depletion in myeloid cells also resulted in accelerated bone healing via enhanced osteoclastogenesis within a non-compromised calvarial defect model. While in the 5th chapter, lacking TLR4 signal after allograft

implantation leaded to decreased osteoclast-mediated graft remodeling and subsequential inhibited bone healing, establishing an important and novel role of TLR4 in graft-mediated bone repair. Taken together, my study suggests that TLR4 might have a regulatory role in skeletal homeostasis, due to its regulating of osteoclastogenesis. As such, in the future, appropriate modulation of TLR4 signaling can be used to initiate early healing after fracture or adding TLR4 signaling for graft-mediated therapy to improve clinical outcomes.

BIBLIOGRAPHY

1 Coronado, V. G. *et al.* Surveillance for traumatic brain injury-related deaths--United States, 1997-2007. *Morbidity and mortality weekly report. Surveillance summaries* **60**, 1-32,(2011).

2 Finkelstein, E., Corso, P. S. & Miller, T. R. *The incidence and economic burden of injuries in the United States*. (Oxford University Press, 2006).

3 Surgeons, A. A. o. N. in *National Neurosurgical Procedural Statistics* (2006).

4 Mark Faul, L. X., Marlena M. Wald, Victor G. Coronado. *Traumatic Brain Injury in the United States: Emergency Department Visits, Hospitalizations and Deaths 2002–2006*. 1-74 (Centers for Disease Control, 2010).

5 Fazzalari, N. L. Bone remodeling: A review of the bone microenvironment perspective for fragility fracture (osteoporosis) of the hip. *Seminars in cell & developmental biology* **19**, 467-472,(2008).

6 Franz-Odendaal, T. A. Induction and patterning of intramembranous bone. *Frontiers in bioscience* **16**, 2734-2746,(2011).

7 Szpalski, C., Barr, J., Wetterau, M., Saadeh, P. B. & Warren, S. M. Cranial bone defects: current and future strategies. *Neurosurgical focus* **29**, E8,(2010).

8 Noden, D. M. Patterns and organization of craniofacial skeletogenic and myogenic mesenchyme: a perspective. *Progress in clinical and biological research* **101**, 167-203,(1982).

9 Couly, G. F., Coltey, P. M. & Le Douarin, N. M. The triple origin of skull in higher vertebrates: a study in quail-chick chimeras. *Development* **117**, 409-429,(1993).

10 Weston, J. A. & Thiery, J. P. Pentimento: Neural Crest and the origin of mesectoderm. *Developmental biology*,(2015).

11 Chung, U. I., Kawaguchi, H., Takato, T. & Nakamura, K. Distinct osteogenic mechanisms of bones of distinct origins. *Journal of orthopaedic science : official journal of the Japanese Orthopaedic Association* **9**, 410-414,(2004).

12 Leucht, P. *et al.* Embryonic origin and Hox status determine progenitor cell fate during adult bone regeneration. *Development* **135**, 2845-2854,(2008).

13 Chan, Charles K. F. *et al.* Identification and Specification of the Mouse Skeletal Stem Cell. *Cell* **160**, 285-298,(2015).

14 Kobayashi, T. & Kronenberg, H. in *Skeletal Development and Repair* Vol. 1130 *Methods in Molecular Biology* (ed Matthew J. Hilton) Ch. 1, 3-12 (Humana Press, 2014).

15 Provot, S. & Schipani, E. Molecular mechanisms of endochondral bone development. *Biochemical and biophysical research communications* **328**, 658-665,(2005).

16 Hunziker, E. B. Mechanism of longitudinal bone growth and its regulation by growth plate chondrocytes. *Microscopy research and technique* **28**, 505-519,(1994).

17 Eames, B. F. & Helms, J. A. Conserved molecular program regulating cranial and appendicular skeletogenesis. *Developmental dynamics : an official publication of the American Association of Anatomists* **231**, 4-13,(2004).
18 Lefebvre, V., Li, P. & de Crombrugghe, B. A new long form of Sox5 (L-Sox5), Sox6 and Sox9 are coexpressed in chondrogenesis and cooperatively activate the type II collagen gene. *The EMBO journal* **17**, 5718-5733,(1998).
19 Eames, B. F., de la Fuente, L. & Helms, J. A. Molecular ontogeny of the skeleton. *Birth defects research. Part C, Embryo today : reviews* **69**, 93-101,(2003).
20 Holleville, N., Quilhac, A., Bontoux, M. & Monsoro-Burq, A. H. BMP signals regulate Dlx5 during early avian skull development. *Developmental biology* **257**, 177-189,(2003).
21 Beniash, E. Biominerals--hierarchical nanocomposites: the example of bone. *Wiley interdisciplinary reviews. Nanomedicine and nanobiotechnology* **3**, 47-69,(2011).
22 Aszodi, A., Hunziker, E. B., Olsen, B. R. & Fassler, R. The role of collagen II and cartilage fibril-associated molecules in skeletal development. *Osteoarthritis and cartilage / OARS, Osteoarthritis Research Society* **9 Suppl A**, S150-159,(2001).
23 Prince, M. *et al.* Expression and regulation of Runx2/Cbfa1 and osteoblast phenotypic markers during the growth and differentiation of human osteoblasts. *Journal of cellular biochemistry* **80**, 424-440,(2001).
24 Wigner, N. A., Soung do, Y., Einhorn, T. A., Drissi, H. & Gerstenfeld, L. C. Functional role of Runx3 in the regulation of aggrecan expression during cartilage development. *Journal of cellular physiology* **228**, 2232-2242,(2013).
25 Lai, L. P. & Mitchell, J. Indian hedgehog: Its roles and regulation in endochondral bone development. *Journal of cellular biochemistry* **96**, 1163-1173,(2005).
26 St-Jacques, B., Hammerschmidt, M. & McMahon, A. P. Indian hedgehog signaling regulates proliferation and differentiation of chondrocytes and is essential for bone formation. *Genes & development* **13**, 2072-2086,(1999).
27 Yang, J. *et al.* HMGB1 is a bone-active cytokine. *Journal of cellular physiology* **214**, 730-739,(2008).
28 Taniguchi, N. *et al.* Stage-specific secretion of HMGB1 in cartilage regulates endochondral ossification. *Molecular and cellular biology* **27**, 5650-5663,(2007).
29 Protasoni, M. *et al.* The collagenic architecture of human dura mater. *Journal of neurosurgery* **114**, 1723-1730,(2011).
30 Levi, B. *et al.* Dura mater stimulates human adipose-derived stromal cells to undergo bone formation in mouse calvarial defects. *Stem cells* **29**, 1241-1255,(2011).
31 Petrie, C., Tholpady, S., Ogle, R. & Botchwey, E. Proliferative capacity and osteogenic potential of novel dura mater stem cells on poly-lactic-co-glycolic acid. *Journal of biomedical materials research. Part A* **85**, 61-71,(2008).
32 Peptan, I. A., Hong, L. & Evans, C. A. Multiple differentiation potentials of neonatal dura mater-derived cells. *Neurosurgery* **60**, 346-352; discussion 352,(2007).
33 Wan, D. C. *et al.* Global age-dependent differences in gene expression in response to calvarial injury. *The Journal of craniofacial surgery* **19**, 1292-1301,(2008).
34 Yu, J. C. *et al.* Regional differences of dura osteoinduction: squamous dura induces osteogenesis, sutural dura induces chondrogenesis and osteogenesis. *Plastic and reconstructive surgery* **100**, 23-31,(1997).

35 Hobar, P. C., Schreiber, J. S., McCarthy, J. G. & Thomas, P. A. The role of the dura in cranial bone regeneration in the immature animal. *Plastic and reconstructive surgery* **92**, 405-410,(1993).
36 Cowan, C. M., Quarto, N., Warren, S. M., Salim, A. & Longaker, M. T. Age-related changes in the biomolecular mechanisms of calvarial osteoblast biology affect fibroblast growth factor-2 signaling and osteogenesis. *The Journal of biological chemistry* **278**, 32005-32013,(2003).
37 Hassler, W. & Zentner, J. Radical osteoclastic craniectomy in sagittal synostosis. *Neurosurgery* **27**, 539-543,(1990).
38 Sirola, K. Regeneration of defects in the calvaria. An experimental study. *Annales medicinae experimentalis et biologiae Fenniae* **38(Suppl 2)**, 1-87,(1960).
39 Feng, L. *et al.* Pentamethoxyflavanone regulates macrophage polarization and ameliorates sepsis in mice. *Biochemical pharmacology* **89**, 109-118,(2014).
40 Malizos, K. N. & Papatheodorou, L. K. The healing potential of the periosteum molecular aspects. *Injury* **36 Suppl 3**, S13-19,(2005).
41 Tawonsawatruk, T., Spadaccino, A., Murray, I. R., Peault, B. & Simpson, H. A. Growth kinetics of rat mesenchymal stem cells from 3 potential sources: bone marrow, periosteum and adipose tissue. *Journal of the Medical Association of Thailand = Chotmaihet thangphaet* **95 Suppl 10**, S189-197,(2012).
42 Agata, H. *et al.* Effective bone engineering with periosteum-derived cells. *Journal of dental research* **86**, 79-83,(2007).
43 Murao, H., Yamamoto, K., Matsuda, S. & Akiyama, H. Periosteal cells are a major source of soft callus in bone fracture. *Journal of bone and mineral metabolism* **31**, 390-398,(2013).
44 Ball, M. D., Bonzani, I. C., Bovis, M. J., Williams, A. & Stevens, M. M. Human periosteum is a source of cells for orthopaedic tissue engineering: a pilot study. *Clinical orthopaedics and related research* **469**, 3085-3093,(2011).
45 Hutmacher, D. W. & Sittinger, M. Periosteal cells in bone tissue engineering. *Tissue engineering* **9 Suppl 1**, S45-64,(2003).
46 Hayashi, O., Katsube, Y., Hirose, M., Ohgushi, H. & Ito, H. Comparison of osteogenic ability of rat mesenchymal stem cells from bone marrow, periosteum, and adipose tissue. *Calcified tissue international* **82**, 238-247,(2008).
47 Hoffman, M. D., Xie, C., Zhang, X. & Benoit, D. S. The effect of mesenchymal stem cells delivered via hydrogel-based tissue engineered periosteum on bone allograft healing. *Biomaterials* **34**, 8887-8898,(2013).
48 Zhao, L., Zhao, J., Wang, S., Wang, J. & Liu, J. Comparative study between tissue-engineered periosteum and structural allograft in rabbit critical-sized radial defect model. *Journal of biomedical materials research. Part B, Applied biomaterials* **97**, 1-9,(2011).
49 Ma, D. *et al.* Enhancing bone formation by transplantation of a scaffold-free tissue-engineered periosteum in a rabbit model. *Clinical oral implants research* **22**, 1193-1199,(2011).
50 Reid, C. A., McCarthy, J. G. & Kolber, A. B. A study of regeneration in parietal bone defects in rabbits. *Plastic and reconstructive surgery* **67**, 591-596,(1981).
51 Uddstromer, L. & Ritsila, V. Healing of membranous and long bone defects. An experimental study in growing rabbits. *Scandinavian journal of plastic and reconstructive surgery* **13**, 281-287,(1979).

52 Gosain, A. K., Gosain, S. A., Sweeney, W. M., Song, L. S. & Amarante, M. T. Regulation of osteogenesis and survival within bone grafts to the calvaria: the effect of the dura versus the pericranium. *Plastic and reconstructive surgery* **128**, 85-94,(2011).
53 Paulo Ade, O. *et al.* Repair of critical-size defects with autogenous periosteum-derived cells combined with bovine anorganic apatite/collagen: an experimental study in rat calvaria. *Brazilian dental journal* **22**, 322-328,(2011).
54 Byron, C. D. *et al.* Effects of increased muscle mass on mouse sagittal suture morphology and mechanics. *The anatomical record. Part A, Discoveries in molecular, cellular, and evolutionary biology* **279**, 676-684,(2004).
55 Saito, K., Shimizu, Y. & Ooya, K. Age-related morphological changes in squamous and parietomastoid sutures of human cranium. *Cells, tissues, organs* **170**, 266-273,(2002).
56 Morriss-Kay, G. M. & Wilkie, A. O. Growth of the normal skull vault and its alteration in craniosynostosis: insights from human genetics and experimental studies. *Journal of anatomy* **207**, 637-653,(2005).
57 Opperman, L. A. Cranial sutures as intramembranous bone growth sites. *Developmental dynamics : an official publication of the American Association of Anatomists* **219**, 472-485,(2000).
58 Tholpady, S. S. & Ogle, R. C. Expression of transforming growth factor-beta-responsive smads in cranial suture development and closure. *The Journal of craniofacial surgery* **22**, 324-328,(2011).
59 Maeno, T. *et al.* Early onset of Runx2 expression caused craniosynostosis, ectopic bone formation, and limb defects. *Bone* **49**, 673-682,(2011).
60 Chen, F. *et al.* NELL-1, an osteoinductive factor, is a direct transcriptional target of Osterix. *PloS one* **6**, e24638,(2011).
61 Ang, B. U., Spivak, R. M., Nah, H. D. & Kirschner, R. E. Dura in the pathogenesis of syndromic craniosynostosis: fibroblast growth factor receptor 2 mutations in dural cells promote osteogenic proliferation and differentiation of osteoblasts. *The Journal of craniofacial surgery* **21**, 462-467,(2010).
62 Li, W. *et al.* Nell-1 enhances bone regeneration in a rat critical-sized femoral segmental defect model. *Plastic and reconstructive surgery* **127**, 580-587,(2011).
63 Isenmann, S. *et al.* TWIST family of basic helix-loop-helix transcription factors mediate human mesenchymal stem cell growth and commitment. *Stem cells* **27**, 2457-2468,(2009).
64 Lee, M. S., Lowe, G. N., Strong, D. D., Wergedal, J. E. & Glackin, C. A. TWIST, a basic helix-loop-helix transcription factor, can regulate the human osteogenic lineage. *Journal of cellular biochemistry* **75**, 566-577,(1999).
65 Huang, Y. *et al.* Twist1- and twist2-haploinsufficiency results in reduced bone formation. *PloS one* **9**, e99331,(2014).
66 Sadr, A. M., Cardenas, F. & Tavassoli, M. Functional potential of ectopic marrow autotransplants. *Experientia* **36**, 605-606,(1980).
67 Ma, J. *et al.* Bone forming capacity of cell- and growth factor-based constructs at different ectopic implantation sites. *Journal of biomedical materials research. Part A*,(2014).
68 Chan, C. K. *et al.* Endochondral ossification is required for haematopoietic stem-cell niche formation. *Nature* **457**, 490-494,(2009).

69 Chan, C. K. *et al.* Clonal precursor of bone, cartilage, and hematopoietic niche stromal cells. *Proceedings of the National Academy of Sciences of the United States of America*,(2013).
70 Scadden, D. T. The stem-cell niche as an entity of action. *Nature* **441**, 1075-1079,(2006).
71 Calvi, L. M. *et al.* Osteoblastic cells regulate the haematopoietic stem cell niche. *Nature* **425**, 841-846,(2003).
72 Tamplin, Owen J. *et al.* Hematopoietic Stem Cell Arrival Triggers Dynamic Remodeling of the Perivascular Niche. *Cell* **160**, 241-252,(2015).
73 Ferguson, C., Alpern, E., Miclau, T. & Helms, J. A. Does adult fracture repair recapitulate embryonic skeletal formation? *Mechanisms of development* **87**, 57-66,(1999).
74 Ai-Aql, Z. S., Alagl, A. S., Graves, D. T., Gerstenfeld, L. C. & Einhorn, T. A. Molecular mechanisms controlling bone formation during fracture healing and distraction osteogenesis. *Journal of dental research* **87**, 107-118,(2008).
75 Eming, S. A., Hammerschmidt, M., Krieg, T. & Roers, A. Interrelation of immunity and tissue repair or regeneration. *Seminars in cell & developmental biology* **20**, 517-527,(2009).
76 Eming, S. A., Krieg, T. & Davidson, J. M. Inflammation in wound repair: molecular and cellular mechanisms. *The Journal of investigative dermatology* **127**, 514-525,(2007).
77 Schmidt-Bleek, K. *et al.* Inflammatory phase of bone healing initiates the regenerative healing cascade. *Cell and tissue research* **347**, 567-573,(2012).
78 Wang, D. *et al.* Accelerated calvarial healing in mice lacking Toll-like receptor 4. *PloS one* **7**, e46945,(2012).
79 Park, S. H., Silva, M., Bahk, W. J., McKellop, H. & Lieberman, J. R. Effect of repeated irrigation and debridement on fracture healing in an animal model. *Journal of orthopaedic research : official publication of the Orthopaedic Research Society* **20**, 1197-1204,(2002).
80 Kim, B. J. *et al.* Risk factors of delayed surgical evacuation for initially nonoperative acute subdural hematomas following mild head injury. *Acta neurochirurgica* **156**, 1605-1613,(2014).
81 Schmidt-Bleek, K. *et al.* Cellular composition of the initial fracture hematoma compared to a muscle hematoma: a study in sheep. *Journal of orthopaedic research : official publication of the Orthopaedic Research Society* **27**, 1147-1151,(2009).
82 Lee, J. S. *et al.* Changes in serum levels of receptor activator of nuclear factor-kappaB ligand, osteoprotegerin, IL-6 and TNF-alpha in patients with a concomitant head injury and fracture. *Archives of orthopaedic and trauma surgery* **129**, 711-718,(2009).
83 Miyake, K. Innate immune sensing of pathogens and danger signals by cell surface Toll-like receptors. *Seminars in immunology* **19**, 3-10,(2007).
84 Szczesny, G. *et al.* Genetic factors responsible for long bone fractures non-union. *Archives of orthopaedic and trauma surgery* **131**, 275-281,(2011).
85 Schindeler, A., McDonald, M. M., Bokko, P. & Little, D. G. Bone remodeling during fracture repair: The cellular picture. *Seminars in cell & developmental biology* **19**, 459-466,(2008).
86 Fayaz, H. C. *et al.* The role of stem cells in fracture healing and nonunion. *International orthopaedics* **35**, 1587-1597,(2011).
87 Eriksen, E. F. Cellular mechanisms of bone remodeling. *Reviews in endocrine & metabolic disorders* **11**, 219-227,(2010).

88 Gerstenfeld, L. C., Cullinane, D. M., Barnes, G. L., Graves, D. T. & Einhorn, T. A. Fracture healing as a post-natal developmental process: molecular, spatial, and temporal aspects of its regulation. *Journal of cellular biochemistry* **88**, 873-884,(2003).
89 Raggatt, L. J. & Partridge, N. C. Cellular and molecular mechanisms of bone remodeling. *The Journal of biological chemistry* **285**, 25103-25108,(2010).
90 Mountziaris, P. M. & Mikos, A. G. Modulation of the inflammatory response for enhanced bone tissue regeneration. *Tissue engineering. Part B, Reviews* **14**, 179-186,(2008).
91 Levy, R. M. *et al.* Systemic inflammation and remote organ damage following bilateral femur fracture requires Toll-like receptor 4. *American journal of physiology. Regulatory, integrative and comparative physiology* **291**, R970-976,(2006).
92 Nagy, A., Perrimon, N., Sandmeyer, S. & Plasterk, R. Tailoring the genome: the power of genetic approaches. *Nature genetics* **33 Suppl**, 276-284,(2003).
93 Lorenzo, J., Horowitz, M. & Choi, Y. Osteoimmunology: interactions of the bone and immune system. *Endocrine reviews* **29**, 403-440,(2008).
94 Kobbe, P. *et al.* Patterns of cytokine release and evolution of remote organ dysfunction after bilateral femur fracture. *Shock* **30**, 43-47,(2008).
95 Strecker, W. *et al.* Early biochemical characterization of soft-tissue trauma and fracture trauma. *The Journal of trauma* **47**, 358-364,(1999).
96 Takayanagi, H. Osteoimmunology and the effects of the immune system on bone. *Nature reviews. Rheumatology* **5**, 667-676,(2009).
97 Zhang, X. *et al.* Cyclooxygenase-2 regulates mesenchymal cell differentiation into the osteoblast lineage and is critically involved in bone repair. *The Journal of clinical investigation* **109**, 1405-1415,(2002).
98 Toben, D. *et al.* Fracture healing is accelerated in the absence of the adaptive immune system. *Journal of bone and mineral research : the official journal of the American Society for Bone and Mineral Research* **26**, 113-124,(2011).
99 Brown, J., Wang, H., Hajishengallis, G. N. & Martin, M. TLR-signaling networks: an integration of adaptor molecules, kinases, and cross-talk. *Journal of dental research* **90**, 417-427,(2011).
100 Takami, M., Kim, N., Rho, J. & Choi, Y. Stimulation by toll-like receptors inhibits osteoclast differentiation. *Journal of immunology* **169**, 1516-1523,(2002).
101 Hayashi, S. *et al.* Distinct osteoclast precursors in the bone marrow and extramedullary organs characterized by responsiveness to Toll-like receptor ligands and TNF-alpha. *Journal of immunology* **171**, 5130-5139,(2003).
102 Kikuchi, T. *et al.* Gene expression of osteoclast differentiation factor is induced by lipopolysaccharide in mouse osteoblasts via Toll-like receptors. *Journal of immunology* **166**, 3574-3579,(2001).
103 Nair, S. P. *et al.* Bacterially induced bone destruction: mechanisms and misconceptions. *Infection and immunity* **64**, 2371-2380,(1996).
104 Kobbe, P. *et al.* Local exposure of bone components to injured soft tissue induces Toll-like receptor 4-dependent systemic inflammation with acute lung injury. *Shock* **30**, 686-691,(2008).
105 Kolar, P. *et al.* The early fracture hematoma and its potential role in fracture healing. *Tissue engineering. Part B, Reviews* **16**, 427-434,(2010).

106 Nakashima, T. & Takayanagi, H. Osteoimmunology: crosstalk between the immune and bone systems. *Journal of clinical immunology* **29**, 555-567,(2009).
107 Choudhary, S., Halbout, P., Alander, C., Raisz, L. & Pilbeam, C. Strontium ranelate promotes osteoblastic differentiation and mineralization of murine bone marrow stromal cells: involvement of prostaglandins. *Journal of bone and mineral research : the official journal of the American Society for Bone and Mineral Research* **22**, 1002-1010,(2007).
108 Gosain, A. K. *et al.* Osteogenesis in cranial defects: reassessment of the concept of critical size and the expression of TGF-beta isoforms. *Plastic and reconstructive surgery* **106**, 360-371; discussion 372,(2000).
109 Dimitriou, R., Tsiridis, E. & Giannoudis, P. V. Current concepts of molecular aspects of bone healing. *Injury* **36**, 1392-1404,(2005).
110 de Gorter, D. J., van Dinther, M., Korchynskyi, O. & ten Dijke, P. Biphasic effects of transforming growth factor beta on bone morphogenetic protein-induced osteoblast differentiation. *Journal of bone and mineral research : the official journal of the American Society for Bone and Mineral Research* **26**, 1178-1187,(2011).
111 Zimmermann, G. *et al.* TGF-beta1 as a marker of delayed fracture healing. *Bone* **36**, 779-785,(2005).
112 Cho, T. J., Gerstenfeld, L. C. & Einhorn, T. A. Differential temporal expression of members of the transforming growth factor beta superfamily during murine fracture healing. *Journal of bone and mineral research : the official journal of the American Society for Bone and Mineral Research* **17**, 513-520,(2002).
113 Lange, J. *et al.* Action of IL-1beta during fracture healing. *Journal of orthopaedic research : official publication of the Orthopaedic Research Society* **28**, 778-784,(2010).
114 Lee, Y. M., Fujikado, N., Manaka, H., Yasuda, H. & Iwakura, Y. IL-1 plays an important role in the bone metabolism under physiological conditions. *International immunology* **22**, 805-816,(2010).
115 Balto, K., Sasaki, H. & Stashenko, P. Interleukin-6 deficiency increases inflammatory bone destruction. *Infection and immunity* **69**, 744-750,(2001).
116 Hoyland, J. A., Freemont, A. J. & Sharpe, P. T. Interleukin-6, IL-6 receptor, and IL-6 nuclear factor gene expression in Paget's disease. *Journal of bone and mineral research : the official journal of the American Society for Bone and Mineral Research* **9**, 75-80,(1994).
117 Darowish, M. *et al.* Reduction of particle-induced osteolysis by interleukin-6 involves anti-inflammatory effect and inhibition of early osteoclast precursor differentiation. *Bone* **45**, 661-668,(2009).
118 Wallace, A., Cooney, T. E., Englund, R. & Lubahn, J. D. Effects of interleukin-6 ablation on fracture healing in mice. *Journal of orthopaedic research : official publication of the Orthopaedic Research Society* **29**, 1437-1442,(2011).
119 Mountziaris, P. M., Spicer, P. P., Kasper, F. K. & Mikos, A. G. Harnessing and modulating inflammation in strategies for bone regeneration. *Tissue engineering. Part B, Reviews* **17**, 393-402,(2011).
120 Seeman, E. & Delmas, P. D. Bone quality--the material and structural basis of bone strength and fragility. *The New England journal of medicine* **354**, 2250-2261,(2006).
121 Balogh, Z. J. *et al.* Advances and future directions for management of trauma patients with musculoskeletal injuries. *Lancet* **380**, 1109-1119,(2012).

122 Kaczorowski, D. J., Tsung, A. & Billiar, T. R. Innate immune mechanisms in ischemia/reperfusion. *Frontiers in bioscience* **1**, 91-98,(2009).
123 Rakoff-Nahoum, S. & Medzhitov, R. Toll-like receptors and cancer. *Nature reviews. Cancer* **9**, 57-63,(2009).
124 Kawasaki, T. & Kawai, T. Toll-like receptor signaling pathways. *Frontiers in immunology* **5**, 461,(2014).
125 Gao, Y. *et al.* Toll-like receptor 4-mediated myeloid differentiation factor 88-dependent signaling pathway is activated by cerebral ischemia-reperfusion in hippocampal CA1 region in mice. *Biological & pharmaceutical bulletin* **32**, 1665-1671,(2009).
126 Hyakkoku, K. *et al.* Toll-like receptor 4 (TLR4), but not TLR3 or TLR9, knock-out mice have neuroprotective effects against focal cerebral ischemia. *Neuroscience* **171**, 258-267,(2010).
127 Yang, Q. W. *et al.* HMBG1 mediates ischemia-reperfusion injury by TRIF-adaptor independent Toll-like receptor 4 signaling. *Journal of cerebral blood flow and metabolism : official journal of the International Society of Cerebral Blood Flow and Metabolism* **31**, 593-605,(2011).
128 Sachdev, U. *et al.* TLR2 and TLR4 Mediate Differential Responses to Limb Ischemia through MyD88-Dependent and Independent Pathways. *PloS one* **7**, e50654,(2012).
129 Vartanian, K. B. *et al.* LPS preconditioning redirects TLR signaling following stroke: TRIF-IRF3 plays a seminal role in mediating tolerance to ischemic injury. *Journal of neuroinflammation* **8**, 140,(2011).
130 Brickey, W. J. *et al.* MyD88 provides a protective role in long-term radiation-induced lung injury. *International journal of radiation biology* **88**, 335-347,(2012).
131 Watanabe, T. *et al.* Activation of the MyD88 signaling pathway inhibits ischemia-reperfusion injury in the small intestine. *American journal of physiology. Gastrointestinal and liver physiology* **303**, G324-334,(2012).
132 Park, J. E. & Barbul, A. Understanding the role of immune regulation in wound healing. *American journal of surgery* **187**, 11S-16S,(2004).
133 Geissmann, F. *et al.* Development of monocytes, macrophages, and dendritic cells. *Science* **327**, 656-661,(2010).
134 Nace, G. W. *et al.* Cellular-specific role of toll-like receptor 4 in hepatic ischemia-reperfusion injury in mice. *Hepatology* **58**, 374-387,(2013).
135 Hui, W., Jinxiang, Z., Heshui, W., Zhuoya, L. & Qichang, Z. Bone marrow and non-bone marrow TLR4 regulates hepatic ischemia/reperfusion injury. *Biochemical and biophysical research communications* **389**, 328-332,(2009).
136 Liu, S. *et al.* Role of toll-like receptors in changes in gene expression and NF-kappa B activation in mouse hepatocytes stimulated with lipopolysaccharide. *Infection and immunity* **70**, 3433-3442,(2002).
137 Zhang, Y. & Li, X. Lipopolysaccharide-regulated production of bone sialoprotein and interleukin-8 in human periodontal ligament fibroblasts: the role of toll-like receptors 2 and 4 and the MAPK pathway. *Journal of periodontal research* **50**, 141-151,(2015).
138 Lin, J. *et al.* Porphyromonas gingivalis exacerbates ligature-induced, RANKL-dependent alveolar bone resorption via differential regulation of Toll-like receptor 2 (TLR2) and TLR4. *Infection and immunity* **82**, 4127-4134,(2014).
139 Chen, Q. *et al.* Involvement of toll-like receptor 2 and pro-apoptotic signaling pathways in bone remodeling in osteomyelitis. *Cellular physiology and biochemistry :*

international journal of experimental cellular physiology, biochemistry, and pharmacology **34**, 1890-1900,(2014).

140 Kaczorowski, D. J. *et al.* Mechanisms of Toll-like receptor 4 (TLR4)-mediated inflammation after cold ischemia/reperfusion in the heart. *Transplantation* **87**, 1455-1463,(2009).

141 Liu, Y., Yin, H., Zhao, M. & Lu, Q. TLR2 and TLR4 in autoimmune diseases: a comprehensive review. *Clinical reviews in allergy & immunology* **47**, 136-147,(2014).

142 Mu, H. *et al.* Sinomenine decreases MyD88 expression and improves inflammation-induced joint damage progression and symptoms in rat adjuvant-induced arthritis. *Inflammation* **36**, 1136-1144,(2013).

143 Madeira, M. F. *et al.* MyD88 is essential for alveolar bone loss induced by Aggregatibacter actinomycetemcomitans lipopolysaccharide in mice. *Molecular oral microbiology* **28**, 415-424,(2013).

144 Zhang, P. *et al.* TLR2-dependent modulation of osteoclastogenesis by Porphyromonas gingivalis through differential induction of NFATc1 and NF-kappaB. *The Journal of biological chemistry* **286**, 24159-24169,(2011).

145 Castoldi, A. *et al.* TLR2, TLR4 and the MYD88 signaling pathway are crucial for neutrophil migration in acute kidney injury induced by sepsis. *PloS one* **7**, e37584,(2012).

146 Sachdev, U., Cui, X., Xu, J., Xu, J. & Tzeng, E. MyD88 and TRIF mediate divergent inflammatory and regenerative responses to skeletal muscle ischemia. *Physiological reports* **2**,(2014).

147 Rodriguez, N. *et al.* Polymorphonuclear neutrophils improve replication of Chlamydia pneumoniae in vivo upon MyD88-dependent attraction. *Journal of immunology* **174**, 4836-4844,(2005).

148 Negishi, H. *et al.* Evidence for licensing of IFN-gamma-induced IFN regulatory factor 1 transcription factor by MyD88 in Toll-like receptor-dependent gene induction program. *Proceedings of the National Academy of Sciences of the United States of America* **103**, 15136-15141,(2006).

149 Huebener, P. & Schwabe, R. F. Regulation of wound healing and organ fibrosis by toll-like receptors. *Biochimica et biophysica acta* **1832**, 1005-1017,(2013).

150 Macedo, L. *et al.* Wound healing is impaired in MyD88-deficient mice: a role for MyD88 in the regulation of wound healing by adenosine A2A receptors. *The American journal of pathology* **171**, 1774-1788,(2007).

151 Gasse, P. *et al.* IL-1R1/MyD88 signaling and the inflammasome are essential in pulmonary inflammation and fibrosis in mice. *The Journal of clinical investigation* **117**, 3786-3799,(2007).

152 Jiang, D. *et al.* Regulation of lung injury and repair by Toll-like receptors and hyaluronan. *Nature medicine* **11**, 1173-1179,(2005).

153 Hayashi, F., Means, T. K. & Luster, A. D. Toll-like receptors stimulate human neutrophil function. *Blood* **102**, 2660-2669,(2003).

154 Clausen, B. E., Burkhardt, C., Reith, W., Renkawitz, R. & Forster, I. Conditional gene targeting in macrophages and granulocytes using LysMcre mice. *Transgenic research* **8**, 265-277,(1999).

155 Maitra, R. *et al.* Dendritic cell-mediated in vivo bone resorption. *Journal of immunology* **185**, 1485-1491,(2010).

156 Alnaeeli, M., Park, J., Mahamed, D., Penninger, J. M. & Teng, Y. T. Dendritic cells at the osteo-immune interface: implications for inflammation-induced bone loss. *Journal of bone and mineral research : the official journal of the American Society for Bone and Mineral Research* **22**, 775-780,(2007).
157 Rivollier, A. *et al.* Immature dendritic cell transdifferentiation into osteoclasts: a novel pathway sustained by the rheumatoid arthritis microenvironment. *Blood* **104**, 4029-4037,(2004).
158 Oh, Y., Oh, I., Morimoto, J., Uede, T. & Morimoto, A. Osteopontin has a crucial role in osteoclast-like multinucleated giant cell formation. *Journal of cellular biochemistry* **115**, 585-595,(2014).
159 Huebener, P. & Schwabe, R. F. Regulation of wound healing and organ fibrosis by toll-like receptors. *Biochimica et biophysica acta*,(2012).
160 Lin, Q., Li, M., Fang, D., Fang, J. & Su, S. B. The essential roles of Toll-like receptor signaling pathways in sterile inflammatory diseases. *International immunopharmacology* **11**, 1422-1432,(2011).
161 Poltorak, A. *et al.* Defective LPS signaling in C3H/HeJ and C57BL/10ScCr mice: mutations in Tlr4 gene. *Science* **282**, 2085-2088,(1998).
162 Smiley, S. T., King, J. A. & Hancock, W. W. Fibrinogen stimulates macrophage chemokine secretion through toll-like receptor 4. *J Immunol* **167**, 2887-2894,(2001).
163 Gondokaryono, S. P. *et al.* The extra domain A of fibronectin stimulates murine mast cells via toll-like receptor 4. *J Leukoc Biol* **82**, 657-665,(2007).
164 Ohashi, K., Burkart, V., Flohe, S. & Kolb, H. Cutting edge: heat shock protein 60 is a putative endogenous ligand of the toll-like receptor-4 complex. *J Immunol* **164**, 558-561,(2000).
165 Biragyn, A. *et al.* Toll-like receptor 4-dependent activation of dendritic cells by beta-defensin 2. *Science* **298**, 1025-1029,(2002).
166 Wang, H. *et al.* HMG-1 as a late mediator of endotoxin lethality in mice. *Science* **285**, 248-251,(1999).
167 Bar-Shavit, Z. Taking a toll on the bones: regulation of bone metabolism by innate immune regulators. *Autoimmunity* **41**, 195-203,(2008).
168 Liu, J. *et al.* Molecular mechanism of the bifunctional role of lipopolysaccharide in osteoclastogenesis. *The Journal of biological chemistry* **284**, 12512-12523,(2009).
169 Tomofuji, T. *et al.* Involvement of toll-like receptor 2 and 4 in association between dyslipidemia and osteoclast differentiation in apolipoprotein E deficient rat periodontium. *Lipids in health and disease* **12**, 1,(2013).
170 Ukai, T., Yumoto, H., Gibson, F. C., 3rd & Genco, C. A. Macrophage-elicited osteoclastogenesis in response to bacterial stimulation requires Toll-like receptor 2-dependent tumor necrosis factor-alpha production. *Infection and immunity* **76**, 812-819,(2008).
171 Vijayan, V., Khandelwal, M., Manglani, K., Gupta, S. & Surolia, A. Methionine down-regulates TLR4/MyD88/NF-kappaB signalling in osteoclast precursors to reduce bone loss during osteoporosis. *British journal of pharmacology* **171**, 107-121,(2014).
172 Uzar, I. *et al.* The importance of 8993C>T (Thr399Ile) TLR4 polymorphism in etiology of osteoporosis in postmenopausal women. *Ginekologia polska* **85**, 180-184,(2014).

173 Huang, R. L. *et al.* LPS-stimulated inflammatory environment inhibits BMP-2-induced osteoblastic differentiation through crosstalk between TLR4/MyD88/NF-kappaB and BMP/Smad signaling. *Stem cells and development* **23**, 277-289,(2014).
174 Amcheslavsky, A. & Bar-Shavit, Z. Toll-like receptor 9 ligand blocks osteoclast differentiation through induction of phosphatase. *Journal of bone and mineral research : the official journal of the American Society for Bone and Mineral Research* **22**, 1301-1310,(2007).
175 Chiu, W. S. *et al.* Transgenic mice that express Cre recombinase in osteoclasts. *Genesis* **39**, 178-185,(2004).
176 Hilliard, T. J., Meadows, G. & Kahn, A. J. Lysozyme synthesis in osteoclasts. *Journal of bone and mineral research : the official journal of the American Society for Bone and Mineral Research* **5**, 1217-1222,(1990).
177 Seledtsov, V. I. & Seledtsova, G. V. A balance between tissue-destructive and tissue-protective immunities: a role of toll-like receptors in regulation of adaptive immunity. *Immunobiology* **217**, 430-435,(2012).
178 Olmedo, M. L. *et al.* Regulation of osteoblast levels during bone healing. *Journal of orthopaedic trauma* **13**, 356-362,(1999).
179 Matsumoto, C. *et al.* Toll-like receptor 2 heterodimers, TLR2/6 and TLR2/1 induce prostaglandin E production by osteoblasts, osteoclast formation and inflammatory periodontitis. *Biochemical and biophysical research communications* **428**, 110-115,(2012).
180 Dasu, M. R. *et al.* TLR2 expression and signaling-dependent inflammation impair wound healing in diabetic mice. *Laboratory investigation; a journal of technical methods and pathology* **90**, 1628-1636,(2010).
181 Moles, A. *et al.* A TLR2/S100A9/CXCL-2 signaling network is necessary for neutrophil recruitment in acute and chronic liver injury in the mouse. *Journal of hepatology* **60**, 782-791,(2014).
182 Hurst, S. M. *et al.* Il-6 and its soluble receptor orchestrate a temporal switch in the pattern of leukocyte recruitment seen during acute inflammation. *Immunity* **14**, 705-714,(2001).
183 Kasama, T., Strieter, R. M., Standiford, T. J., Burdick, M. D. & Kunkel, S. L. Expression and regulation of human neutrophil-derived macrophage inflammatory protein 1 alpha. *The Journal of experimental medicine* **178**, 63-72,(1993).
184 Lee, S. *et al.* Distinct macrophage phenotypes contribute to kidney injury and repair. *Journal of the American Society of Nephrology : JASN* **22**, 317-326,(2011).
185 Lech, M. *et al.* Macrophage phenotype controls long-term AKI outcomes--kidney regeneration versus atrophy. *Journal of the American Society of Nephrology : JASN* **25**, 292-304,(2014).
186 Alexiou, G. A., Sfakianos, G. & Prodromou, N. Pediatric head trauma. *Journal of emergencies, trauma, and shock* **4**, 403-408,(2011).
187 Chung, E. H. *et al.* Biomimetic artificial ECMs stimulate bone regeneration. *Journal of biomedical materials research. Part A* **79**, 815-826,(2006).
188 Zimmermann, G. & Moghaddam, A. Allograft bone matrix versus synthetic bone graft substitutes. *Injury* **42 Suppl 2**, S16-21,(2011).
189 Copeland, C. E., Mitchell, K. A., Brumback, R. J., Gens, D. R. & Burgess, A. R. Mortality in patients with bilateral femoral fractures. *Journal of orthopaedic trauma* **12**, 315-319,(1998).

190 Daly, K. A. *et al.* Damage associated molecular patterns within xenogeneic biologic scaffolds and their effects on host remodeling. *Biomaterials* **33**, 91-101,(2012).
191 Piccinini, A. M. & Midwood, K. S. DAMPening inflammation by modulating TLR signalling. *Mediators of inflammation* **2010**,(2010).
192 Dasu, M. R. & Isseroff, R. R. Toll-like receptors in wound healing: location, accessibility, and timing. *The Journal of investigative dermatology* **132**, 1955-1958,(2012).
193 Kaczorowski, D. J., Mollen, K. P., Edmonds, R. & Billiar, T. R. Early events in the recognition of danger signals after tissue injury. *Journal of leukocyte biology* **83**, 546-552,(2008).
194 Li, C. *et al.* Lipopolysaccharide differentially affects the osteogenic differentiation of periodontal ligament stem cells and bone marrow mesenchymal stem cells through Toll-like receptor 4 mediated nuclear factor kappaB pathway. *Stem cell research & therapy* **5**, 67,(2014).
195 Sohn, D. H. *et al.* Plasma proteins present in osteoarthritic synovial fluid can stimulate cytokine production via Toll-like receptor 4. *Arthritis research & therapy* **14**, R7,(2012).
196 Schelbergen, R. F. *et al.* Alarmins S100A8 and S100A9 elicit a catabolic effect in human osteoarthritic chondrocytes that is dependent on Toll-like receptor 4. *Arthritis and rheumatism* **64**, 1477-1487,(2012).
197 Edwin E. Osgood , A. J. S. The cellular composition of normal bone marrow as obtained by sternal puncture. *Physiological Reviews* **24**, 46-69,(1944).
198 De Bari, C. *et al.* Mesenchymal multipotency of adult human periosteal cells demonstrated by single-cell lineage analysis. *Arthritis and rheumatism* **54**, 1209-1221,(2006).
199 Gnecchi, M. & Melo, L. G. Bone marrow-derived mesenchymal stem cells: isolation, expansion, characterization, viral transduction, and production of conditioned medium. *Methods in molecular biology* **482**, 281-294,(2009).
200 Zheng, R. C. *et al.* Characteristics and response of mouse bone marrow derived novel low adherent mesenchymal stem cells acquired by quantification of extracellular matrix. *The journal of advanced prosthodontics* **6**, 351-360,(2014).
201 Kozloff, K. M., Volakis, L. I., Marini, J. C. & Caird, M. S. Near-infrared fluorescent probe traces bisphosphonate delivery and retention in vivo. *Journal of bone and mineral research : the official journal of the American Society for Bone and Mineral Research* **25**, 1748-1758,(2010).
202 Bastian, O. *et al.* Systemic inflammation and fracture healing. *Journal of leukocyte biology* **89**, 669-673,(2011).
203 Thomas, M. V. & Puleo, D. A. Infection, inflammation, and bone regeneration: a paradoxical relationship. *Journal of dental research* **90**, 1052-1061,(2011).
204 Bryant, C. D. The blessings and curses of C57BL/6 substrains in mouse genetic studies. *Annals of the New York Academy of Sciences* **1245**, 31-33,(2011).
205 Cornejo, A. *et al.* Effect of adipose tissue-derived osteogenic and endothelial cells on bone allograft osteogenesis and vascularization in critical-sized calvarial defects. *Tissue engineering. Part A* **18**, 1552-1561,(2012).
206 Navarro, S. J. *et al.* The C57BL/6J Mouse Strain Background Modifies the Effect of a Mutation in Bcl2l2. *G3* **2**, 99-102,(2012).

207 Huang, C., Tang, M., Yehling, E. & Zhang, X. Overexpressing sonic hedgehog peptide restores periosteal bone formation in a murine bone allograft transplantation model. *Molecular therapy : the journal of the American Society of Gene Therapy* **22**, 430-439,(2014).
208 Ito, H. *et al.* Remodeling of cortical bone allografts mediated by adherent rAAV-RANKL and VEGF gene therapy. *Nature medicine* **11**, 291-297,(2005).
209 Levi, B. *et al.* Human adipose derived stromal cells heal critical size mouse calvarial defects. *PloS one* **5**, e11177,(2010).
210 Yu, X. *et al.* The effect of fresh bone marrow cells on reconstruction of mouse calvarial defect combined with calvarial osteoprogenitor cells and collagen-apatite scaffold. *Journal of tissue engineering and regenerative medicine*,(2012).